POLITECNICO

MILANO 1863

DIPARTIMENTO DI ELETTRONICA INFORMAZIONE E BIOINGEGNERIA

SCUOLA DI INGEGNERIA INDUSTRIALE E DELL'INFORMAZIONE

Corso di Laurea Magistrale in Ingegneria dell'Automazione

TESI DI LAUREA MAGISTRALE

Predictive Control of Voltages and Frequency in an Islanded Microgrid

Relatore:
Prof. Riccardo Scattolini

Correlatori:
Dr. Stefano Raimondi Cominesi
Ing. Carlo Sandroni
Prof. Carlo Novara

Candidato:
Alessio La Bella
Matricola: 813547

Anno Accademico 2014–2015

Alla mia famiglia

L'uomo deve perseverare nella credenza
che l'incomprensibile sia comprensibile;
altrimenti rinuncerebbe a cercare.

J. W. Goethe, Massime e riflessioni, 1833.

Abstract

A microgrid can be considered as a cluster of generators, renewable sources, storage units and loads, working either in grid-connection or in islanded mode. The undeterministic nature of both renewable sources and loads represents the main issue for the reliability of microgrids, resulting in frequent unbalances between the total generated and absorbed power. While in grid-connected mode any power mismatch is compensated by a power exchange with the main grid, unbalances in islanded mode have a considerable impact on the network frequency and voltages, leading to significant deviations from their nominal values. The main objective of this work is to design a supervising controller for the coordination of generators in an islanded microgrid. The control objective is to keep frequency and voltages as close as possible to their nominal values while satisfying the actual load absorption. Moreover, also some economic factors are taken into account in order to implement some resource management strategies. For this purpose, a two-layer control architecture has been devised. The primary controller, based on the largely studied *Droop Control*, relies on a decentralized control action that promptly minimizes the power unbalances. A higher control layer is instead entitled to both restore voltages and frequency to their nominal values and efficiently distribute the power generation among the different sources. The designed secondary control layer relies on a *Model Predictive Control* approach, that at each iteration defines the optimal production plan. Moreover, the inclusion of an integral action ensures the convergence of the frequency to its nominal value. The proposed hierarchical control structure, besides improving the performances with respect to those provided by the primary layer alone, allows for a better distribution of the regulating action among the controllable generators. The results show the effectiveness of the algorithm in presence of different control objectives. Moreover, the robustness of the control system have been tested, taking into account different contexts which may correspond to realistic implementations.

Sommario

Una microgrid corrisponde ad un insieme di generatori, sorgenti rinnovabili, batterie e carichi, il quale può funzionare sia in isola che connessa alla rete. La natura non deterministica sia delle risorse rinnovabili che dei carichi causa frequenti sbilanci fra la potenza totale generata e quella assorbita. Mentre quando la microgrid è connessa, ogni sbilancio è compensato da uno scambio di potenza con la rete, in modalità in isola gli sbilanci hanno un considerevole impatto sulla frequenza di rete e sulle tensioni, portandole a deviare significativamente dai loro valori nominali. Lo scopo di questo lavoro è quello di progettare un sistema di controllo per il coordinamento dei generatori in una rete isolata. L'obiettivo è quello di mantenere la frequenza e le tensioni più vicine possibile ai loro valori nominali e nel mentre soddisfare la potenza di carico richiesta. Inoltre, anche fattori economici sono stati presi in considerazione per implementare diverse strategie per la gestione delle risorse. É stata ideata una struttura di controllo gerarchica, che consiste in due principali livelli. Il controllo primario si basa sul *Controllo Droop* e implementa un'azione di controllo decentralizzata che minimizza velocemente gli sbilanci di potenza. In seguito, è stato progettato sistema di controllo di più alto livello, che ha come obiettivo sia di riportare le tensioni e la frequenza ai loro valori nominali, sia di distribuire la potenza generata alle diverse sorgenti. Questo si basa su una tecnica di controllo predittivo, il quale decide ad ogni iterazione qual è il piano di produzione ottimale. Inoltre, per assicurare che la frequenza converga al suo valore nominale, è stata inserita un' azione di controllo integrale. La struttura di controllo definita, oltre che migliorare le prestazioni rispetto al caso in cui sia implementato solo il controllo primario, permette una migliore distribuzione dell'azione regolante ai diversi generatori. I risultati ottenuti hanno mostrato infatti l'efficienza dell'algoritmo in presenza di differenti obiettivi. Infine, la robustezza del sistema di controllo è stata valutata prendendo in considerazione un' implementazione più realistica.

Contents

Chapter 1

Introduction

1.1 Motivations

The need of reducing CO_2 emissions from energy generation, as well as the objective of having a more efficient and reliable electrical system, have pushed a growing research interest in Distributed Energy Resources (DER). There has been in fact an increasing penetration of microgeneration sources, such as photovoltaics, CHP systems [1] or small wind turbines, and this process is actually reshaping the traditional electrical structure. Given the presence of distributed generation, the current electrical system is actually becoming more decentralized and there is less and less distinction between generating sites and consumption areas as each small portion of the main grid could be also an energy producer, as well as an energy consumer.

The reason why distributed generation is becoming an attractive technology relies on its decentralized nature; it allows in fact to overcome many shortfalls of the actual system. The current grid structure is quite inefficient because of energy losses on the long transmission lines and, what is more, it is not by far a reliable system. There have been indeed plenty of black-outs events, for instance in Italy or North-East United States both in 2003, where a small problem in one part of the grid affected the whole system through a domino-effect process, causing eventually many money losses and technical problems.

Moreover, this centralized electrical structure relies on big power plants that, producing energy for great portions of countries, can not depend on green technologies but they are usually fossil-fuel based, becoming today the main cause of the high level of carbon dioxide emissions.

---

[1] A combined heat and power system corresponds to a small fuel cell or heat engine driving a generator which provides electric and heat power for building heating or air conditioning.

To overcome these issues, the future system could consist in a more flexible and distributed electrical framework which can be seen as a big set of many small-scale grids, called microgrids, where each of these elements is a cluster of several energy microgeneration sources, storage units and loads.

Although microgrids could still export and import energy to the main grid through single-point connections, called points of common coupling (PCC), they are no more strictly dependent on the main electrical system. In fact in this future view, if a fault occurred in the main grid, this smart microgrid would be able to isolate itself and to work as an autonomous system thanks only to its sources, including renewable ones. Furthermore, the microgrid could also intentionally decide to disconnect itself from the main grid for economical or security reasons. These configurations are generally called islanded or stand-alone operating modes.

Nevertheless, the islanded condition requires that all microgrids' elements must be properly coordinated in order to avoid network collapse. Without the support of the main grid, this condition is somehow critical as some generating sources, such as photovoltaics and wind turbines, are not fully controllable and therefore peaks of power demand do not necessarily coincide with generation peaks. Moreover, network frequency and voltages must be also taken into account as they are extremely sensitive to the uncertain power variations and mismatches. Without a proper control system, these variables would greatly diverge leading the system to a possible black-out event.

Given the research interest and the above-mentioned issues, this work focuses on the design of a control system that, during the islanded operating mode, is not only able to efficiently manage the microgrid's energy flows, but it also ensures that the power quality, in terms of network frequency and voltages, is never compromised.

1.2   Microgrids

Microgrids can not properly be designed as a new concept since small-scale grids have already existed in remote areas, where the interconnection with the main grid is not possible due to technical or economical reasons. Nevertheless, combustion-based generators, which are fully deterministic and dispatchable, have been so far the most common choice for the electrical supply.

The next challenge is to make microgrids ensure the system correct operation without relying on fossil fuel combustion but only thanks to the efficient coordination of many different zero carbon emission technologies. Although microgrids may have arbitrary configurations, some elements are generally present, such as renewable energy sources, storage systems, and some controllable generation units.

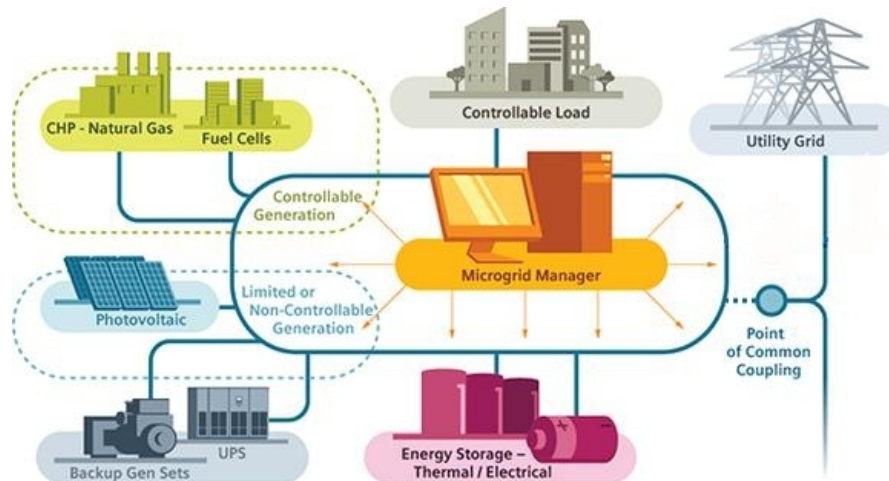A possible microgrid structure is presented below.

Figure 1.1: Microgrid general structure

However, it should be underlined that the high integration of greener technologies, in spite of many environmental advantages, raises some new technical concerns which must be solved in order to ensure system reliability.

The most relevant challenges in microgrid management and control include:

- **Intermittent power:** Renewable sources can not deliver as much power as requested but their contributions depend on external factors, mainly regarding the weather and the different hours of the day. Therefore, there could be some situations where the power balance is not feasible. To overcome this issue, the microgrid is equipped with several batteries that can be charged when there is high power availability and discharged when a load peak occurs. However, also storage units are not fully controllable power sources since they depend on their states of charge.

- **Bidirectional power flows:** Distribution feeders were initially designed for unidirectional power flows. However, the introduction of DERs to low voltage levels can cause reverse power flows, given for instance the presence of batteries that can either absorb or deliver power. This may lead to complications in protection coordination, undesirable power flow patterns, fault current distribution or voltage control.

- **Low inertia:** Unlike today power systems where the high number of synchronous generators ensures a large system inertia, microgrids are characterized by a low-inertia characteristic as most distributed generation sources are controlled through power electronics converters. This interface is necessary since many microgeneration units directly produce DC power, such as photovoltaics and batteries, or not synchronous AC power, like wind turbines, and therefore power converters, such as inverters, are needed. Although such an interface enhances the dynamic performance, the lack of synchronous and high-inertia rotating generators make the system control more critical as relevant voltage or frequency deviations can occur, especially if the microgrid is not supported by the host grid.

- **Uncertainty:** This is another issue for the correct system coordination since neither generation sources nor loads are deterministic systems. Indeed, even though load profiles and weather forecasts are often available, their reliability is controversial. This factor is more critical in microgrids than in bulk power systems due to the reduced number of loads and the high correlation variations of available energy resources, limiting so the averaging effect that a big electrical system may have.

All these issues may be overcome through the presence of a supervising control system that will be in charge of the coordination of all microgrid's systems. It has to ensure that reliability is never compromised, especially in islanded operation, and it could also take into account economical factors for an efficient resources' management.

1.3 Control Structure

In the field of power system's control, two distinctive approaches can be identified: centralized and decentralized. A fully centralized control requires that all microgrid's data and measures are delivered to a central controller that determines the control actions for the whole systems.

On the other hand, in a decentralized control structure each unit is independently managed by its local controller and so there is no interaction between the different controllers of the microgrid.

The electrical complexity and extension of a microgrid make a fully centralized approach infeasible due to the extensive communication and required computation. At the same time, a complete distributed approach is not recommended since, given the strong coupling between the operations of the microgrid's elements, a high coordination level is needed. A compromise between the two approaches could be achieved by implementing a hierarchical control structure consisting of many local controllers coordinated by a high level control system. The adoption of this control structure is quite appealing also because it allows to deal with the different involved time constants, such as the fast dynamics of voltage output controls and the slower ones for the economical dispatch.

In the context of power systems control, the hierarchical control structure has a typical structure consisting in three control levels: primary, secondary and tertiary control. Each of these layers provides supervisory control over lower-levels and it differs from the others in the time frame in which it operates, as well as in the interconnections with the other system elements. A brief description of the hierarchical structure is now presented.

1.3.1   Primary Control

The primary control layer constitutes the lower level of this hierarchical control architecture and it has the responsibility to deal with the fastest dynamics of the system. Given the computational time frame, it has generally a decentralized structure and it is locally implemented at each distributed generation source. Its main objective is to regulate the inverters of the generation units so that frequency and voltages do not considerably diverge from their nominal values. Although primary control can have different configurations, it generally consists of two sequential control stages: the inverter output control and the droop control.

Inverter output control represents the inner loop and it is in charge of maintaining the inverter output set-points with a series of current and voltage control loops.

Droop control is a particular scheme designed to quickly stabilize frequency and voltages of the microgrid during large variations of powers, as well as during the islanding event. Its purpose is to set the set-points for the inverter output control through a proportional action linking the variations of generated active power and generated reactive power to the variations of network frequency and voltages.

An example of a possible droop static relationship is reported in Figure 1.2. Looking to the graph on the left, it possible to see that, depending on the generated active power, the output inverter frequency is set to a certain value. The same reasoning holds for the right graph, where the output voltage is decided based on the delivered reactive power. These relatioships are based on several reasons, most related to network characteristics; all the details of this control strategy will be explained in next chapters.

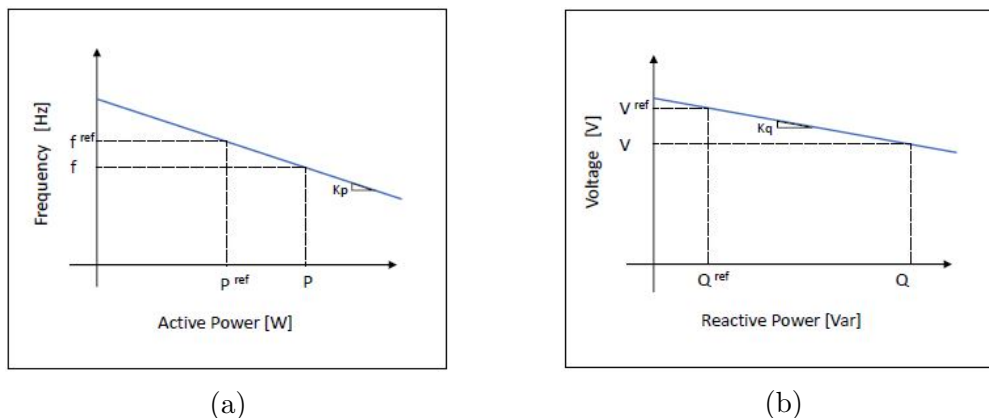(a)   (b)

Figure 1.2: Inductive droop characteristics

Since the aim of droop control is not to keep voltages and frequency at their nominal values but only to avoid that they significantly deviate, its action usually results in steady-state biases from reference values. An additional control loop is needed so that these electrical variables can be restored to their reference values. This can be done by means of secondary control.

1.3.2 Secondary Control

The secondary control layer operates at a ... respect to the previously described primary control. This allows both to consider primary dynamics at steady state and also to have enough time to perform complex computations. Actually, the purpose of this layer could be not only to restore frequency and voltages deviations but it may also be responsible for the economical operation of the microgrid either in grid-connected and stand-alone mode.

Also in this case, two main approaches are generally adopted: centralized and decentralized. The first one surely enables the implementation of online algorithms that can achieve relevant results in terms of efficient and secure operation. However

a centralized control is not a flexible framework since even a small change on the microgrid structure implies that the controller setting must be modified.

On the other hand, the decentralized approach exhibits the desirable plug-and-play feature since it can easily incorporate new DER elements without changing the control scheme; nevertheless at the same time this approach can not ensure an optimal high level coordination. Generally, in islanded mode it could be preferred to implement a centralized structure since power balances must be properly managed in order to avoid serious frequency or voltage deviations.

1.3.3   Tertiary Control

This is the highest control level and it typically operates in the order of several minutes or hours. It has not a fixed purpose, but it is generally designed to optimize power flows between different microgrids or between the single microgrid and the main grid. Hence, this control layer could be needed only in grid connected mode, while during stand-alone operation the highest coordination is usually performed by secondary control.

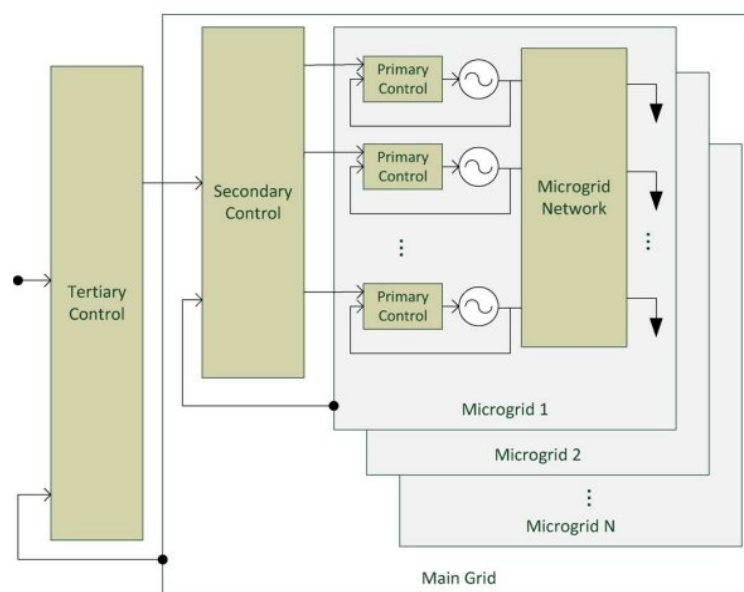A possible hierarchical control structure is depicted in Figure 1.3.

Figure 1.3: Hierarchical control structure

1.4   Literature Review

The recent interest in islanded microgrids' management has motivated many research activities concerning the definition and analysis of their control system. With regard to the primary control, the so called droop control has attracted the most attention since it ensures a fast network stabilization through its decentralized structure. Although several studies have been carried out [1]-[4], it has been rarely rigoursly analysed. Because of this, J. W. Simpson-Porco, F. Dörfler and F. Bullo performed a nonlinear analysis of this control layer proving that, under certain assumptions, a stable steady-state solution exists [5]. Moreover, by precisely tuning the droop static relationships, it is possible to achieve a proportional power sharing between the different generation units.

As droop control leads to steady state deviations, a slower secondary control loop can be used to regulate frequency and voltages towards their nominal values. Therefore, the previous authors developed a distributed secondary scheme, called distributed averaging proportional integral controller (DAPI), that, thanks to its integral action, is able to eliminate steady-state offsets, preserving also the power sharing performed by primary control [5], [6]. Other interesting examples of distributed secondary control, implemented using multiagent or consensus techniques, are explained in [7], [8]. As aforementioned, although the decentralized approach represents a more flexible and simpler structure, it can not provide a high level and economical coordination.

Some centralized secondary control structures have been discussed in the literature, such as in [9] and [10], but it is rarely the case that an efficient control scheme taking into account both network variables restoration and economical factors has been developed. The intent of this work is so to propose a novel control structure that is able to accomplish both tasks during the critical stand-alone operation since in this case power unbalances can results in unstable behaviours. In the next paragraph a brief description of the proposed solution is given.

1.5   Proposed Solution

The designed control scheme relies on a hierarchical control structure consisting in two layers: primary and secondary control. The primary control is characterized by a decentralized framework and it is locally implemented at each generation unit. It is based on the droop control approach since, as previously explained, it provides a fast stabilization of network variables.

Regarding the secondary control layer, it implements a centralized controller in order to both restore variables' shifts and to efficiently manage microgrid energy flows. It should be noted that the frequency is required to be as close all possible to 50 Hz. This is a more relevant issue if the islanded microgrid need to be reconnected again to the main grid; indeed the two systems must be synchronized at the same nominal frequency and phase at the interconnection point. To accomplish this task, an integrator is first placed on the frequency error, so as to guarantee a zero steady-state frequency error. Then, a Model Predictive Controller (MPC) is designed. This control strategy is based on a detailed and structured theory but, to put it briefly, this control algorithm performs an optimization process on a predefined time span so that the optimal control variables are chosen. Moreover, weather and load profiles forecasts are usually available and they could be used to perform a more accurate optimization over a defined prediction horizon.

Although the system has a continuous dynamics, it has been quantized into a discrete-time based system. The sampling time can be arbitrary decided but there are however some limitations. In fact, a too slow control action could not be enough effective, while it may be not possible to implement a too fast one due both to computational limits and to the fact that it is assumed that the primary dynamics have already reached the steady-state condition. Therefore, the time frame is chosen to be in the order of some minutes. All the details regarding this solution will be extensively discussed in next chapters, explaining both the theoretical definition and the actual implementation. However, in order to have a first insight of the proposed hierarchical control structure, a simplified scheme is reported in Figure 1.4.
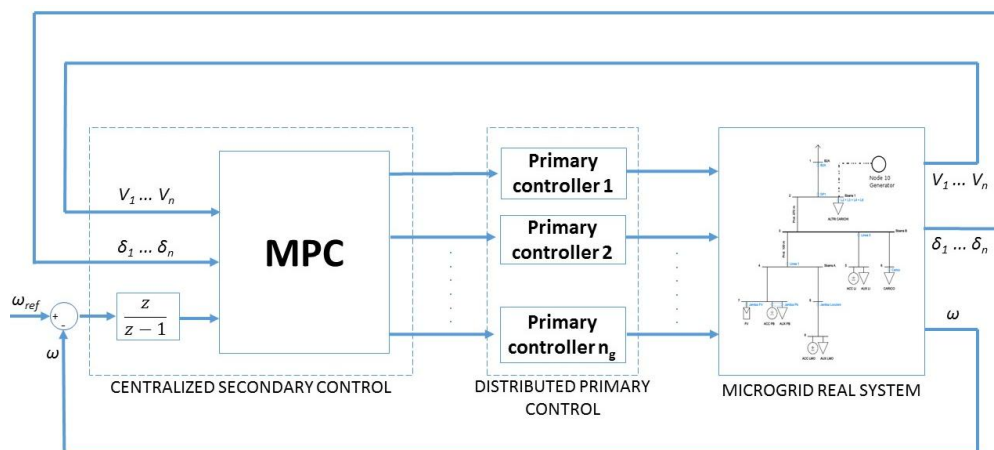

Figure 1.4: Proposed control scheme

11

1.6 Thesis Outlook

The thesis is structured as follows.

After this introduction, the second chapter will focus on a detailed description of the issues that involve the islanded condition. An overview of the primary control theory will be also given, explaining how its implementation can actually give a first resolution to the mentioned issues. It will be shown that different primary control configurations exist and their implementations actually depend on the network parameters and loads. However, as already mentioned, a primary control layer is not enough to efficiently manage an islanded microgrid and therefore an additional and more complex control layer is needed.

Since the secondary control layer is based on the Model Predictive Control theory, a mathematical model of the system is needed. The third chapter will show how the network model has been derived starting from the power flow theory. Moreover, also the main microgrid elements need to be modeled so that the corresponding main variables can be taken into account during the optimization process. Finally, the system simulator developed by RSE S.p.A. will be presented.

Once the system model has been presented, the fourth chapter will be focused on the actual design of the secondary control layer. The prediction approach will be described and the implemented cost function and variable constraints will be discussed in details.

Starting from the designed hierarchical control structure, its performances will be analysed in the fifth chapter. Firstly, the microgrid test case, as well as its main elements, will be described. Then, the effectiveness of the defined control system will be shown through several simulations. Additional tests will be also performed, taking into account more realistic implementations and features of the designed control framework.

Finally, a chapter will cover some conclusive considerations about the treated control problem, showing also the additional features which could be investigated in future research developments.

Chapter 2

Primary Control

2.1 Islanding Issues

The Tellegen's theorem states that the sum of the generated, lost and absorbed power in an electrical network must be always equal to zero [16]. This is formalized in (2.1) and (2.2) by considering separately active (P) and reactive (Q) powers.

$$\sum_{k=1}^{n} P_k^{generated} \;+\; \sum_{k=1}^{n} P_k^{lost} \;+\; \sum_{k=1}^{n} P_k^{absorbed} \;=\; 0 \tag{2.1}$$

$$\sum_{k=1}^{n} Q_k^{generated} \;+\; \sum_{k=1}^{n} Q_k^{lost} \;+\; \sum_{k=1}^{n} Q_k^{absorbed} \;=\; 0 \tag{2.2}$$

where n corresponds to the number of nodes of the network [1].

In grid-connected mode this theorem is always valid since any unbalance between generated and absorbed power is compensated by an energy import or export from/to the main grid. On the other hand, the islanded operating mode becomes a critical situation for the absence of grid-connection and because generated and absorbed powers easily mismatch due to the intermittent and stochastic nature of most renewable sources.

It should be noted that the electrical power, especially if related to transmission losses and to loads, is not a fixed quantity but it depends on the network variables such as voltages (V), currents (I) and frequency (ω).

---

[1] An electrical network can be represented by a graph where nodes correspond to either generation or load units and branches correspond to the interconnections between utilities.

Because of this, it would be more correct to rewrite equations (2.1) and (2.2) as reported in (2.3) and (2.4), explicating the dependence of the powers from the network variables. Moreover, at steady state the whole network reaches a unique system frequency, therefore it is not defined as a nodal variable, like voltages, but it is a global variable. It is important to underline that, since lost powers are mainly related to line losses, they do not depend only on the electrical variables of their own node but they are defined from the voltages of all the interconnected nodes, as well as from the system frequency.

$$\sum_{k=1}^{n} P_k^{generated}(V_k, \omega) \; + \; \sum_{k=1}^{n} P_k^{lost}(V_1, ..., V_n, \omega) \; + \; \sum_{k=1}^{n} P_k^{absorbed}(V_k, \omega) \; = \; 0 \quad (2.3)$$

$$\sum_{k=1}^{n} Q_k^{generated}(V_k, \omega) \; + \; \sum_{k=1}^{n} Q_k^{lost}(V_1, ..., V_n, \omega) \; + \; \sum_{k=1}^{n} Q_k^{absorbed}(V_k, \omega) \; = \; 0 \quad (2.4)$$

The dependence between powers and network variables has a considerable impact on the management of an islanded microgrid. Since the Tellegen's theorem must always be verified, it happens that when an unbalance occurs, for example due to a sudden load peak, voltages and microgrid frequency naturally vary bringing the system to a new equilibrium condition where the sum of powers is again zero. However, depending on the size of the unbalance, microgrid voltages and frequency may largely deviate from their reference values, resulting in an equilibrium condition that is not allowed for the system correct operation. In low voltage grids (LV grids) the network variables have to respect some predefined limitations to not compromise the power quality, as well as to not damage microgrid physical devices.

The Italian Electrotechnical Committee (CEI) defined several regulations for power quality of low voltage networks [12]; however they are mostly related to microgrids in grid-connected mode since the islanding mode is quite a new concept. A norm that can be applied in the islanded case is the CEI 8-6 [13], that is related to the power quality of low voltage networks in real geographic islands; these in fact do not have a connection with the main grid if located too far from the shore. The defined requirements are:

$$f \; = \; 50 \text{ Hz} \; \pm \; 2\%$$
$$V \; = \; 400 \text{ V} \; \pm \; 10\%$$

where f corresponds to the microgrid frequency and V to the amplitude of the line-to-line voltage in three-phase interconnections. This means that the frequency can deviate only by 1 Hz around the nominal value, while line voltages are bounded between 440 V and 360 V.

14

Given the aforementioned issues, a primary control level is designed to limit the variables' deviations. Practically, this control layer consists in a decentralized structure that quickly modifies the generated power of each source so that the network power balance becomes feasible without making voltages and frequency reach values that are not allowed by the regulations. This primary control scheme is composed of two sub-layers: the inverter output control and the droop control.
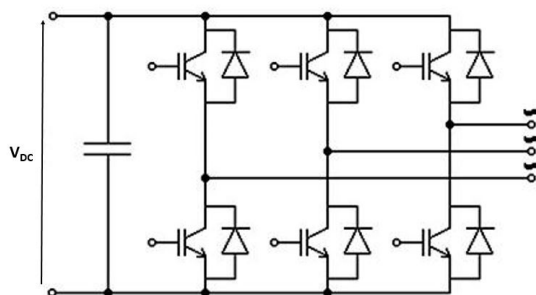
2.2 Inverter Output Control

Figure 2.1: Inverter simplified circuit

The inverter represents one of the most used power converters and it is designed to transform a DC power source into an AC one. Even though the literature provides a detailed description of its physical structure and control [14], it is not of interest for this work to go into a detailed explanation. To put it briefly, the inverter circuit consists in a series of switching valves and diodes (see Figure 2.1) that, through an accurate control, can generate a three-phase sinusoidal voltage waveform from a DC power source. Moreover, there are some configurations that implements also an AC/AC conversion through the sequence of an AC/DC stage and a DC/AC stage; in this way it is possible to decouple two distinct AC powers which can have different frequencies, as well as different voltage magnitudes.

Given the potentialities of these power converters, they will become fundamental devices for future microgrids. This is confirmed by the fact that some generation sources produce DC power, such as energy storage units and photovoltaics, while others, such as wind turbines, produce AC power that is not synchronous with the grid frequency. Moreover, this interface allows also to independently control the output power or voltage waveform of each source, based on the set-points imposed by the droop control. To accomplish this task, a series of cascade loops and modulation techniques are designed that act on the inverter switching valves in order to track the chosen output variable, such as the output voltage or current [14].

Depending on the selected controlled variable, two inverter control strategies can be adopted for distributed energy control: the Voltage Source Control (VSC) and the Current Source Control (CSC).

The Voltage Source Control aims to feed the grid with a predefined voltage waveform by imposing the output voltage magnitude and frequency. In this case, depending on the load power and on the power losses, the resulting generated active and reactive power are defined. The actual control is implemented with the d-q frame-based voltage controller and a inner current loop that tracks the predefined values of i_d^o and i_q^o [15].

As far as the Current Source Control is concerned, it has an opposite purpose since the inverters are controlled to provide predefined values of active and reactive powers (this configuration is also called PQ control). The inner control loop consists in a current and a voltage control loop that provide the values of i_d^o and i_q^o in order to generate the power values imposed by the droop control [17]. In this case, the inverter output voltage magnitude and frequency are not predefined but they come from the network power balance equations since, as stated before, the network variables will assume the values that ensure the validity of Tellegen's theorem.

Having decided whether the inverter is controlled as a voltage source or a current source, then another sub-layer needs to be designed.

2.3   Droop Control

The droop method is an efficient and simple decentralized control strategy. This layer, having no need of intercommunications with other units and being characterized by a proportional control action, ensures a rapid control action that minimizes power unbalances and consequently the system frequency and voltages. This is a relevant feature since, as stated in the first chapter, the inverter interface implies a low system inertia, resulting in fast dynamics that must be properly managed.

Although the droop proportional actions have not a unique definition, they are implemented such in order to link the network variables' deviations and the generated powers' deviations from their nominal values. In other words, this control layer varies a defined network variable, such as the inverter output frequency, based on the variation of another electrical variable, such as the actual generated active power. The dependency between the variables that motivates the control action will be furtherly discussed in the following paragraph.

2.3.1 Droop Relationships

There are three possible droop couplings: the resistive, the inductive and the mixed relationship.

- *Resistive*: The active power variation is linked to the nodal voltage one, while the reactive power variation to the network frequency one (P-V, Q-ω).

- *Inductive*: The active power variation is linked to network frequency one, while the reactive power variation to the nodal voltage one (P-ω, Q-V).

- *Mixed*: In this case both active and reactive power variations have an impact both on frequency and voltages; although this can express more realistic cases, this relationship is not very used given its complex definition.

The droop relationships are usually chosen based on the line impedances [18], and, in particular, the key factor is represented by the ratio between resistive and the inductive impedance of the line, known as the R/X factor. A network characterized by lines with small values of the R/X factor is said to have a mainly inductive characteristic and suggests to exploit, for the droop control, the active power - frequency and reactive power - voltage relationship. On the other hand, large values of the R/X factors result in stronger correlations between active power and voltage and between reactive power and frequency. Being the resistive characteristic is typical of small grid systems like the one considered in this work, the resistive droop relatioship will be considered.

Although a rigorous proof of the reasons why the resistive and the inductive relationship impose these precise links would be beyond the purpose of this work, a shorter intuitive explanation can be given considering the simple case reported in Figure 2.2.
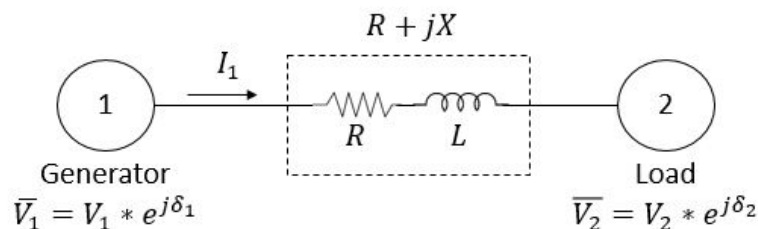

Figure 2.2: Simple electrical network

The network is composed of one generator and one load, interconnected through a line with a defined impedance. It is assumed that this AC network has already reached the steady state condition, therefore each variable has a sinusoidal waveform that pulsates at a steady-state frequency, $\bar{\omega}$. This allows to study the system in the phasor domain, where each voltage can be represented in the complex plane as a phase vector that rotates at the steady-state frequency [19], as reported in Figure 2.3.
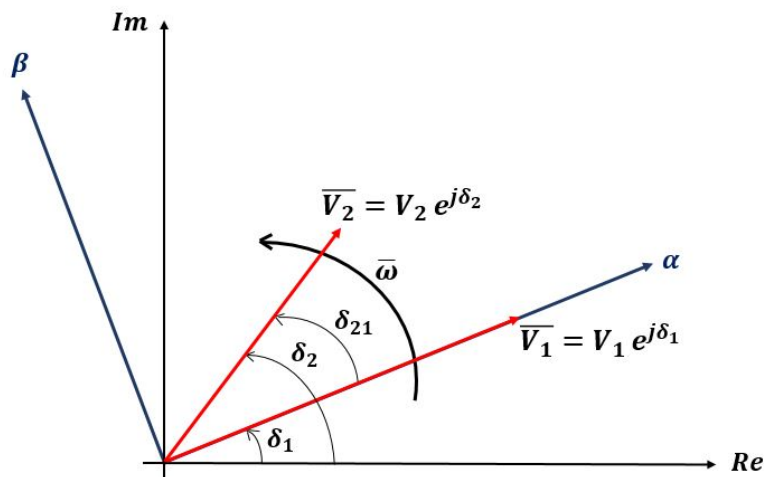

Figure 2.3: Phasor representation of nodal voltages

Node 1 is assumed to be the reference node, called also *slack node*. This means that all phase vectors are defined with respect to a new coordinate system (α, β), which is synchronous and aligned with $\bar{V}_1$. Therefore:

$$\bar{V}_1^{\alpha\beta} = V_1$$
$$\bar{V}_2^{\alpha\beta} = V_2\, e^{j\,\delta_{21}}$$

Given the nodal voltages and the line impedance, the line current can be easily computed:

$$\bar{I}_1^{\alpha\beta} = \frac{(\bar{V}_1^{\alpha\beta} - \bar{V}_2^{\alpha\beta})}{R + jX} = \frac{(V_1 - V_2\, cos(\delta_{21}) - j\, V_2\, sin(\delta_{21}))}{R + jX} =$$

$$= \frac{-R\, V_2\, cos(\delta_{21}) + R\, V_1 - X\, V_2\, sin(\delta_{21})}{R^2 + X^2} +$$
$$+ j\, \frac{X\, V_2\, cos(\delta_{21}) - X\, V_1 - R\, V_2\, sin(\delta_{21})}{R^2 + X^2}$$

Knowing both voltage and output current of Node 1, now it is possible to compute the complex delivered power:

$$S_1 \;=\; \bar{V_1}^{\alpha\beta} \cdot (\bar{I_1}^{\alpha\beta})^* \;=\; V_1 \, \frac{(R\,(V_1 \,-\, V_2\, cos(\delta_{21})) \,-\, X\, V_2\, sin(\delta_{21}))}{R^2 + X^2} \;+$$
$$+\, j\, V_1 \, \frac{(X\,(V_1 \,-\, V_2\, cos(\delta_{21})) \,+\, R\, V_2\, sin(\delta_{21}))}{R^2 + X^2}$$

Finally, the output active and reactive power are computed by considering separately the real and the imaginary part of the complex power:

$$P_1 \;=\; \mathrm{Re}(S_1) \;=\; V_1 \, \frac{(R\,(V_1 \,-\, V_2\, cos(\delta_{21})) \,-\, X\, V_2\, sin(\delta_{21}))}{R^2 + X^2}$$

$$Q_1 \;=\; \mathrm{Im}(S_1) \;=\; V_1 \, \frac{(X\,(V_1 \,-\, V_2\, cos(\delta_{21})) \,+\, R\, V_2\, sin(\delta_{21}))}{R^2 + X^2}$$

Starting from the expressions of the active and reactive generated power with the explicit dependence on the network variables, now it is possible to understand why the resistive and the inductive relationships have these precise links between powers, frequency and voltages. Considering first the inductive droop coupling: it is applied when the network R/X factor is very small. Therefore, by considering $X \gg R$ and by linearizing around $\delta_{21} \simeq 0$ (in a single line interconnection it can be assumed that voltages have nearly the same phase), we obtain:

$$P_1^{\,inductive} \;=\; -\,(\frac{V_2\, V_1\, X}{R^2 + X^2})\, \delta_{21} \qquad\qquad (2.5)$$

$$Q_1^{\,inductive} \;=\; V_1 \, \frac{(V_1 \,-\, V_2)\, X}{R^2 + X^2} \qquad\qquad (2.6)$$

While for a resistive network, where $R \gg X$, it results that:

$$P_1^{\,resistive} \;=\; V_1 \, \frac{(V_1 \,-\, V_2)\, R}{R^2 + X^2} \qquad\qquad (2.7)$$

$$Q_1^{\,resistive} \;=\; (\frac{V_2\, V_1\, R}{R^2 + X^2})\, \delta_{21} \qquad\qquad (2.8)$$

By looking to the equations (2.5) and (2.8), it is possible to see that an increment in the phase difference between the two nodes has an impact on the active

19

power in the inductive case and on the reactive power in the resistive case. Actually, the phase difference is strictly related to the frequency. An increase of δ_{21} means that V_2 waveform tends dynamically to anticipate the V_1 one, which in turn implies that the frequency of Node 2 tends to be higher with respect to Node 1 [20]. Therefore, in order to control the frequency, for inductive microgrids it is better to vary the generated active power, while for the resistive case it is better to act on the variation of reactive power.

Regarding the voltages, it should be noted that there is not a perfect decoupling since a voltage variation affects both the active and reactive powers. However, in some cases, such as in (2.6) and in (2.7), there is a squared dependence from the generation voltage V_1 and the relative power. Although the effects are not completely decoupled as for the frequency, in the inductive case the generation voltage is linked with the delivered reactive power, while in the resistive case the generated active power is usually used to control the nodal voltage.

The explained relationships are not perfectly decoupled; however, for the sake of simplicity the droop is always designed as it had separate effects on the different variables. This approximation is well accepted since the aim of droop control is not to perform a precise control action but only to allow the network to properly work without large deviations of variables.

Remark: For small scale networks it is not true that only line impedances have to be taken into account, but the whole system should be considered. Actually, since microgrids are characterized by short lines, load characteristics have a great impact on the relationships between network variables and generated powers. There are some loads, such as linear RLCs, that are characterized by a resistive coupling (P-V, Q-ω), while others, such as asynchronous rotating motors, show an inductive relationship (P-ω, Q-V). Depending on the prevailing load characteristics, the droop coupling should be chosen. Taking into account the experiments carried out in [20], it can be stated that the resistive relationship is the one that ensures the system stability for most types of microgrids. Actually, it is quite difficult to have a small-scale network characterized by a prevailing inductive characteristic, since it is not frequent to have rotating loads directly connected to the line but they are usually interfaced through inverters.

Having chosen the droop relationships that link the variations of powers to the variations of voltage and the frequency, there are however different droop control approaches. Although they all have the same objective, they are based on different control actions. In the following section a more detailed explanation is given.

2.3.2 Droop control strategies

Depending on the chosen controlled and control variables, two droop methods can be adopted: the Conventional and the Inverse Droop.

The *Conventional Droop* relies on a direct action since, through proportional gains, it varies directly the output voltage magnitude and frequency based on the variation of the delivered active and reactive power. This droop strategy is interfaced with inverters controlled as voltage sources (VSC). Indeed, as the droop layer defines the output voltage waveform, its magnitude and frequency are then sent as set-points to the inverter output control (see Figure 2.4).

On the contrary, the *Inverse Droop* control acts in an opposite way. It modifies the generated output power depending on the deviations of nodal voltage magnitude and frequency from their nominal values. This droop strategy is usually implemented together with Current Source Controlled inverters, since they are able to track active and reactive power set-points. As stated before, with this approach it is not possible to have a direct control on the voltages and on the microgrid frequency, but they will take the values that guarantee the power balance. A schematic representation of the Inverse Droop Control with resistive relationship is reported in Figure 2.5.
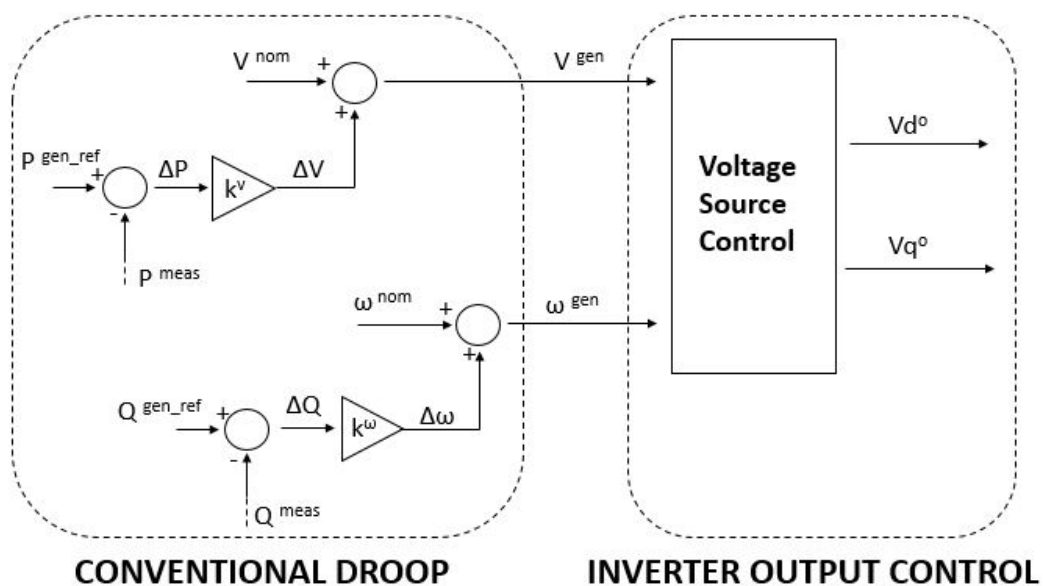

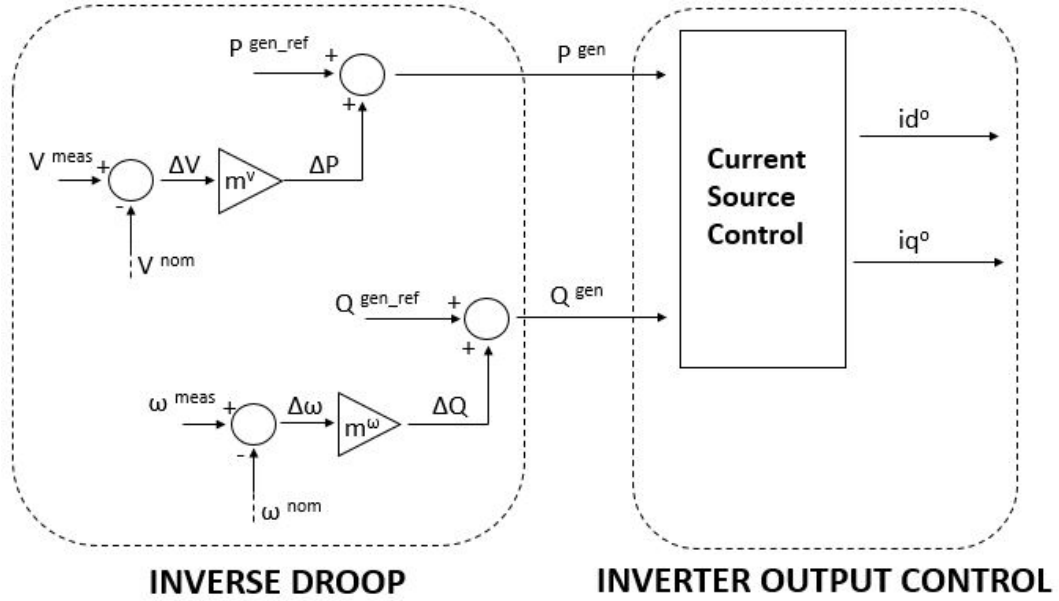
Figure 2.4: Conventional Resistive Droop

Figure 2.5: Inverse Resistive Droop

2.4   Primary control design

After this brief overview on the possible primary control structures, a description of the scheme considered in this work is now given.

It consists in a decentralized structure where at each generation node an Inverse Droop control is located, therefore all generation inverters are controlled as current sources. This implies that there is not a direct control of the network variables, but they will assume the values that make the power balance feasible. Moreover, the resistive relationship (P-V, Q-ω) is implemented since, as aforementioned, it allows the network stability for most types of loads.

Therefore, the output powers are defined by the droop control as:

$$P_j^{gen} \;=\; m_j^v * (V_i - V^{nom}) \;+\; P_j^{gen\_ref} \tag{2.9}$$

$$Q_j^{gen} \;=\; m_j^\omega * (\omega - \omega^{nom}) \;+\; Q_j^{gen\_ref} \tag{2.10}$$

where $j \in (1, \ldots, ncg)$, with ncg number of controllable generation units, $V^{nom} = 400\ V$ and $\omega^{nom} = 314.16\ rad/s$ (i.e. 50 Hz), while m_j^v and m_j^ω correspond to the droop proportional gains. Then, the final values of P_j^{gen} and Q_j^{gen} are sent to the inverter output control that is in charge of delivering the defined active and reactive generated powers.

Regarding the proportional gains, their definition is shown in Figure 2.6, where they correspond to the slopes of the droop characteristics.
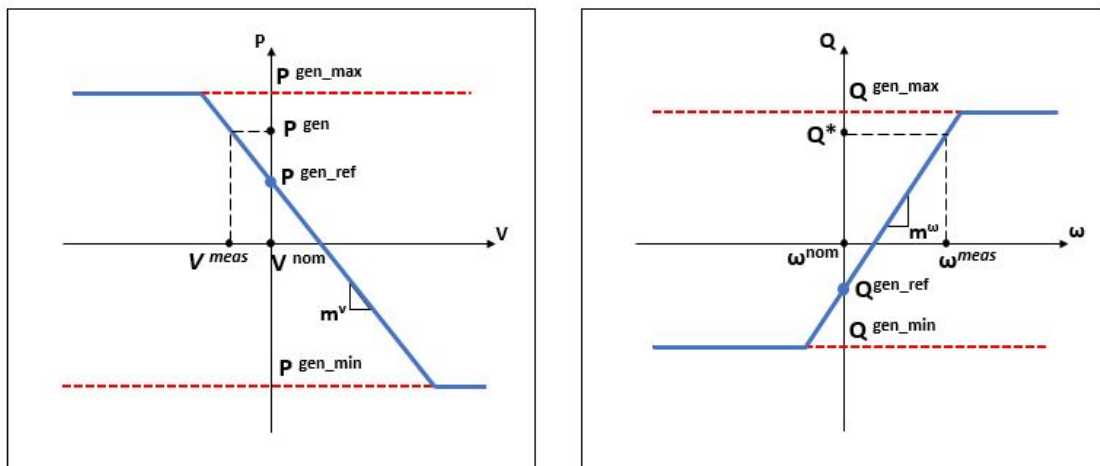
Figure 2.6: Implemented droop characteristics

It is worth noticing that the functions have not constant slopes. Indeed, generators have limited power capabilities and therefore for some values of frequency and voltage magnitude the output powers are saturated to their working limits.

The two droop functions have opposite effects on the outputs. On the one hand, the active power is decreased with the respect the reference value as the voltage deviation increases, while the reactive power offset is directly proportional to the frequency variation. An intuitive explanation of this choice can be given by considering a resistive network with a generator and a parallel RLC load (see Figure 2.7).

In order to study the network, the absorbed power is firstly computed. Since microgrids are characterized by short interconnections and loads represent the most relevant power absorption, power line losses are neglected.
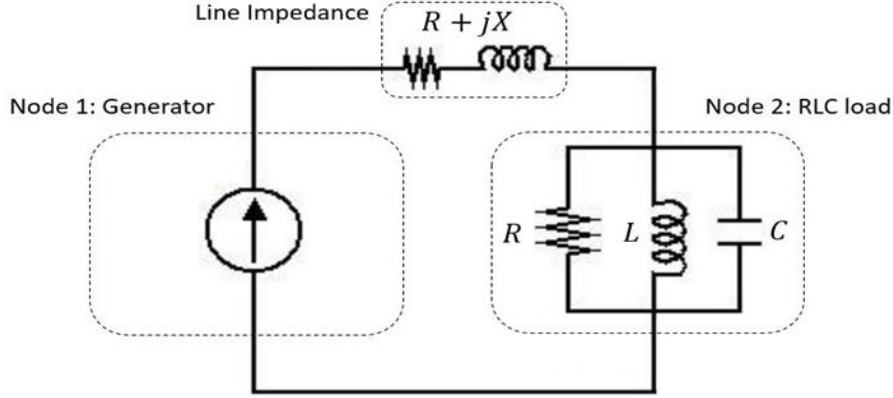
Figure 2.7: Simple network

$$Z \;=\; R \;+\; j\omega L \;+\; \frac{1}{j\omega C}$$

$$S^{load} \;=\; V^{load}\,(I^{load})^* \;=\; V^{load}\,\Big(\frac{V^{load}}{Z^*}\Big) \;=\; \frac{(V^{load})^2}{R} \;+\; j\,\Big(\frac{(V^{load})^2}{\omega L} \;-\; \omega C(V^{load})^2\Big)$$

$$P^{load} \;=\; Re\,(S^{load}) \;=\; \frac{(V^{load})^2}{R} \tag{2.11}$$

$$Q^{load} \;=\; Im\,(S^{load}) \;=\; \frac{(V^{load})^2}{\omega L} \;-\; \omega C(V^{load})^2 \tag{2.12}$$

Through the equations (2.11) and (2.12), it is possible to give an explanation of the droop characteristics shown in Figure 2.6. Taking into account firstly the active power, if a generation peak occurs, there will be an initial unbalance where the generated power exceeds the absorbed one ($P^{gen} > P^{load}$). Given the Tellegen's theorem, this will result in a voltage increase since it is the only way to raise the active absorbed power, as reported by equation (2.11). At steady-state, the condition $P^{gen} = P^{load}$ will be reached. However, if the initial difference between the generated and absorbed power is big, the voltage will largely deviate from its nominal value. To overcome this issue, it is needed to implement a control system that automatically decreases P^{gen} as the nodal voltage exceeds its nominal value. In this way in fact, the unbalance between absorbed and generated power will be reduced and therefore the final equilibrium condition can be reached without relying on a large voltage deviation. This is exactly how the designed droop control acts, as reported in the left graph of Figure 2.6. Indeed, if the voltage has a value beyond the nominal one, the generation active power is reduced with respect to its reference value.

The same reasoning can be carried out regarding reactive powers. Indeed, if an unbalance occurs so that $Q^{gen} > Q^{load}$, the absorbed reactive power need to be raised in order to fulfill the Tellegen's theorem. As reported by (2.12), an increment of Q^{load} can be achieved by a frequency drop. Also in this case, the reached equilibrium could not be allowed by the regulations or it can damage physical devices. Therefore, as the frequency goes down, the droop control decreases also the generated reactive power so that the power balance $Q^{gen} = Q^{load}$ can be reached without having a frequency large steady-state shift. This behavior is coherent with respect to the right graph in Figure 2.6, where reactive power and frequency shows a proportional relationship.

Although the adopted droop strategy has been justified in a simple case, it can be extended to a more structured microgrid equipped with many generators and loads. As reported in [20], the inverse resistive droop control implemented as in Figure 2.6 ensures the network stability for many types of loads, even though it does not impose a direct control on voltage magnitudes and frequency.

2.5 Conclusions

The designed primary control allows the system to properly work in islanded mode, even though power unbalances may occur. However, a control action based only on proportional gains does not ensure that the variables reach their nominal values [11], which is a desirable aspect especially for the frequency. Moreover, at this stage the droop active and reactive power references are fixed parameters (see Figure 2.6). It would be surely better to have an additional control system that efficiently varies the power references depending on the actual microgrid absorption.

Indeed in this way, power unbalances will be of limited size and consequently the variables' steady-state deviations will be reduced. Finally, relying only on a primary control layer, each source is independently controlled and so it is not possible to have a high-level coordination between sources. This would be a relevant feature since it allows to implement several strategies based either on economical reasons or on green energy-oriented policies.

All the mentioned issues can be overcome by a supervising control layer, implemented as a centralized secondary controller. Its control action would consist in shifting the droop characteristics by varying P^{gen_ref} and Q^{gen_ref} based on an optimization algorithm. This structure, if properly designed, can achieve relevant results in terms of network stability and efficient resource management.

Chapter 3

Microgrid Mathematical Model and Simulator

3.1 Introduction

The purpose of the secondary control is both to restore the network variables' deviations and to efficiently manage the microgrid energy flows. The chosen strategy is based on the Model Predictive Control approach (MPC), which is a control algorithm which performs a recursive optimization process over a predefined prediction horizon. As underlined in the previous chapter, this control will be designed to vary the power references of the controllable sources, taking into account the actual state of the network variables. Furthermore, since the network frequency is considered the most critical variable, an integrator has been placed between the frequency error and the centralized MPC controller, so ensuring zero static error.

In order to design the secondary control layer, the state-space model of the whole microgrid, including the primary layer, is needed. Before developing it, at the secondary stage the primary control dynamics have been considered to be always at steady state, therefore represented by the droop final static relationships. This is an acceptable assumption since the inverter interface allows to have relative small time constants. Moreover, since the primary layer reaches the steady-state condition in about 10 seconds and the centralized secondary control is based on a complex optimization algorithm, the variables' sampling time for the secondary layer can not be relatively small but it has to be at least one minute. The developed microgrid model has been chosen to be defined by a discrete time-based system, where the sampling time corresponds precisely to the discrete time step t_k.

By looking at Figure 3.1, it is possible to understand how the designed control system works. Actually, every t_k the network variables are sampled and the MPC algorithm starts its optimization process. After a computation time of few seconds τ_c, the optimization process ends and so the control actions are applied, which means that the MPC varies the reference powers of the droop functions. Then, the primary network layer starts its transient and it reaches the steady state condition in a settling time τ_n of some seconds. Recursively, at the next step the steady state variables' values are sampled and the MPC is performed again in order to the decide the next reference power variations. It should be noted that communication times between the different units are neglected, they are in fact relatively small with respect to the other time frames.
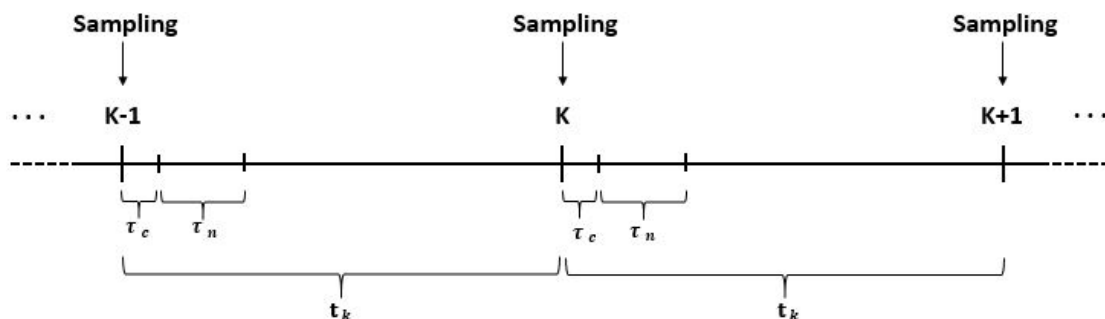

Figure 3.1: Time Discretization

Having defined the secondary control working behavior, now the actual model for the secondary control must be computed. The required model must have as outputs the network variables, such as voltages and frequency, while the active and reactive power references' variations correspond to the inputs. It should be noticed that the secondary layer can vary the power references only of fully controllable units, while some power references are externally imposed, such as loads' or renewable sources' power profiles. This implies that the final model will have the controllable generators' power reference variations as control inputs, while the imposed power reference variations are sent as external disturbances. The notation for inputs and disturbances is reported below.

$$
\text{Inputs:} \quad
\begin{cases}
(\Delta P_1^{gen\_ref},\ \Delta Q_1^{gen\_ref}) \\
\quad\vdots \\
(\Delta P_{ncg}^{gen\_ref},\ \Delta Q_{ncg}^{gen\_ref})
\end{cases}
\qquad
\text{Disturbances:} \quad
\begin{cases}
(\Delta P_1^{ext\_ref},\ \Delta Q_1^{ext\_ref}) \\
\quad\vdots \\
(\Delta P_n^{ext\_ref},\ \Delta Q_n^{ext\_ref})
\end{cases}
$$

27

where ncg corresponds to the number of controllable generation units, while the disturbances are modeled to be $2n$, defining the external power reference variation for each node (if a node is not affected by an imposed power variation, the relative disturbance will be always zero).

An overview of the overall control scheme, with a particular evidence of the system model that need be computed, is reported in Figure 3.2.
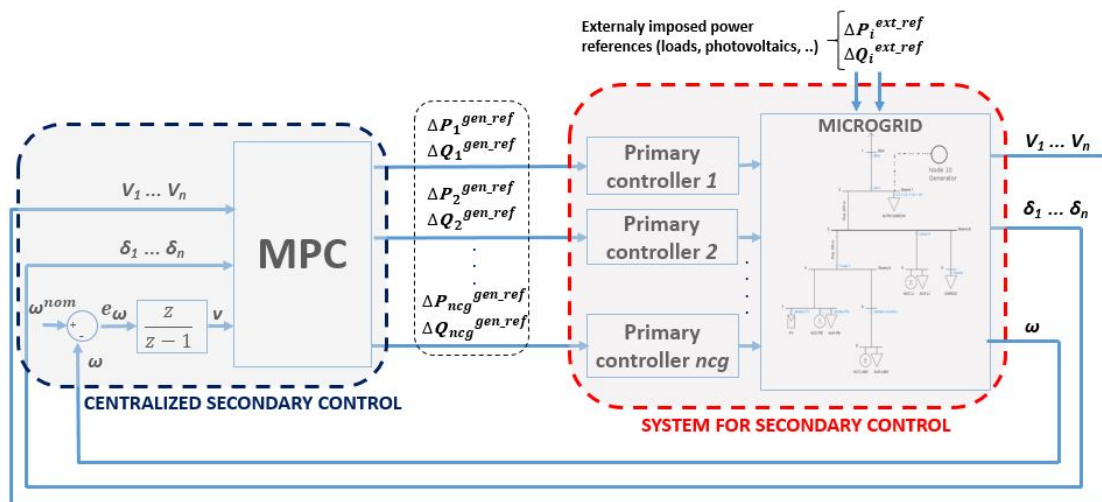

Figure 3.2: Hierarchical control block diagram

The developed system model will be based on the power flow analysis [1] adapted to an islanded network. To better understand its definition, a brief overview of the power flow theory is firstly given.

3.2 Power Flow

The purpose of this approach is to have a complete insight of the powers flowing out from each node in an AC grid system. Taking into account the case issued in this work, it corresponds to a steady-state network characterized by balanced three-phase interconnections. This means that the phasor approach can be adopted, which identifies for each node a single voltage waveform corresponding to the line to line voltage.

---

[1]Also known as "load flow" study

The voltages are represented with phase vectors, where the magnitude corresponds to the amplitude of the waveform, while the vector phase represents the phase shift with respect to the coordinate system aligned to the reference node, called *slack node*. This implies that the vector phase angle of the slack nodal voltage is always zero. When microgrids are in grid-connected mode, the reference node coincides the point of common coupling, while its location can be arbitrarily chosen in the islanded condition.

The first step to perform the power flow analysis is to define the microgrid physical characteristics and this is done through the *admittance matrix*. This matrix contains all the information regarding the network impedances, including the loads' and generators' ones. However, in this case the network characteristics are not expressed in terms of impendances but through the admittance concept, that is defined as the inverse of the impedance. The matrix construction is well explained and documented in the literature, coming from the theory of two-port networks [21].

Its final structure is:

$$[\mathbf{Y}]_{ij} = \begin{cases} y_{ii} + \sum_{k=1,\,k\neq i}^{n} y_{ik} & \text{if } j = i \\ -y_{ij} & \text{otherwise} \end{cases}$$

where, if $j \neq i$, y_{ij} represents the line admittance from node i to node j, otherwise if $j = i$, y_{ii} is referred to the nodal admittance of node i itself, for instance related to the presence of the load impedance. It is important to underline that, given the presence of the inductive and capacitive impedance, the line admittance has not a fixed value but it depends on the network frequency. This implies that, like powers, also the admittance matrix varies as network variables deviate.

Having defined the admittance matrix, it is possible to compute the explicit expression of the powers flowing out from each node. Being $\underline{\mathbf{V}}$ the vector of all nodal voltage phasors, $\underline{\mathbf{I}}$ the vector of all nodal output current ones and $\underline{\mathbf{S}}$ the vector of all nodal complex powers, the active and reactive powers are determined.

$$\underline{\mathbf{I}} = \underline{\mathbf{Y}} \, \underline{\mathbf{V}}$$
$$\underline{\mathbf{S}} = \underline{\mathbf{V}} \, \underline{\mathbf{I}}^*$$

$$\underline{\mathbf{P}}^{\mathbf{T}} = Re(\underline{\mathbf{S}})$$
$$\underline{\mathbf{Q}}^{\mathbf{T}} = Im(\underline{\mathbf{S}})$$

After performing all calculations, the vectors $\underline{\mathbf{P}}^{\mathbf{T}}$ and $\underline{\mathbf{Q}}^{\mathbf{T}}$ result to be:

$$P_i^T\,(V_{(1...n)},\,\delta_{(1...n)},\,\omega)\;=\;V_i\sum_{j=1}^{n}\;[\,V_j*(\mathrm{Re}(Y_{ij}(\omega))*cos(\delta_i-\delta_j)\;+$$

$$+\;\mathrm{Im}(Y_{ij}(\omega))*sin(\delta_i-\delta_j)\,]\qquad\qquad(3.1)$$

$$Q_i^T\,(V_{(1...n)},\,\delta_{(1...n)},\,\omega)\;=\;V_i\sum_{j=1}^{n}\;[\,V_j*(\mathrm{Re}(Y_{ij}(\omega))*sin(\delta_i-\delta_j)\;+$$

$$-\;\mathrm{Im}(Y_{ij}(\omega))*cos(\delta_i-\delta_j)\,]\qquad\qquad(3.2)$$

Through these equations and by knowing the steady-state values of frequency, phase angles and voltages, it is possible to have an exact evaluation of powers flowing in the considered network.

In an electrical network, each node can be characterized by the presence either of a controllable generation unit, e.g. a battery, or of an uncontrollable one, e.g. a load. By defining the power balance at each node, it follows that the active flowing out power is equal to the difference between the active power injected by a controllable generation unit (P^{gen}) and the active power absorbed by an uncontrollable one (P^{ext}), as depicted in Figure 3.3.
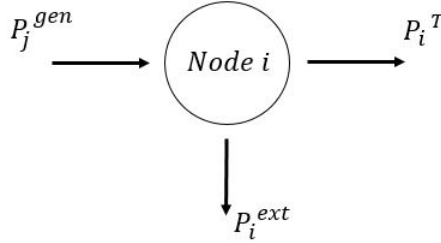

Figure 3.3: Nodal Power Balance

Looking to the above figure, P_j^{gen} corresponds to the active power that the j_{th} generator injects on the i_{th} node. It is assumed that a generator can provide power only to the node where it is placed. On the other hand, P_i^{ext} represents the active power that is absorbed or generated by an uncontrollable unit and it is modeled for each i_{th} node. Obviously, if the i_{th} node is not characterized by the presence of an external power disturbance, the relative P_i^{ext} will be zero. The above described reasoning holds also for the reactive powers.

Putting the nodal balance into equations, it results that for each node i the following equations hold:

$$\begin{cases} P_i^T \left(V_{(1...n)}, \, \delta_{(1...n)}, \, \omega\right) & = & P_j^{gen} \left(V_i, \, \omega\right) \, - \, P_i^{ext} \left(V_i, \, \omega\right) \\ Q_i^T \left(V_{(1...n)}, \, \delta_{(1...n)}, \, \omega\right) & = & Q_j^{gen} \left(V_i, \, \omega\right) \, - \, Q_i^{ext} \left(V_i, \, \omega\right) \end{cases} \qquad (3.3)$$

As aforementioned, by applying the power flow analysis to the islanded microgrid case, it is possible to develop a system model that, taking as inputs the reference nodal powers, gives the network voltages, phase angles and frequency. This will be described in the next section.

3.3 Network Model

The first step to develop the network model is to define all the nodal powers as the sum of a constant quantity (i.e. the reference nodal power) plus a variation due to the impact that the nodal voltages and the frequency have on the related power. This is a true assumption both for generators, where the droop control introduces a power variation because of network variables' deviations, and for loads, since in most cases loads show a dependence between the absorbed power and the network variables, as discussed in paragraph 2.4.

Therefore, for each generator it follows that:

$$\begin{cases} P_j^{gen} \left(V_i, \, \omega\right) & = & P_j^{gen\_ref} & + & \Delta P_j^{gen}(V_i, \omega) \\ Q_j^{gen} \left(V_i, \, \omega\right) & = & Q_j^{gen\_ref} & + & \Delta Q_j^{gen}(V_i, \omega) \end{cases} \qquad (3.4)$$

With regard to the externally imposed powers (such as loads and renewable sources), since they have been modeled for each node, the same equations can be specified.

$$\begin{cases} P_i^{ext} \left(V_i, \, \omega\right) & = & P_i^{ext\_ref} & + & \Delta P_i^{ext}(V_i, \omega) \\ Q_i^{ext} \left(V_i, \, \omega\right) & = & Q_i^{ext\_ref} & + & \Delta Q_i^{ext}(V_i, \omega) \end{cases} \qquad (3.5)$$

31

By putting together (3.3), (3.4) and (3.5), the following holds:

$$\begin{cases} P_j^{gen\_ref} - P_i^{ext\_ref} &= P_i^T\ (V_{(1...n)},\ \delta_{(1...n)},\ \omega)\ -\ \Delta P_j^{gen}(V_i,\omega) - \Delta P_i^{ext}(V_i,\omega) \\ Q_j^{gen\_ref} - Q_i^{ext\_ref} &= Q_i^T\ (V_{(1...n)},\ \delta_{(1...n)},\ \omega)\ -\ \Delta Q_j^{gen}(V_i,\omega) - \Delta Q_i^{ext}(V_i,\omega) \end{cases}$$

For the sake of simplicity, from now on, single active and reactive power reference P_i^{ref}, Q_i^{ref} are defined for each node. If in the same node both a generator and a load are present, the overall power references will be defined as the difference between the generated and the externally imposed reference power.

Therefore, equations (3.6) follow, which actually express how the nodal reference power are linked to the network variables.

$$\begin{cases} P_i^{ref} &= P_i^T\ (V_{(1...n)},\ \delta_{(1...n)},\ \omega)\ -\ \Delta P_j^{gen}(V_i,\omega) - \Delta P_i^{ext}(V_i,\omega) \\ Q_i^{ref} &= Q_i^T\ (V_{(1...n)},\ \delta_{(1...n)},\ \omega)\ -\ \Delta Q_j^{gen}(V_i,\omega) - \Delta Q_i^{ext}(V_i,\omega) \end{cases} \tag{3.6}$$

It should be noted that the above equations are $2n$, where n corresponds to the number of nodes of the network. Regarding the variables, the number of considered phase angles is $(n-1)$ since the slack node phase is always zero. Therefore, with n nodal voltages, $(n-1)$ phase angles and 1 microgrid frequency, $2n$ network variables can be identified.

Given the expressions of flowing powers in (3.1) and (3.2), the equations (3.6) are obviously nonlinear. It is recalled that the developed network model will be fundamental for the secondary control layer to perform the optimization process; moreover, the base formulation of the MPC approach is referred to linear models. To overcome this issue, the secondary controller will sample the steady-state values of the network variables at each control iteration and it will perform a linearization process so that a linear model is obtained. By considering the steady-state values of the network variables as the actual equilibrium point $\bar{x} = (\bar{V}_1,\ ...,\ \bar{V}_n,\ \bar{\delta}_2,\ ...,\ \bar{\delta}_n,\ \bar{\omega})$, the equations (3.6) can be actually linearized through through a first-order Taylor series approximation.

$$\begin{cases} \Delta P_i^{ref} &= (\ \frac{\partial}{\partial \underline{V}} P_i^{ref}\ )^t \Big|_{\bar{x}} \Delta \underline{V}\ +\ (\ \frac{\partial}{\partial \underline{\delta}} P_i^{ref}\ )^t \Big|_{\bar{x}} \Delta \underline{\delta}\ +\ (\ \frac{\partial}{\partial \omega} P_i^{ref}\ )^t \Big|_{\bar{x}} \Delta \omega \\[2em] \Delta Q_i^{ref} &= (\ \frac{\partial}{\partial \underline{V}} Q_i^{ref}\ )^t \Big|_{\bar{x}} \Delta \underline{V}\ +\ (\ \frac{\partial}{\partial \underline{\delta}} Q_i^{ref}\ )^t \Big|_{\bar{x}} \Delta \underline{\delta}\ +\ (\ \frac{\partial}{\partial \omega} Q_i^{ref}\ )^t \Big|_{\bar{x}} \Delta \omega \end{cases} \tag{3.7}$$

In equation (3.7), $\Delta\underline{V} = (\Delta V_1, ..., \Delta V_n)$, $\Delta\underline{\delta} = (\Delta\delta_2, ..., \Delta\delta_n)$, and $\Delta\omega$ correspond to the variations of the network variables with respect to the equilibrium point $\bar{x}$. On the other hand, ΔP_i^{ref} and ΔQ_i^{ref} expresses the reference power variations with respect to $\bar{P}_i^{ref}$ and $\bar{Q}_i^{ref}$, which in turns correspond to the nodal reference powers at the equilibrium point.

Expressing equations (3.7) in matrix form, it follows:

$$
\begin{bmatrix} \Delta P_1^{ref} \\ \vdots \\ \Delta P_n^{ref} \\ \Delta Q_1^{ref} \\ \vdots \\ \Delta Q_n^{ref} \end{bmatrix} = \begin{bmatrix} \left(\frac{\partial P_i^{ref}}{\partial \underline{V}}\right)\Big|_{\bar{x}} & \left(\frac{\partial P_i^{ref}}{\partial \underline{\delta}}\right)\Big|_{\bar{x}} & \left(\frac{\partial P_i^{ref}}{\partial \omega}\right)\Big|_{\bar{x}} \\ & & \\ \left(\frac{\partial Q_i^{ref}}{\partial \underline{V}}\right)\Big|_{\bar{x}} & \left(\frac{\partial Q_i^{ref}}{\partial \underline{\delta}}\right)\Big|_{\bar{x}} & \left(\frac{\partial Q_i^{ref}}{\partial \omega}\right)\Big|_{\bar{x}} \end{bmatrix} \begin{bmatrix} \Delta V_1 \\ \vdots \\ \Delta V_n \\ \Delta \delta_2 \\ \vdots \\ \Delta \delta_n \\ \Delta \omega \end{bmatrix}
$$

The matrix containing all the power derivatives, called network *Jacobian* (J), must be evaluated at the actual equilibrium point $\bar{x}$. This implies that it is not a fixed matrix but it changes at each time step, depending on the reached steady-state equilibrium for the primary dynamic.

The model requested for the designing of the secondary controller must have the network variables as outputs and the reference powers as inputs. Since we are dealing with a $(2n \times 2n)$ matrix, an inversion can be performed so that the network variables are computed based on the reference power variations.

$$
\begin{bmatrix} \Delta V_1 \\ \vdots \\ \Delta V_n \\ \Delta \delta_2 \\ \vdots \\ \Delta \delta_n \\ \Delta \omega \end{bmatrix} = \begin{bmatrix} \left(\frac{\partial P_i^{ref}}{\partial \underline{V}}\right)\Big|_{\bar{x}} & \left(\frac{\partial P_i^{ref}}{\partial \underline{\delta}}\right)\Big|_{\bar{x}} & \left(\frac{\partial P_i^{ref}}{\partial \omega}\right)\Big|_{\bar{x}} \\ & & \\ \left(\frac{\partial Q_i^{ref}}{\partial \underline{V}}\right)\Big|_{\bar{x}} & \left(\frac{\partial Q_i^{ref}}{\partial \underline{\delta}}\right)\Big|_{\bar{x}} & \left(\frac{\partial Q_i^{ref}}{\partial \omega}\right)\Big|_{\bar{x}} \end{bmatrix}^{-1} \begin{bmatrix} \Delta P_1^{ref} \\ \vdots \\ \Delta P_n^{ref} \\ \Delta Q_1^{ref} \\ \vdots \\ \Delta Q_n^{ref} \end{bmatrix}
$$

At this stage, a static relationship between the reference power variations and the network variables ones with respect to the equilibrium point is obtained. Since the variation of the reference power implemented by the secondary controller has an effect on the network variables and since the consequent steady-state values will be sampled at the next time step, the discretized model is formulated by considering a 1-step shift between the cause and the effect.

Therefore it becomes:

$$
\begin{bmatrix} \Delta V_1(k+1) \\ \vdots \\ \Delta V_n(k+1) \\ \Delta \delta_2(k+1) \\ \vdots \\ \Delta \delta_n(k+1) \\ \Delta \omega(k+1) \end{bmatrix} = \begin{bmatrix} \left(\frac{\partial P_i^{ref}}{\partial \underline{V}}\right)\bigg|_{\bar{x}(k)} & \left(\frac{\partial P_i^{ref}}{\partial \underline{\delta}}\right)\bigg|_{\bar{x}(k)} & \left(\frac{\partial P_i^{ref}}{\partial \omega}\right)\bigg|_{\bar{x}(k)} \\ & & \\ & & \\ \left(\frac{\partial Q_i^{ref}}{\partial \underline{V}}\right)\bigg|_{\bar{x}(k)} & \left(\frac{\partial Q_i^{ref}}{\partial \underline{\delta}}\right)\bigg|_{\bar{x}(k)} & \left(\frac{\partial Q_i^{ref}}{\partial \omega}\right)\bigg|_{\bar{x}(k)} \end{bmatrix}^{-1} \begin{bmatrix} \Delta P_1^{ref}(k) \\ \vdots \\ \Delta P_n^{ref}(k) \\ \Delta Q_1^{ref}(k) \\ \vdots \\ \Delta Q_n^{ref}(k) \end{bmatrix}
$$

where

$$
\begin{cases} \Delta V_i(k+1) & = V(k+1) - V(k) \\ \Delta \delta_i(k+1) & = \delta(k+1) - \delta(k) \\ \Delta \omega(k+1) & = \omega(k+1) - \omega(k) \end{cases} \qquad \begin{cases} \Delta P_i^{ref}(k) & = P_i^{ref}(k) - P_i^{ref}(k-1) \\ \Delta Q_i^{ref}(k) & = Q_i^{ref}(k) - Q_i^{ref}(k-1) \end{cases}
$$

and $\bar{x}(k)$ corresponds to the primary steady-state values of network variables at time step k.

By computing the inverse of the Jacobian, the linearized system model dynamics can be obtained.

$$
\begin{cases} V_1(k+1) & = V_1(k) + \alpha_{(1,1)}(k)\,\Delta P_1^{ref}(k) + \dots + \alpha_{(1,2n)}(k)\,\Delta Q_n^{ref}(k) \\ \vdots \\ V_n(k+1) & = V_n(k) + \alpha_{(n,1)}(k)\,\Delta P_1^{ref}(k) + \dots + \alpha_{(n,2n)}(k)\,\Delta Q_n^{ref}(k) \\ \delta_2(k+1) & = \delta_2(k) + \alpha_{(n+1,1)}(k)\,\Delta P_1^{ref}(k) + \dots + \alpha_{(n+1,2n)}(k)\,\Delta Q_n^{ref}(k) \\ \vdots \\ \delta_n(k+1) & = \delta_n(k) + \alpha_{(2n-1,1)}(k)\,\Delta P_1^{ref}(k) + \dots + \alpha_{(2n-1,2n)}(k)\,\Delta Q_n^{ref}(k) \\ \omega(k+1) & = \omega(k) + \alpha_{(2n,1)}(k)\,\Delta P_1^{ref}(k) + \dots + \alpha_{(2n,2n)}(k)\,\Delta Q_n^{ref}(k) \end{cases}
$$

where $\alpha_{i,j}(k)$ corresponds to the (i,j) element of inverted Jacobian, $J^{-1}(k)$.

It is recalled that not all power references are imposed by the secondary control but some of them come from load powers or undeterministic renewable energy sources. The uncontrollable power references are modeled as external disturbances, considered as known if power profiles are assumed to be available.

Therefore, the model can be written in the standard state-space form as follows:

$$\underline{x}(k+1) = A\,\underline{x}(k)\ +\ B(k)\,\Delta\underline{u}(k)\ +\ M(k)\,\Delta\underline{d}(k) \tag{3.8}$$

where

$$\underline{x}\ =\ \begin{bmatrix} V_1 \\ \vdots \\ V_n \\ \delta_2 \\ \vdots \\ \delta_n \\ \omega \end{bmatrix} \qquad A\ =\ \begin{bmatrix} 1 & & & \\ & \cdot & & \\ & & \cdot & \\ & & & \cdot \\ & & & & 1 \end{bmatrix}$$

while $B(k)$ corresponds to a proper partition of $J^{-1}(k)$, depending on where controllable units ($\Delta\underline{u}(k)$) are placed in the network, and $M(k)$ is exactly equal to $J^{-1}(k)$, since the vector $\Delta\underline{d}(k)$ represents the reference power external disturbances for each node of the network. In the case a certain node is not affected by an external imposed power, the relative $\Delta d_i(k)$ is always zero.

3.4 Models of the components

The network power model has been determined. However, all system components must be modelled in order to have a complete description of the microgrid dynamics.

3.4.1 Frequency Integrator

As previously mentioned, an integrator, taking as input the frequency primary steady-state deviation, is implemented. Therefore, this system introduces an additional state variable to be considered, that is the integrator output v.
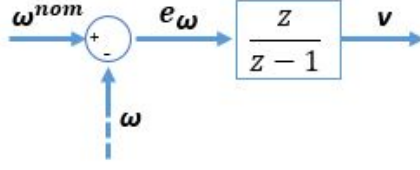
Figure 3.4: Frequency Integrator

Taking into account Figure 3.4, the integrator dynamics can be easily computed through the Z-transform [11].

$$V(z) = \frac{z}{z-1}E_\omega(z)$$

Therefore, it follows:

$$(z-1)\,V(z) = z\,E_\omega(z)$$
$$v(k+1) = v(k) + e_\omega(k+1)$$
$$v(k+1) = v(k) + \omega^{nom} - \omega\,(k+1)$$
$$v(k+1) = v(k) + \omega^{nom} - (\,\omega\,(k) + B_\omega(k)\,\Delta\underline{u}(k) + M_\omega(k)\,\Delta\underline{d}(k)\,)$$

$$v(k+1) = v(k) - \omega\,(k) - B_\omega(k)\,\Delta\underline{u}(k) - M_\omega(k)\,\Delta\underline{d}(k) + \omega^{nom} \qquad (3.9)$$

where $B_\omega(k)$ and $M_\omega(k)$ correspond to the partitions of $J(k)^{-1}$ related to the frequency dynamics (last row of the Jacobian matrix). Moreover, the reference frequency ω^{nom} is included in the disturbance vector $\Delta\underline{d}(k)$ since it is not a input decided by the secondary control.

The actual network model is then augmented with respect to its original formulation. Hence, by inserting equation (3.9) into (3.8), it results:

$$\underline{\tilde{x}}(k+1) = \tilde{A}\,\underline{\tilde{x}}(k) + \tilde{B}(k)\,\Delta\underline{u}(k) + \tilde{M}(k)\,\Delta\underline{\tilde{d}}(k) \qquad (3.10)$$

where

$$
\tilde{\underline{x}} \;=\; \begin{bmatrix} V_1 \\ \vdots \\ V_n \\ \delta_2 \\ \vdots \\ \delta_n \\ \omega \\ \hdashline v \end{bmatrix}
\qquad
\Delta\underline{u} \;=\; \begin{bmatrix} \Delta P_1^{gen\_ref} \\ \vdots \\ \Delta P_{ncg}^{gen\_ref} \\ \Delta Q_1^{gen\_ref} \\ \vdots \\ \Delta Q_{ncg}^{gen\_ref} \end{bmatrix}
\qquad
\Delta\tilde{\underline{d}} \;=\; \begin{bmatrix} \Delta P_1^{ext\_ref} \\ \vdots \\ \Delta P_n^{ext\_ref} \\ \Delta Q_1^{ext\_ref} \\ \vdots \\ \Delta Q_n^{ext\_ref} \\ \hdashline \omega^{nom} \end{bmatrix}
$$

and

$$
\tilde{A} \;=\; \left[\begin{array}{ccc:c} & & & 0 \\ & A & & \vdots \\ & & & 0 \\ \hdashline 0 & \dots & -1 & 1 \end{array}\right]
\qquad
\tilde{B}(k) \;=\; \left[\begin{array}{ccccc} b_{1,1}(k) & . & . & . & b_{1,2ncg}(k) \\ . & . & & & . \\ . & & . & & . \\ . & & & . & . \\ b_{n,1}(k) & . & . & . & b_{n,2ncg}(k) \\ \hdashline -b_{n,1}(k) & . & . & . & -b_{n,2ncg}(k) \end{array}\right]
$$

$$
\tilde{M}(k) \;=\; \left[\begin{array}{cccc:c} m_{1,1}(k) & . & . & m_{1,2n}(k) & 0 \\ . & . & & . & . \\ . & & . & . & . \\ . & & . & . & . \\ m_{n,1}(k) & . & . & m_{n,2n}(k) & 0 \\ \hdashline -m_{n,1}(k) & . & . & -m_{n,2n}(k) & 1 \end{array}\right]
$$

3.4.2 Batteries

Regarding the microgrid storage units, it can be assumed that they have an instantaneous power dynamics since the inverter time constants are negligible for the secondary control time frame. The presence of batteries add however additional dynamics related to their states of charge (SOC), which are function of the battery active power.

The SOC dynamics have been chosen to be modeled by discrete integrator systems [22]. To better understand their dynamical behavior, the time discretization is depicted again in Figure 3.5.
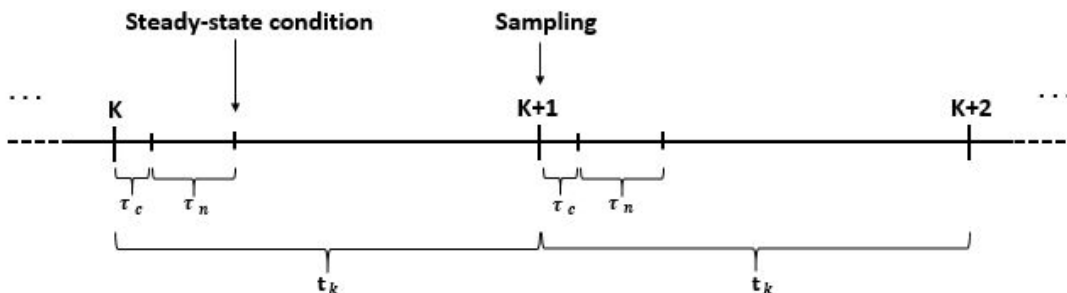

Figure 3.5: Time Discretization (SOC)

The battery integrator model implies that the SOC at $t = (k+1)$ corresponds to the SOC at $t = k$ plus a charge/discharge variation due to the active power that the battery generated between $t = k$ and $t = (k+1)$. Looking at Figure 3.5, since $(\tau_c + \tau_n) << t_k$, it can be assumed that the delivered power between the two time steps coincides with the active power that the battery delivers as the steady-state condition is reached, therefore at $t = (k + \tau_c + \tau_n)$. However, since the steady-state values are sampled at $t = (k+1)$, the steady-state power is conventionally defined as $P^{gen}(k+1)$ instead of $P^{gen}(k + \tau_c + \tau_n)$.

Therefore, taking into account the integrator battery model, the SOC dynamics can be expressed as:

$$SOC_b(k+1) \; = \; SOC_b(k) \; - \; \xi_b * \frac{\tau_s}{60 * C_b^{tot}} * P_j^{gen}(k+1) \qquad (3.11)$$

where

$$\begin{aligned}
\xi_b & \quad : \text{ Charge/Discharge coefficient} \\
\tau_s & \quad : \text{ Sampling time [min]} \\
C_b^{tot} & \quad : \text{ Total battery capacity [kWh]} \\
P_j^{gen}(k+1) & \quad : \text{ Active generated power, positive if delivered}
\end{aligned}$$

$b \in (1...nb)$, where nb corresponds to the number of batteries in the microgrid, and $j \in (1, \; ... \; , ncg)$ represents the number of the controllable generator corresponding to the b_{th} battery.

38

The SOC dynamics need to be added to the microgrid model so that they can be taken into account by the secondary control layer to perform an efficient resource management. However, the actual defined SOC model does not represent a proper discrete dynamic since there is not a time shift between the final SOC and the relative delivered power. Moreover, at this stage the generated powers are unknown quantities since they are neither an input nor an output, but internal variables of the system. Although the secondary scheme sets the power references for the primary layer, the droop control then modifies the generated power based on the network variables' deviation. In order to add the SOCs to the state vector $\tilde{\underline{x}}$, the generated power dynamics must be previously defined.

Generated Powers Discrete Model

The generated active and reactive powers correspond to the sum of the actual power reference plus the variation given by the droop primary control. This means that it can be written as:

$$P_j^{gen}(k+1) \; = \; P_j^{gen\_ref}(k+1) \; + \; \Delta P_j^{droop}(k+1)$$
$$Q_j^{gen}(k+1) \; = \; Q_j^{gen\_ref}(k+1) \; + \; \Delta Q_j^{droop}(k+1)$$

In this case, since the resistive inverse droop has been applied, $\Delta P_j^{droop}(k+1)$ will depend on the voltage deviation with respect to the nominal value, while $\Delta Q_j^{droop}(k+1)$ on the microgrid frequency one.

Therefore:

$$P_j^{gen}(k+1) \; = \; P_j^{gen\_ref}(k+1) \; + \; m_j^v(k+1) * (V_i(k+1) \; - \; V^{nom}) \qquad (3.12)$$
$$Q_j^{gen}(k+1) \; = \; Q_j^{gen\_ref}(k+1) \; + \; m_j^\omega(k+1) * (\omega(k+1) \; - \; \omega^{nom}) \qquad (3.13)$$

where i corresponds to the node where the j_{th} generator is placed.

In order to obtain the generated power dynamics, the state-space equations should be found so that it is possible to know the $P_j^{gen}(k+1)$ and $Q_j^{gen}(k+1)$ given the information at the time step k. Starting with the reference powers $P_j^{gen\_ref}(k+1)$ and $Q_j^{gen\_ref}(k+1)$, they are defined by pretty simple equations since the reference power at $(k+1)$ corresponds to the reference powers at the time step k plus the variation that the secondary control decided to implement.

Hence:

$$P_j^{gen\_ref}(k+1) \; = \; P_j^{gen\_ref}(k) \; + \; \Delta P_j^{gen\_ref}(k) \tag{3.14}$$

$$Q_j^{gen\_ref}(k+1) \; = \; Q_j^{gen\_ref}(k) \; + \; \Delta Q_j^{gen\_ref}(k) \tag{3.15}$$

In equations (3.11) and (3.12) the variables $V_i(k+1)$ and $\omega(k+1)$ can be substituted with the dynamics defined in paragraph 3.3. Regarding the droop parameters, it can be assumed that $m_j^v(k+1) = m_j^v(k)$ and $m_j^\omega(k+1) = m_j^\omega(k)$ since the droop functions have been implemented with constant slopes. Therefore, (3.11) and (3.12) become:

$$P_j^{gen}(k+1) \; = \; P_j^{gen\_ref}(k) \; + \; \Delta P_j^{gen\_ref}(k) \; + \; m_j^v(k) * (V_i(k) + B_{V_i}(k)\,\Delta \underline{u}(k) \; +$$
$$+ \; M_{V_i}(k)\,\Delta \underline{d}(k) \; - \; V^{nom}) \tag{3.16}$$

$$Q_j^{gen}(k+1) \; = \; Q_j^{gen\_ref}(k) \; + \; \Delta Q_j^{gen\_ref}(k) \; + m_j^\omega(k) * (\omega(k) + B_\omega(k)\,\Delta \underline{u}(k) \; +$$
$$+ \; M_\omega(k)\,\Delta \underline{d}(k) \; - \; \omega^{nom}) \tag{3.17}$$

From the equations (3.16) and (3.17), now it is possible to easily derive the state-space equations since V^{nom} and ω^{nom} can be identified as known disturbances, while the remaining variables are either states or inputs.

Having defined the generated power dynamics, by putting equation (3.16) into (3.11), it results:

$$SOC_b(k+1) \; = \; SOC_b(k) \; - \; \xi_b * \frac{\tau_s}{60 * C_b^{tot}} * (\; P_j^{gen\_ref}(k) \; + \; \Delta P_j^{gen\_ref}(k) \; +$$
$$+ \; m_j^v(k) * (V_i(k) + B_{V_i}(k)\,\Delta \underline{u}(k) \; + M_{V_i}(k)\,\Delta \underline{d}(k) \; - \; V^{nom})\,) \tag{3.18}$$

Now, the SOC dynamics can be added to the whole model since they are expressed through a discrete model where all variables are either inputs or states, all known at $t = k$.

Remark: It should be noted that the obtained generated power dynamics might not be realistic in some circumstances. Firstly, it is not always true that $m_j^v(k+1) = m_j^v(k)$ and $m_j^\omega(k+1) = m_j^\omega(k)$, since, if the powers reach their limits, the droop function slope becomes zero (see paragraph 2.4); this means that there could be some instants where $m_j^v(k+1) \neq m_j^v(k)$ or $m_j^\omega(k+1) \neq m_j^\omega(k)$. On the other hand, the network model is based on a linearization process and therefore the variables that the model computes at $t = (k+1)$ might have a slightly different value from the real ones; indeed the linearized model at time $t = k$ is valid only in the neighborhood of the system equilibrium point.

However, in spite of these approximations, these equations allow the secondary controller to have a good estimation of the effective generated power after the action of the primary control, which is fundamental to estimate the charge or discharge of the batteries.

By properly putting together all the analysed dynamics, it is possible to derive a final state-space equation that takes into account both the network variables, the generated powers and the batteries' SOCs.

This is defined as:

$$\tilde{\tilde{\underline{x}}}(k+1) = \tilde{\tilde{A}}(k)\,\tilde{\tilde{\underline{x}}}(k) \; + \; \tilde{\tilde{B}}(k)\,\Delta\underline{u}(k) \; + \; \tilde{\tilde{M}}(k)\,\Delta\tilde{\tilde{\underline{d}}}(k) \tag{3.19}$$

where

$$
\tilde{\tilde{\underline{x}}} \;=\;
\begin{bmatrix}
\tilde{x} \\
\hline
P_1^{gen\_ref} \\
\vdots \\
P_{ncg}^{gen\_ref} \\
Q_1^{gen\_ref} \\
\vdots \\
Q_{ncg}^{gen\_ref} \\
\hline
P_1^{gen} \\
\vdots \\
P_{ncg}^{gen} \\
Q_1^{gen} \\
\vdots \\
Q_{ncg}^{gen} \\
\hline
SOC_1 \\
\vdots \\
SOC_{nb}
\end{bmatrix}
\qquad
\Delta\underline{u} \;=\;
\begin{bmatrix}
\Delta P_1^{gen\_ref} \\
\vdots \\
\Delta P_{ncg}^{gen\_ref} \\
\Delta Q_1^{gen\_ref} \\
\vdots \\
\Delta Q_{ncg}^{gen\_ref}
\end{bmatrix}
\qquad
\Delta\tilde{\underline{d}} \;=\;
\begin{bmatrix}
\Delta P_1^{ref} \\
\vdots \\
\Delta P_n^{ref} \\
\Delta Q_1^{ref} \\
\vdots \\
\Delta Q_n^{ref} \\
\omega^{nom} \\
V^{nom}
\end{bmatrix}
$$

41

while the complete structures of $\tilde{\tilde{A}}(k)$, $\tilde{\tilde{B}}(k)$, $\tilde{\tilde{M}}(k)$ are not reported for simplicity. However, they can be easily computed taking into account the dynamics defined in (3.14), (3.15), (3.16), (3.17) and (3.18).

3.4.3 Rotating Generators

The rotating generators dynamics have been neglected in the considered model, as well their internal control loops. This means that it is assumed that the requested power by the hierarchical control structure will be immediately delivered by the generators. This is acceptable in our case since the time constants of controllable generators are much smaller with respect to the secondary control time frame.

3.4.4 Loads

Although the load units are not controllable by the secondary controller, their internal models are needed in order to describe how the network variables influence the absorbed power. As far as parallel RLC loads are concerned, the corresponding static model has been already introduced in paragraph 2.4, where the active and reactive power expressions have been computed as functions of the network variables.

However, for more complex loads it quite difficult to mathematically compute these expression since there are not detailed information about their internal impedances. Because of this, identification experiments are performed in order to find static expressions defining how the absorbed powers depend on the load output voltage and frequency. These models are usually characterized by nonlinear functions, and their general structure is depicted in (3.20).

$$\begin{cases} P_i^{load} = h_p \cdot f_{pv}\left(V_i,\ k_{pv}\right) \cdot f_{p\omega}\left(\omega,\ k_{p\omega}\right) \\ Q_i^{load} = h_q \cdot f_{qv}\left(V_i,\ k_{qv}\right) \cdot f_{q\omega}\left(\omega, k_{q\omega}\right) \end{cases} \tag{3.20}$$

where f_{pv}, $f_{p\omega}$, f_{qv}, $f_{q\omega}$ correspond to the predefined nonlinear functions that express the static model used in the identification experiment. On the contrary h_p, h_q, k_{pv}, $k_{p\omega}$, k_{qv}, $k_{p\omega}$ are parameters that need to be identified and they depend on the actual load characteristics.

The first two parameters are related to the amount of active and reactive power that the load absorbs at nominal conditions, while the others are referred to dependence that the final absorbed power has on the corresponding network variable. Moreover, the load models are defined such that the parameters k_{pv}, $k_{p\omega}$, k_{qv}, $k_{p\omega}$ are set to zero if the load does not show a dependence between the corresponding power and the network variable.

For instance, if we want to define a model for a RLC load through the above equations, the parameter $k_{p\omega}$ must be set to zero since there is not a dependence between the active power and the network frequency, as reported by equation (2.13).

Although the knowledge of these models is not always available, they are fundamental to choose the droop coupling to implement. Indeed, through their definitions and the line characteristics is possible to estimate which is the prevailing impedance of the network.

Having defined the models of the main system dynamics, now a brief description of the implemented simulator is given.

3.5   Simulator

In order to test the control performances of both the primary and the secondary control, a simulation environment must be developed. To do that, the MATLAB$^{\text{TM}}$ programming code has been used, thanks for its potentialities for system modelling and control. Regarding the microgrid components, they have been simulated by actually implementing the previous developed dynamics. On the other hand, the network model is a nonlinear system and so it must be simulated through numerical methods.

It is possible to find many network simulators in the literature; however, most of them are related to grid-connected microgrids and so they do not suit to our case. Thanks to the collaboration with RSE SpA, it has been possible to use a simulator developed by the istitution itself that can be easily adapted to an islanded microgrid with all sources controlled with the Inverse Droop configuration [23].

This network simulator is based on the Newton-Raphson method, which actually is a well-known numerical algorithm to solve nonlinear equations [24]. It relies on a sequential linearization process that continues to iterate until a convergent solution is reached. Adapting it to the power flow case, starting from the equations in (3.3), it is possible to identify $2n$ nonlinear functions represented as $f(x) = 0$, as reported below.

$$\begin{cases} f_i^P(\underline{x}) = P_i^T(\underline{x}) - P_j^{gen}(\underline{x}) + P_i^{ext}(\underline{x}) = 0 \\ f_i^Q(\underline{x}) = Q_i^T(\underline{x}) - Q_j^{gen}(\underline{x}) + Q_i^{ext}(\underline{x}) = 0 \end{cases} \qquad (3.21)$$

At this point, the Newton-Raphson algorithm is used until it eventually finds a convergent solution, if it exists. The convergence is defined as the condition where the solution residual, that is the difference between the solutions of two sequential iterations, remains inside some predefined tolerance bounds for a fixed number of iterations (at least 2). Since these bounds are usually chosen to be considerably small with respect to the values of the variables, this means that, when convergence is reached, it is not necessary to continue the iteration process since a solution for the nonlinear problem has been found.

Relying on this algorithm, the adopted network simulator receives as inputs the network characteristics (topology, impedances, number of nodes etc.), the nodal power references and the functions that describe the dependence of the nodal powers to the network variables (droop functions, load impedances etc.). Finally, the primary steady-state values of voltages, phase angles and frequency are given back as outputs.

3.6   Conclusions

The developed models are fundamental for the definition of the secondary layer. Indeed, as aforementioned, it will rely on a Model Predictive Control approach, making so the state-space model essential to predict the future behavior of the system based on the chosen control actions. Having the system model, as well as the relative simulator, now a complete presentation of the secondary control design is given, which actually can be considered as the main innovation of this work.

Chapter 4

Secondary Control

4.1 Introduction

In this chapter a description of the secondary control design will be given. As underlined in the previous chapters, its implementation is based on a Model Predictive Control approach (MPC), that eventually will modify the reference powers of the primary layer. The schema representing the overall closed-loop system is again represented.
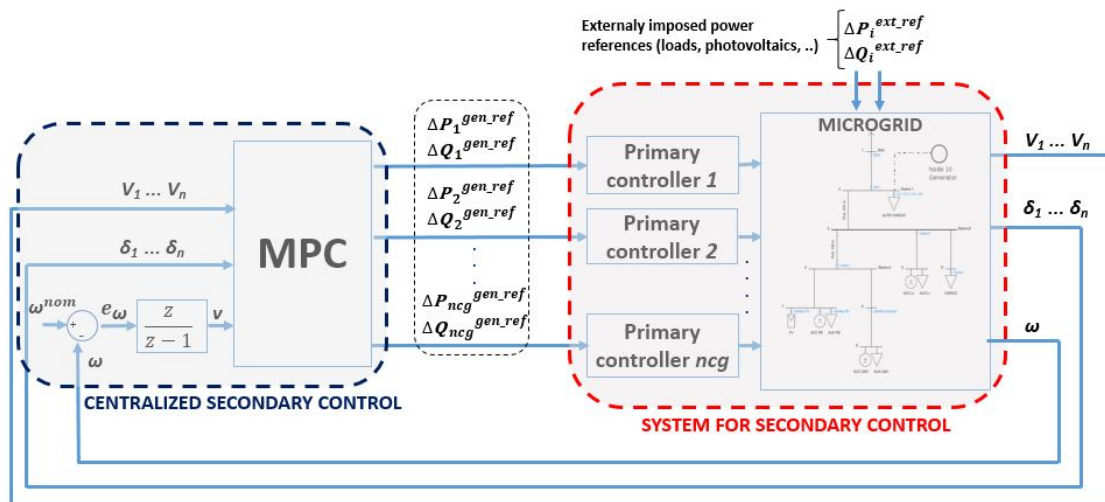
Figure 4.1: Hierarchical control block diagram

The Model Predictive Control is an advanced control technique, considerably different from the traditional linear control approaches, has been defined during the 1980s as a new control strategy for process control, mainly used in chemical plants and oil refineries. At the beginning, its diffusion was pretty limited since, being based on an on-line optimization process, this algorithm could not be applied to fast systems, but only to slow ones, such as the chemical processes. However, the recent progresses in computing processing power allowed to implement advanced control strategies to faster and faster systems, such as the ones related to the energy sector. Actually, applying predictive control becomes surely an interesting solution to solve many electrical issues since it may provide relevant results in terms of energy efficiency.

The reason why the MPC became such an attractive control scheme relies in its innovative features with respect to traditional control techniques. Although they have been rigorously discussed in the literature [25], [26], [27], the MPC main features can be briefly summarized in the following points.

- **Optimization:** It is possible to express the control problem as a typical optimization problem where different objectives can be identified. These are defined through a *cost function J*, whose minimization gives back the best control actions to implement. One of the main advantages is that the the cost function has not a fixed structure but it is completely flexible and adaptable based on the control objectives.

- **Constrained problem:** Another relevant feature corresponds to the possibility of defining the constraints for the optimization problem. This becomes an effective tool since the control actions will be chosen in order to respect the defined bounds on the system variables, which may be referred either to some design choices or to some physical limits that the variables have to satisfy.

- **Prediction approach:** Although other control strategies are based on an optimizing procedure (e.g. LQ, LQG and H-infinity control), the prediction aspect is a feature typical of the MPC algorithm. Actually, this control strategy at each iteration tries to predict the future behavior of the system on a predefined temporal horizon. Based on this information, the optimal control actions are computed so that they both minimize the cost function and they also respect the predefined bounds for the whole prediction horizon.

Moreover, this control strategy is based on the *Receding Horizon* approach. This is a recursive procedure where at a certain time step $t = k$ the control performs the optimization algorithm taking into account also the variables' values for a fixed number of future time slots N, and then it decides the control actions to implement between $t = k$ and $t = (k + N)$. However, according to this approach only the control actions of the actual time step $t = k$ will be implemented. Being a recursive approach, at the next step, $t = (k + 1)$, the variables will be sampled again and the MPC will perform the same procedure by taking into account the system behavior between $t = (k + 1)$ and $t = (k + 1 + N)$ in order to choose the control actions to implement at the time step $t = (k + 1)$.

- **Possible use of identification models:** To perform the prediction of the future system behavior, the MPC uses the system dynamical model. However, it is not fundamental to define it through the real physical equations but it can be obtained with system identification techniques performed through simple tests on the system itself.

Given the potentialities of this control approach, it becomes an interesting solution to apply it to the management of an islanded microgrid. Indeed, implementing a secondary scheme based on an optimization strategy may allow an efficient management of microgrid resources, like storage systems and generators, and it also could ensure that the voltages and the frequency are kept as near as possible to the nominal values even though absorbed powers may considerably vary during the day. A complete overview of the secondary control design is now given.

4.2 Model Predictive Control Design

The Model Predictive Control relies on three fundamental parts: the system model, the problem constraints and the cost function. A description of these parts is now given, underlining how they have been implemented.

4.2.1 Predictive Model

The final state-space equation, describing all the relevant system dynamics for the secondary time frame, was defined in the previous chapter in (3.19).

This model is reported again in (4.1) (for the sake of readability from now on all variables are expressed without the $\sim$ symbol).

$$\underline{x}(k+1) = A(k)\,\underline{x}(k)\ +\ B(k)\,\Delta\underline{u}(k)\ +\ M(k)\,\Delta\underline{d}(k) \tag{4.1}$$

The model expressed in (4.1) is time varying since the matrices $A(k)$, $B(k)$, $M(k)$ are not fixed quantities. This is due both to the droop parameters, which vary if the power limits are reached, and to the fact that these matrices come from a linearization procedure, evaluated at the equilibrium steady-state condition at the current time step. Moreover, it is recalled that the MPC algorithm tries to predict the system future behavior by exploiting the model linearized in the relative equilibrium condition. This means that, from the MPC prospective, it can be assumed that the system model does not vary over time but it is represented through a time-invariant linear model, expressed in (4.2).

$$\underline{x}(k+1) = \bar{A}_k\,\underline{x}(k)\ +\ \bar{B}_k\,\Delta\underline{u}(k)\ +\ \bar{M}_k\,\Delta\underline{d}(k) \tag{4.2}$$

where $\bar{A}_k$, $\bar{B}_k$, $\bar{M}_k$ refer to the matrices $A(k)$, $B(k)$, $M(k)$ evaluated at the steady-state condition represented by $\underline{x}(k)$.

Since the linearization is valid only in the neighborhood of the equilibrium, this implies that the prediction will be less and less precise as the time horizon increases. However, for small prediction horizons (e.g. $N = 3, 4, 5, 6...$) this represents a quite acceptable approximation in order to compute the future behavior of the system based on the chosen control strategies and on the known disturbances.

Starting from this model, the prediction is performed through a simple and recursive procedure. For instance, given the information of the system state at $t = k$, as well as the forecasts of the future disturbances (which in our case correspond to the power profiles of the uncontrollable units, like renewable sources or loads), it is possible to know the system state vector at $t = (k+2)$ based on the chosen control actions.

$\underline{x}(k+2) = \bar{A}_k\,\underline{x}(k+1)\ +\ \bar{B}_k\,\Delta\underline{u}(k+1)\ +\ \bar{M}_k\,\Delta\underline{d}(k+1)$

$\underline{x}(k+2) = \bar{A}_k[\,\bar{A}_k\underline{x}(k) + \bar{B}_k\Delta\underline{u}(k) +\ \bar{M}_k\Delta\underline{d}(k)\,]\ + \bar{B}_k\Delta\underline{u}(k+1) + \bar{M}_k\Delta\underline{d}(k+1)$

$\underline{x}(k+2) = \bar{A}_k^{\,2}\underline{x}(k) + \bar{A}_k\bar{B}_k\Delta\underline{u}(k) + \bar{A}_k\bar{M}_k\Delta\underline{d}(k) + \bar{B}_k\Delta\underline{u}(k+1) + \bar{M}_k\Delta\underline{d}(k+1)$

Applying the same procedure for the whole prediction horizon, the following formula holds, also known as the Lagrange equation for discrete time systems.

$$\underline{x}(k+i) = \bar{A}_k{}^i \underline{x}(k) \; + \; \sum_{j=0}^{i-1} \bar{A}_k{}^{i-j-1} \bar{B}_k \Delta \underline{u}(k+j) \; + \; \sum_{j=0}^{i-1} \bar{A}_k{}^{i-j-1} \bar{M}_k \Delta \underline{d}(k+j)$$

where $i \in (1, \, ..., \, N)$.

Expressing everything in matrix form, the system dynamic for the whole prediction horizon is defined in (4.3).

$$\underline{X}(k) \; = \; \boldsymbol{A}_k \, \underline{x}(k) \; + \; \boldsymbol{B}_k \, \Delta \underline{U}(k) \; + \; \boldsymbol{M}_k \, \Delta \underline{D}(k) \tag{4.3}$$

where

$$\underline{X}(k) = \begin{bmatrix} \underline{x}(k+1) \\ \underline{x}(k+2) \\ \vdots \\ \underline{x}(k+N-1) \\ \underline{x}(k+N) \end{bmatrix}, \quad \Delta \underline{U}(k) = \begin{bmatrix} \Delta \underline{u}(k) \\ \Delta \underline{u}(k+1) \\ \vdots \\ \Delta \underline{u}(k+N-2) \\ \Delta \underline{u}(k+N-1) \end{bmatrix}, \quad \Delta \underline{D}(k) = \begin{bmatrix} \Delta \underline{d}(k) \\ \Delta \underline{d}(k+1) \\ \vdots \\ \Delta \underline{d}(k+N-2) \\ \Delta \underline{d}(k+N-1) \end{bmatrix}$$

$$\boldsymbol{A}_k \; = \; \begin{bmatrix} \bar{A}_k \\ \bar{A}_k^2 \\ \vdots \\ \bar{A}_k^{N-1} \\ \bar{A}_k^N \end{bmatrix}, \qquad \boldsymbol{B}_k = \begin{bmatrix} \bar{B}_k & 0 & 0 & 0 & \ldots & 0 & 0 \\ \bar{A}_k \bar{B}_k & \bar{B}_k & 0 & 0 & \ldots & 0 & 0 \\ \ldots & \ldots & \ldots & \ldots & \ldots & \ldots & \ldots \\ \ldots & \ldots & \ldots & \ldots & \ldots & \ldots & \ldots \\ \bar{A}_k^{N-2} \bar{B}_k & \bar{A}_k^{N-3} \bar{B}_k & \ldots & \ldots & \bar{A}_k \bar{B}_k & \bar{B}_k & 0 \\ \bar{A}_k^{N-1} \bar{B}_k & \bar{A}_k^{N-2} \bar{B}_k & \ldots & \ldots & \ldots & \ldots & \bar{B}_k \end{bmatrix}$$

and

$$\boldsymbol{M}_k = \begin{bmatrix} \bar{M}_k & 0 & 0 & 0 & \ldots & 0 & 0 \\ \bar{A}_k \bar{M}_k & \bar{M}_k & 0 & 0 & \ldots & 0 & 0 \\ \ldots & \ldots & \ldots & \ldots & \ldots & \ldots & \ldots \\ \ldots & \ldots & \ldots & \ldots & \ldots & \ldots & \ldots \\ \bar{A}_k^{N-2} \bar{M}_k & \bar{A}_k^{N-3} \bar{M}_k & \ldots & \ldots & \bar{A}_k \bar{M}_k & \bar{M}_k & 0 \\ \bar{A}_k^{N-1} \bar{M}_k & \bar{A}_k^{N-2} \bar{M}_k & \ldots & \ldots & \ldots & \ldots & \bar{M}_k \end{bmatrix}$$

The equation (4.3) has the great advantage of having a fixed structure; therefore at each iteration the MPC will be able to predict the whole system behavior for the next N steps by simply evaluating the above defined matrices in the relative equilibrium point $\underline{x}(k)$.

Given the presented predictive model, now the actual optimization problem will be introduced. It will consist of two main parts: the constraints and the cost function. These are equally important since the first limits the values of the main variables so that only real and implementable solutions can be found, while the second defines the control objectives in order to compute the best solution.

4.2.2 Constraints

Defining the constraints for an optimization problem is not always a straightforward issue. This is due to the fact that the feasibility of the problem strongly depends on the adopted solution bounds. In other words, if the the optimization problem is characterized by too tight constraints a solution could not be found and therefore there will be no way to know which control actions the MPC has to implement. This is a more challenging issue in predictive algorithms since during the optimization process the variables must respect the defined bounds for the whole horizon and not only for the current time step.

Being the feasibility of the problem such a priority, some constraints will be not defined as mandatory, but they will be "relaxed". This means that, in case the problem feasibility is compromised, these constraints can be violated. In the theory of optimization there is in fact a difference between *Hard Constraints*, that must be fulfilled in each system condition, and *Soft Constraints*, which might be not respected. The *Soft Constraints* are implemented through the use of additional optimization variables, called *slack variables*, which have the function of widening the variables' bounds so that the constraint can be satisfied. Their standard implementation follows, X is a general variable and ϵ corresponds to the slack variable.

$$-\epsilon \ + \ X_{MIN} \ \leq X \ \leq \ X_{MAX} \ + \ \epsilon$$
$$\epsilon \ \geq \ 0$$

It can be easily noted that through this implementation the greater is the slack variable, the more "extended" the bounds are. Obviously the ideal case is when the slack variables are equal to zero, meaning that the variables will stay inside the defined limits. To do that, one of the objectives defined in the cost function will be to minimize as much as possible the values of the slack variables.

Regarding the problem considered in this work, the variables' bounds will be mainly related either to physical or to safety limitations imposed by the regulations. Concerning the implemented problem constraints, they can be summarized in four categories. A description of their definitions is now given.

Implemented Constraints

1) Voltages Bounds: As mentioned in paragraph 2.1, the microgrid line to line voltages must respect some limits since they can cause serious damages to physical devices. In the optimization problem, this implies that the voltages will be bounded between a maximum and a minimum value for the whole prediction horizon. However, it should be noted that, being the voltage an output affected by external disturbances, in some circumstances the constraint could be not respected. It may happen in fact that large load power variations occur, and therefore the relative nodal voltages will considerably deviate, so exceeding the defined bounds. This implies that the voltage constraints will be relaxed through the use of *Soft Constraints* as reported below.

$$- \epsilon_V + V^{min} \leq V_i(k+j) \leq V^{max} + \epsilon_V$$

where $i \in (1, ..., n)$, with n being the number of nodes of the network and $j \in (1, ..., N)$, with N being the chosen prediction horizon. Moreover, V^{max} and V^{min} correspond to the defined voltage bounds, while finally ϵ_V, defined to take positive values, is the slack variable that makes the constraint of "soft" type.

2) SOC Bounds: The state of charge of a battery is a system variable that must be intrinsically limited between 0% and 100%. However, it should be noted that excessive charges, or discharges, negatively affect the batteries' capacities and therefore they should be avoided in most cases. To accomplish these requirements, two constraints will be defined for the SOC: a *Hard Constraint* to set the physical limits, and a *Soft Constraint* that expresses a recommended region where the states of charge should evolve in order to not ruin the batteries' life. In other words, in some circumstances the SOCs could exceed the recommended bounds, but they obviously can never take values beyond 100% or below 0%.

$$0 \leq SOC_b(k+j) \leq 100$$

$$- \epsilon_{SOC} + SOC^{min} \leq SOC_b(k+j) \leq SOC^{max} + \epsilon_{SOC}$$

where $b \in (1, \ ..., \ n_b)$, with n_b being the number batteries in the network and $j \in (1, \ ..., \ N)$, with N being the chosen prediction horizon. Moreover, SOC^{max} and SOC^{min} represent the defined operational bounds for the states of charge, and they are obviously set such that $SOC^{min} > 0$ and $SOC^{max} < 100$. Finally, $\epsilon_{SOC} > 0$ corresponds to the slack variable.

3) Generator Power Capabilities: Each generation source is characterized by active and reactive power limits. This implies that the variations of the reference powers that the secondary control implements have to respect the generators' capabilities. Moreover, as underlined in paragraph 2.4, the droop action is saturated if the power limits are reached and therefore also the states representing the effective generated powers will be limited through a constraint. Since these constraints refer to physical limits, they are both expressed as *Hard Constraints*.

$$P_i^{\ min} \ \leq \ P_i^{gen\_ref}(k+j) \ \leq \ P_i^{\ max}$$
$$Q_i^{\ min} \ \leq \ Q_i^{gen\_ref}(k+j) \ \leq \ Q_i^{\ max}$$

$$P_i^{\ min} \ \leq \ P_i^{gen}(k+j) \ \leq \ P_i^{\ max}$$
$$Q_i^{\ min} \ \leq \ Q_i^{gen}(k+j) \ \leq \ Q_i^{\ max}$$

where $i \in (1, \ ..., \ ncg)$ and $j \in (1, \ ..., \ N)$. $P_i^{\ max}$, $P_i^{\ min}$, $Q_i^{\ max}$, $Q_i^{\ min}$ represent the i_{th} generator's limits both for active and reactive powers.

It can be noted that the with regard to the above defined constraints, additional physical limitations could exist that limit the reactive power based on the generated active one. This means that depending of the additional bounds that characterize the generation sources, some other constraints could be required to be implemented.

4) Reference Power Variations Bounds: It is recalled that the variations of reference powers correspond to the control inputs of the secondary control. These variables must be also limited since, being the model based on a linearization procedure, too large control actions could bring the system states too far from the considered equilibrium, affecting so the reliability of the linearized predictive model. Moreover, since the control inputs are not affected by external disturbances but they are completely defined by the optimization problem, their bounds will be defined through *Hard Constraints*, as follows.

$$\Delta u^{\ min} \quad \leq \quad \Delta u_i(k+j-1) \quad \leq \quad \Delta u^{\ max}$$

where $i \in (1, \ ..., \ ncg)$ and $j \in (1, \ ..., \ N)$. $\Delta u^{\ min}$, $\Delta u^{\ max}$ are the chosen bounds for the variations of reference powers.

However, it should be noted that there is a case where this constraint is needed to be relaxed. For instance, if the state of charge of a battery reaches its lower bound, the control system should be able to force the battery to not generate power, which means to force the output power to take values smaller or equal to zero, requiring also prompt and large variation of the power references. Therefore, for batteries the above-reported constraint will be defined as a soft one, making it violable in case of an excessive charge or discharge. It follows:

$$- \ \epsilon_{\Delta U_{batt}} \quad + \quad \Delta u_{\ min} \quad \leq \quad \Delta u_i(k+j) \quad \leq \quad \Delta u_{\ max} + \quad \epsilon_{\Delta U_{batt}}$$

where $i \in (1, \ ..., \ ncg)$ refers in this case to the controllable generators implemented as batteries, while $\epsilon_{\Delta U_{batt}}$ is the slack variable, which also in this case is defined to take only positive values.

Having defined all the constraints for the optimization problem, now the cost function will be presented. Its minimization in fact will provide the best solution that is possible to implement given the solution space $S(k)$, that results from the above defined constraints at each iteration.

4.2.3   Cost Function

As already mentioned, the main objectives of the secondary control structure are both to restore the network variables' deviations to their nominal values and also to efficiently manage the microgrid generation sources. In order to define them as the objectives of the optimization problem, the cost function must be implemented so that its minimization will provide the optimal solution.

The cost function $J(\underline{x}(k))$ is defined as the sum of terms related to the variables to be minimized, properly multiplied by some constants, called "weights".

Actually, through their use it is possible to give different importance to the elements during the minimization process. Furthermore, since the optimization problem tries to find the minimum, the cost function must be properly defined so that an absolute real minimum always exists. This means that for each state condition defined by the constraints, the cost function must be always below bounded, which means:

$$J(\underline{x}(k)) \in (-\infty, +\infty] \ \ \forall \underline{x}(k) \in S(k)$$

where $S(k)$ correspond to the resulting solution space from the constraints applied at $t = k$.

To accomplish this issue, the cost function has been defined to be always positive. Moreover, it is worth noticing that the cost function has not a unique form but different objectives can be implemented given its flexibility. For the purpose of this work, a precise form has been defined and implemented. To better understand its structure, the involved variables are now presented.

Implemented Cost Function

1) Slack Variables: As already mentioned, although soft constraints allow to violate the defined bounds if the problem feasibility is compromised, the main objective is obviously to respect the variables' limits keeping the slack variables as close to zero as possible. To do that, these will be highly weighted in the cost function.

2) Frequency Integrator Output: In order to keep the frequency close to its nominal value, the output of the integrator will be also weighted in the cost function. It is recalled that by placing an integrator between the steady-state frequency deviation and the MPC, it is ensured that in steady-state conditions the frequency converges to its nominal value. By increasing, or decreasing, the weight of the frequency integrator, it will result that the transient to reach the nominal frequency will be decreased, or increased. Moreover, since the integrator output can take also negative values, it may lead so the cost function to be unbounded below; therefore the squared integrator output value will be taken into account to be minimized.

3) Voltages' deviations: The nodal voltages are allowed to deviate from its nominal value, reaching also in some cases their bounds without causing many problems to the network. However, it is surely better to make these variables stay as close as possible to the nominal value for each power condition; in this way in fact also line currents will not take high values. To express that, the voltage deviation with respect to the nominal value will be weighted in the cost function in order to be minimized. However, since also in this case the deviation can take negative values, its squared value will be taken into account.

4) Reference Power Variations: Also control inputs are requested to be minimized since this will result in smoother variations of the generator reference powers. Actually, it may happen that, if reference power variations are not weighted in the cost function, they will take the extreme values imposed by the constraints, leading the system to continuous and relevant variations of voltages and frequency. Moreover, it is surely better to minimize the variation of reference powers since in this way the linearized predictive model will more accurately represent the system future behavior.

5) Total Reference Powers: These variables are the ones that determine the efficient management of the microgrid. Actually, by weighting them in the cost function, the minimization will lead to use the minimum amount of power such that the actual load absorption is satisfied and the steady-state variable deviations are restored. It is recalled that the reference powers are not what is effectively generated since the droop control will modifies them in order to reduce network variables' deviations; however, they represent a good approximation of which generators will be more exploited with respect to others. Based on the defined weights, different management strategies may be implemented. For instance, if in the islanded condition the main objective is to use green technologies, the batteries' reference powers will be less weighted with respect to the ones of other controllable generators, like turbines, so that the power generation will rely only on storage units and renewable sources, which in our case are not managed by secondary control.

Having presented all the objectives and fundamental elements that have been taken into account, the complete formulation of the cost function follows.

$$
\begin{aligned}
J(\underline{x}(k),\ \underline{U}(k),\ \underline{D}(k)) \quad = \quad & \sum_{j=1}^{N} \rho_V \cdot \epsilon_V(k+j-1) \\
+ & \sum_{j=1}^{N} \rho_{SOC} \cdot \epsilon_{SOC}(k+j-1) \\
+ & \sum_{j=1}^{N} \rho_{\Delta U_{batt}} \cdot \epsilon_{\Delta U_{batt}}(k+j-1) \\
+ & \sum_{j=1}^{N} w_v\, v^2(k+j) \\
+ & \sum_{j=1}^{N} \sum_{i=1}^{n} w_V^i\, (V_i(k+j) - V_{nom})^2 \\
+ & \sum_{j=1}^{N} \sum_{i=1}^{2*ncg} w_{\Delta U}^i\, (\Delta u_i(k+j-1))^2 \\
+ & \sum_{j=1}^{N} \sum_{i=1}^{ncg} w_{gen\_ref}^i\, (P_i^{gen\_ref}(k+j))^2 \\
+ & \sum_{j=1}^{N} \sum_{i=1}^{ncg} w_{gen\_ref}^{i+ncg}\, (Q_i^{gen\_ref}(k+j))^2
\end{aligned}
$$

where ρ_V, ρ_{SOC}, $\rho_{\Delta U_{batt}}$, w_v, w_V^i, $w_{\Delta U}^i$, $w_{gen\_ref}^i$ correspond to the weights of the relative variables.

The minimization of the above function, performed at each control iteration, will give the optimal control sequence to implement accordingly to the previously defined objectives and constraints. However, as underlined before, only the control action at the relative time step will be implemented since the *Receding Horizon* approach has been adopted.

4.3 Conclusions

With this chapter, all the theoretical aspects and the formulation of the developed control structure have been presented. In the following chapters, the relative control performances will be tested, taking into account a real microgrid test case.

Chapter 5

Microgrid benchmark and Simulations Tests

5.1 Introduction

In this chapter the effectiveness of the primary and secondary control architectures is tested. As already mentioned, this work has been carried out in collaboration with RSE S.p.A. (Research Energy System), a research institution, which provided a microgrid test case. The considered microgrid corresponds to a real low voltage grid that RSE owns in order to test new control algorithms for the energy management.

This network is equipped with a communication infrastructure able to monitor all grid electrical variables, as well as to send control inputs to the different units. This framework is implemented through a SCADA system (Supervisory Control and Data Acquisition), a famous computer-based industrial system used to control large-scale processes. The considered test network has not a fixed structure but it can be configured according to several topologies; moreover, different generation and load units can be plugged in or disconnected depending on the chosen test. This can be done by acting on the physical switches and commuters displaced in the network, and a switch placed in the Point of Common Coupling allows to operate the microgrid either in grid-connected or stand-alone mode. A picture of the RSE Test Falicity is illustrated in Figure 5.1, where the main units are highlighted.

According to the main goals of this work, the hierarchical control structure will be tested on a defined microgrid topology.

This corresponds to an islanded small grid, which includes both controllable generators, storage units, renewable sources, and some loads through which is possible to externally vary the amount of absorbed powers.

LEGEND:

1. Control Room
2. Lithium Battery
3. Cogenerator
4. Electrical Loads
5. Redox Battery
6. Lead Battery
7. Photovoltaic System
8. Small Wind Turbine

Figure 5.1: RSE Test Facility

Before showing the main results, a brief description of considered network configuration is given.

5.2 Test Facility

The examinated microgrid configuration has a simple radial structure composed of 13 nodes, and its electrical scheme is depicted in Figure 5.2. In the simulation environment, the real network and units parameters have been implemented in order to represent the real behavior of the system. In the next section a description of the main elements is given.
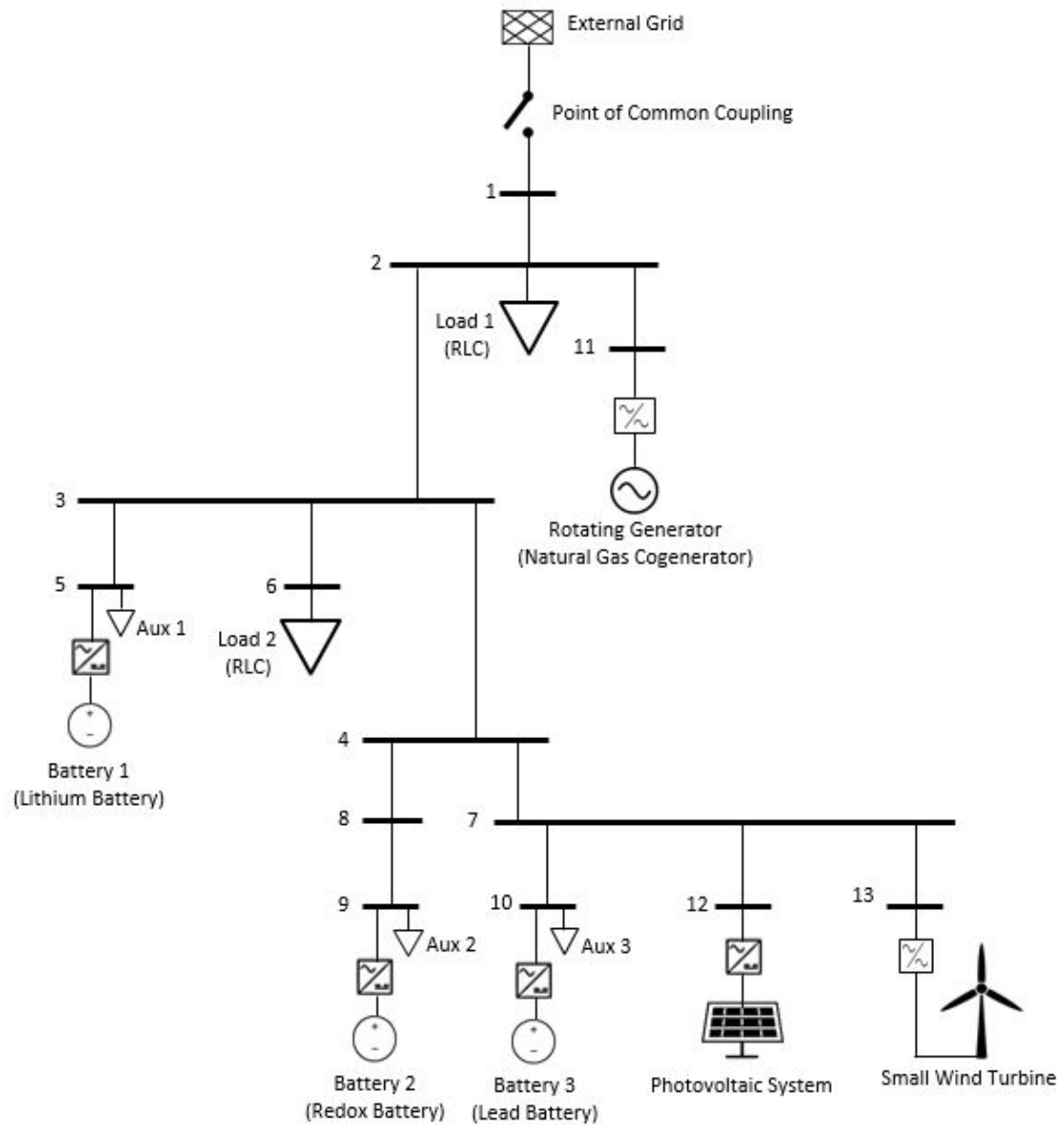
Figure 5.2: Test Facility Schematic

5.2.1 Test facility Elements

The main microgrid elements are presented below.

Storage Units: The network is equipped with three batteries, placed in nodes 5, 9 and 10, respectively. Being DC sources, each of them is interfaced with an inverter controlling both the active and the reactive output power. These batteries are characterized by a rectangular power capability curve [1], which in turn implies that the power factor [2] is not limited. The batteries parameters are shown in Table 5.1, and, to have a better understanding of their meanings, the battery model is reported again.

$$SOC(k+1) \;=\; SOC(k) \;-\; \xi * \frac{\tau_s}{60 * C^{tot}} * P^{gen}(k+1)$$

	Node	C^{tot}	ξ	P^{max}	P^{min}	Q^{max}	Q^{min}
Battery 1	5	32 kWh	0.96	30 kW	-11 kW	60 kVar	-60 kVar
Battery 2	9	30 kWh	0.86	25 kW	-25 kW	15 kVar	-15 kVar
Battery 3	10	55 kWh	0.92	12 kW	- 9 kW	13 kVar	-11 kVar

Table 5.1: Batteries Parameters

It is recalled that ξ corresponds to the battery charge/discharge coefficient and C^{tot} to the total battery capacity.

It should be considered that batteries tend to overheat because of frequent charge and discharge operations, resulting in an aging effect that the decrease batteries' life. This implies that an auxiliary cooling system must be placed next to each battery. These systems have been modeled as a constant active and reactive power absorption at the node where they are located and their real characteristics are shown in Table 5.2.

---

[1]The power capability curve expresses the active and reactive power limits for a generator. In other words, taking a cartesian plot with the delivered active power at the y-axis and the reactive one at the x-axis, the capability curve delimits the working region for the two powers. A rectangular capability curve means that this region is limited only by the maximum and the minimum powers.

[2]The power factor is a largely used electrical quantity, strictly related to the ratio between the delivered reactive and active power. It is defined as p.f.=cos(arctan (Q/P)),

	Node	P	Q
Auxiliary Cooling System 1	5	4.50 kW	-4.96 kVar
Auxiliary Cooling System 2	9	0.19 kW	-2.12 kVar
Auxiliary Cooling System 3	10	0.28 kW	-0.83 kVar

Table 5.2: Auxiliary Cooling Systems for Batteries

Rotating Generator: A rotating generator is placed at node 11, which in the real microgrid corresponds to a natural gas-fueled cogeneration source. This is a fundamental element since, being batteries limited by their available states of charge and being renewable sources undeterministic, it is the only source that can provide power in most conditions. Moreover, although this generator provides AC power, it is however interfaced with an inverter to fully control the output active and reactive power.

Regarding the power capability curve, it has not a simple definition for rotating generators but it comes from many factors such as limits on the power factor and on the maximum apparent power [3], defined as $|S|_{MAX}$. However, given some limitations due to the coupling with the power electronics interface, it was decided to make the generator work in a smaller region as depicted in Figure 5.3, where the active and reactive powers are expressed in p.u. with respect to the nominal apparent power, $|S|_n$ and the relative parameters are reported in Table 5.3.

It is worth underlining that the rotating generator can not absorb active power but only deliver it; this does not hold for the reactive power where the generator can also absorb it through an appropriate inverter control. Moreover, looking at Figure 5.3, it can be noted that for small values of generated active power (below 0.2 p.u.) the limitation on the minimum power factor reduces the maximum, or minimum, generating reactive.

---

[3] The apparent power corresponds to the magnitude of the complex power. It is defined as $|S| = |P + jQ| = \sqrt{P^2 + Q^2}$. A limitation on the maximum apparent power means that the capability region is delimited by a circle, which implies that the more active power is delivered, the less reactive power can be generated and vice versa.
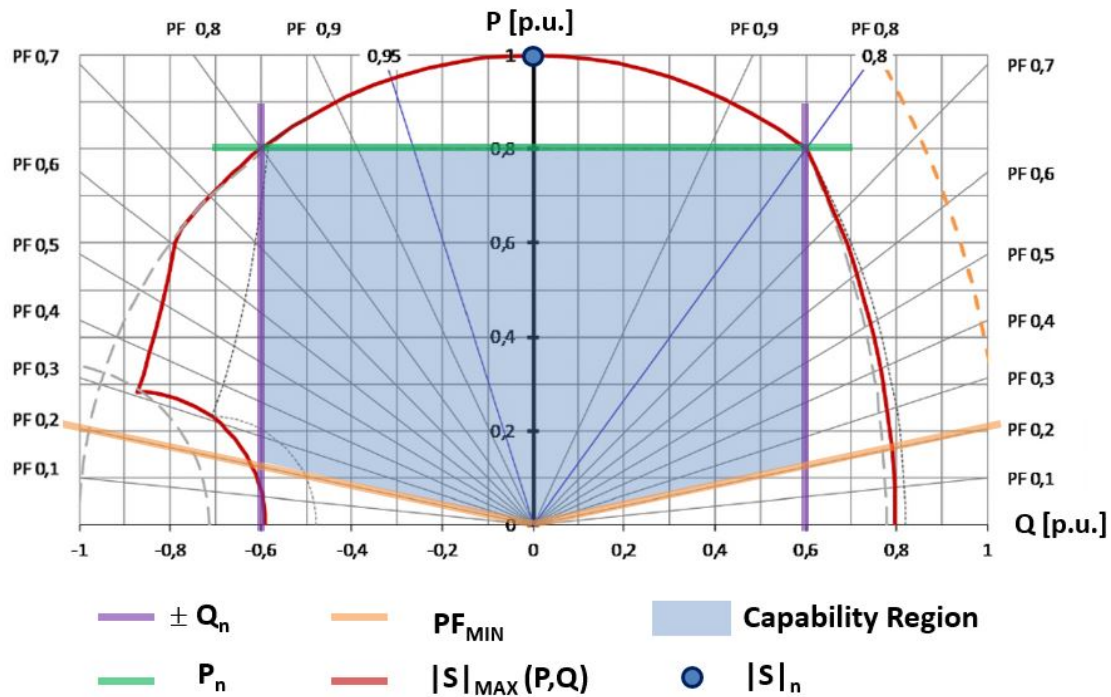
Figure 5.3: Rotating Generator Capability Region

	Node	PF_{MIN}	$|S|_n$	P_n	Q_n
Rotating Generator	11	0.2	63 kVA	50.4 kW	37.8 kVar

Table 5.3: Rotating Generator Parameters

Renewable Sources: The microgrid is equipped with two renewable sources: a photovoltaic system located at node 12 and a small wind turbine at node 13. They are both small renewable systems since in a realistic view it is not possible to place into a microgrid a big wind turbine or a large number of solar panels. These systems have been equipped only with primary controllers since their reference powers are not determined by the secondary control layer but they depend on the actual weather conditions. Both the photovoltaic system and the wind turbine are characterized by some output power limits, which are depicted in Table 5.4.

	Node	P^{max}	Q^{max}	Q^{min}
Solar Panel	12	30 kW	10 kVar	-10 kVar
Wind Turbine	13	10 kW	10 kVar	-10 kVar

Table 5.4: Renewable Sources Power Limits

Variable Loads: In the considered test facility, two variable loads are present, located in nodes 2 and 6. These consist in two parallel RLC loads (like the one shown in Figure 2.7), that, by externally adjusting their internal impedances, can absorb predefined values of active and reactive powers. These elements are extremely important to test the control strategies for different power situations, and they also allow to understand which power conditions would lead the network to possible collapses. Moreover, it should be noted that the imposed absorbed powers are defined at nominal conditions, meaning that the final power absorption will vary as voltages and frequency shift from their nominal values.

Transmission Lines: Although network interconnections are not active elements, they have a significant influence on the network variables' behavior. As it was underlined in paragraph 2.3.1, the transmission lines are defined by the R/X factor which determines if the lines have either a resistive or an inductive characteristic.

The considered microgrid is characterized by resistive transmission lines ($R/X = 2.47$), and their lengths vary from 65 to 375 meters. This is quite normal, since the inductive characteristic is typical of long trasmission lines used for power distribution in the actual centralized network system. Looking to the simulation environment, the lines have been modeled through the π-model, that is depicted in Figure 5.4. This represents all the passive elements of the three-phase interconnections through a simple one-phase schematic and by adopting the phasor approach mentioned in the previous chapters. The real line impedances have been implemented in the simulation environment.
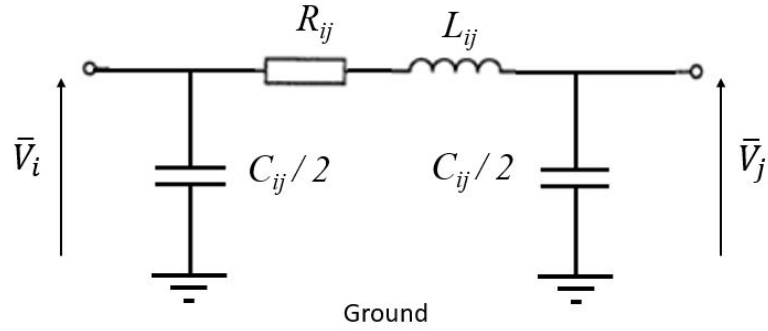
Figure 5.4: Trasmission Line π-model

Having described the features of the main microgrid elements, now the results of several simulations will be presented.

5.3 Numerical Results

In this section the numerical results will be presented. However, before showing the final results, some specifications about the simulation environment need to be defined.

5.3.1 Simulation specifications

The simulations refer to a defined scenario: the microgrid has just entered in the islanded operating mode and therefore the whole system needs to be managed without the support of the main grid. It is recalled that the islanding event could be either intentional, due for example to economic reasons, or it can be due to a fault that occurred in the external grid, leading the microgrid to isolate itself in order to not be affected.

In the reported simulations, the islanded condition will be supposed to last a whole day. The whole simulation time will be then discretized in 2880 steps, where the time difference between two consequential steps corresponds to 30 seconds. It is recalled that, since most units are interfaced through power electronics converters, the system is characterized by an overall low inertia, implying in turn that the network transients last only few seconds. This means that, since the time difference between two steps is longer with respect to the time transients, it can be assumed that at each simulation step the steady-state condition has been already reached.

Regarding the network power conditions, loads and renewable sources will be supposed to vary their powers according to predefined daily power profiles. Obviously, as the corresponding powers change, there will be an initial power unbalance between the total generated and absorbed power that will eventually result in a new transient for the network variables. The power trends for the uncontrollable units have been designed in order to test the hierarchical control structure in different network conditions, trying at the same time to represent the power absorption, or generation, of the real units.

The implemented daily profiles of the photovoltaic system and of the wind microturbine are depicted in Figure 5.5. Their trends are based on real measurements that have been carried at the RSE Test Facility. Only the generated active power is shown since these sources do not generate reactive power by themselves but only through of the primary control.
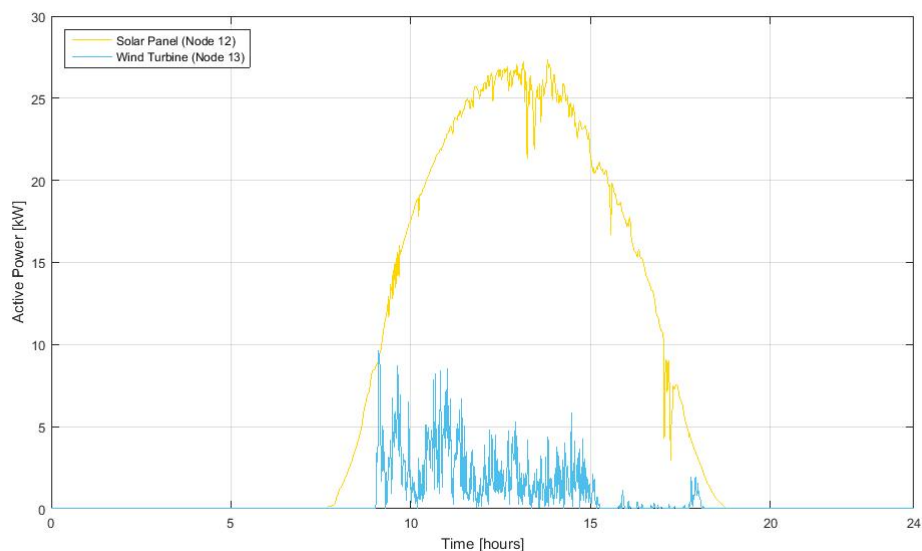
Figure 5.5: Renewable Energy Sources: Power Profiles

Looking at the figure, it is possible to notice that the wind-based source generates a smaller amount of active power with respect to the solar panel. This is due to the fact that small wind turbines can not generate a great deal of power since the wind at low heights never reaches a high speed. Moreover, these systems also require a very smooth airflow in order to be sufficiently efficient. This is not the case of small turbines that, since they are likely to be placed near other buildings, are often subject to a turbulent wind flow. This is witnessed by the Figure 5.5 where the wind power shows a noisy behavior.

65

Regarding the power absorption, it is recalled that five loads are present in the considered microgrid test case. Three of them correspond to the auxiliary cooling systems of batteries, while the others to two RLC loads, which can be regulated to absorb predefined values of active and reactive power. For the varying loads, the implemented nominal active and reactive power trends are illustrated in Figure 5.6 and Figure 5.7. These are not referred to real power measurements as for the renewable sources, but they have been designed according to the maximum power that the network can generate. It is recalled that the final effective power absorption will not be the one showed in the figures but it will vary as voltages and frequency shift from their nominal values. Moreover, the power trends have been designed to be sufficiently noisy in order to test the control performances in the presence of sudden power steps of the corresponding loads.

Finally, the auxiliary systems absorb constant powers, which entities have been previously illustrated in Table 5.2.
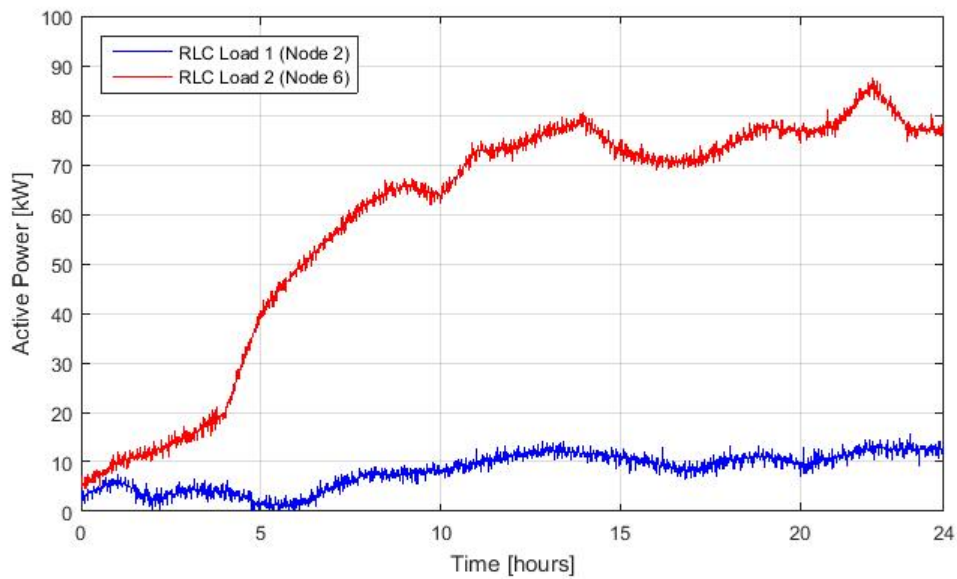
Figure 5.6: RLC Loads: Active Power Profiles
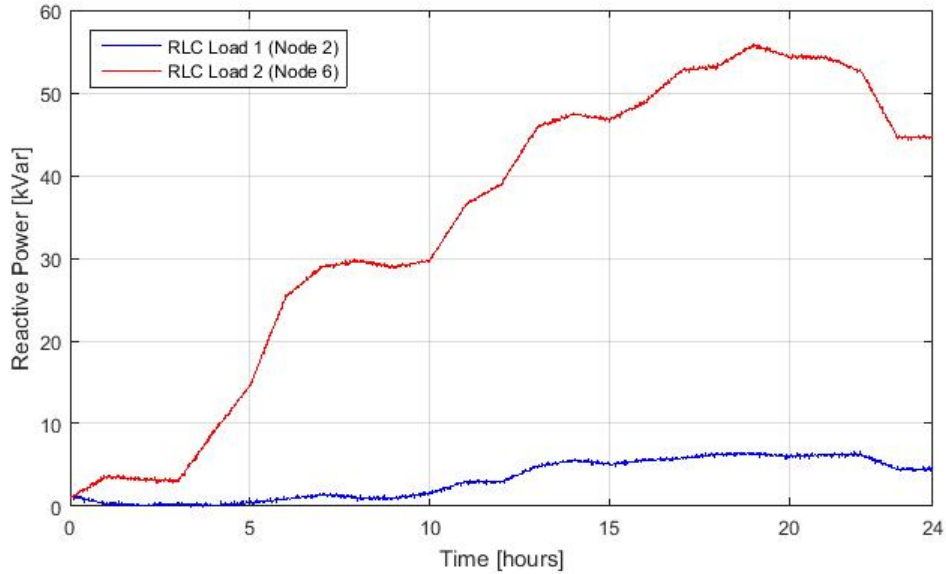
Figure 5.7: RLC Loads: Reactive Power Profiles

Also some specifications for the generation units need to be defined, and these are related to the initial states of charge of batteries and power references' of the controllable generation sources. Finally, as discussed in the previous chapters, it is required that a slack node is defined since each phase is refereed to this node. In the following simulations, it is assumed that the Node 1 is the slack one.

Having defined all the simulation details, now the system simulations can be performed. Before testing the designed control structure, the open-loop system responses are evaluated. Actually, although these are not of specific interest for the purpose of this work, they will show the problems characterizing an islanded microgrid, as previously described in the paragraph 2.1.

5.3.2 Open-loop system responses

It is recalled that during the islanded mode any power mismatch between the absorbed and the generated power is no more compensated by an import or an export with the main grid, but it directly impacts the network variables, possibly taking the values that ensure the balance between the total generated and absorbed power. In the following simulations, frequent unbalances will occur since the microgrid is subject to varying absorbed and generated powers due to the presence of loads and renewable sources.

67

In the open loop simulation, the uncontrollable sources will follow the power trends presented in the previous paragraph, while the dispatchable generators will be characterized by the initial conditions defined in Table 5.5.

	P^{gen_ref}	Q^{gen_ref}	SOC
Battery 1	1 kW	0 kVar	30%
Battery 2	1 kW	0 kVar	70%
Battery 3	1 kW	0 kVar	70%
Rotating Generator	5 kW	0 kVar	——

Table 5.5: Initial Conditions

The initial reference powers have been chosen to satisfy the initial load power absorption, which, as shown in the previous figures, is considerably small in the initial time instants. What is more, it is recalled that, being the system simulated without the action of the hierarchical control structure, the generation units will deliver constant powers for whole simulation time.

Having defined the power condition for each microgrid element, now the system open loop simulations are presented. In Figure 5.8 and Figure 5.9 the frequency and voltages responses are illustrated for a 15 hours simulation. By looking at the graphs, it is possible to actually realize which problems are related to the islanded operating mode. In fact, neither the microgrid frequency nor the voltages evolve inside the regulation bounds (which correspond to the black horizontal dashed lines depicted in the figures), but they are characterized by serious large deviation from their nominal values.

To ensure the system correct operation, the frequency should be kept at 50 Hz, while the line-to-line voltages must evolve around 400 V. As explained in paragraph 2.1, since the Tellengen's theorem must be valid in each power condition, the network variables considerably deviate from their nominal values so that the actual power generation can balance the absorbed and lost powers. Obviously, the depicted responses are not realistic and they could not be obtained in a real microgrid given the presence of many protection devices and given the fact that all the microgrid elements are designed to work around nominal conditions.
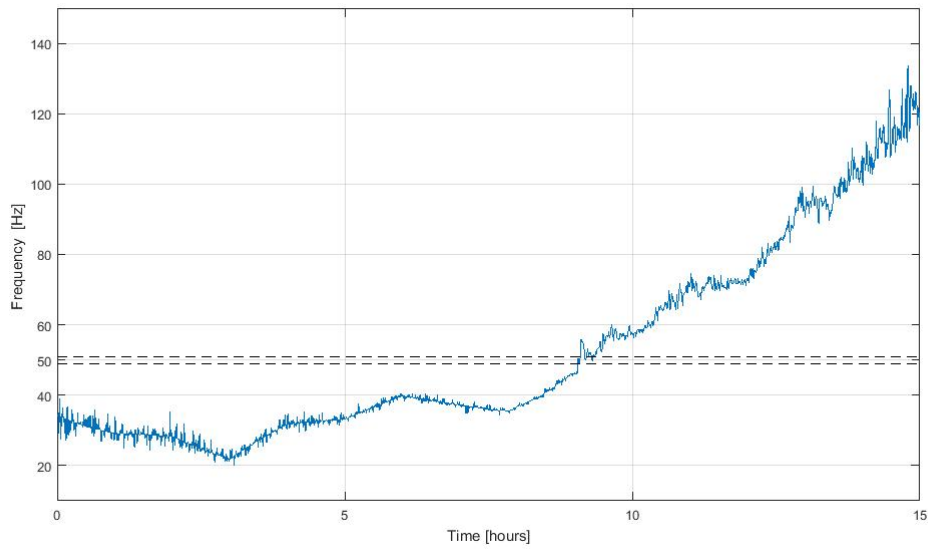
Figure 5.8: Open-Loop system: network frequency response
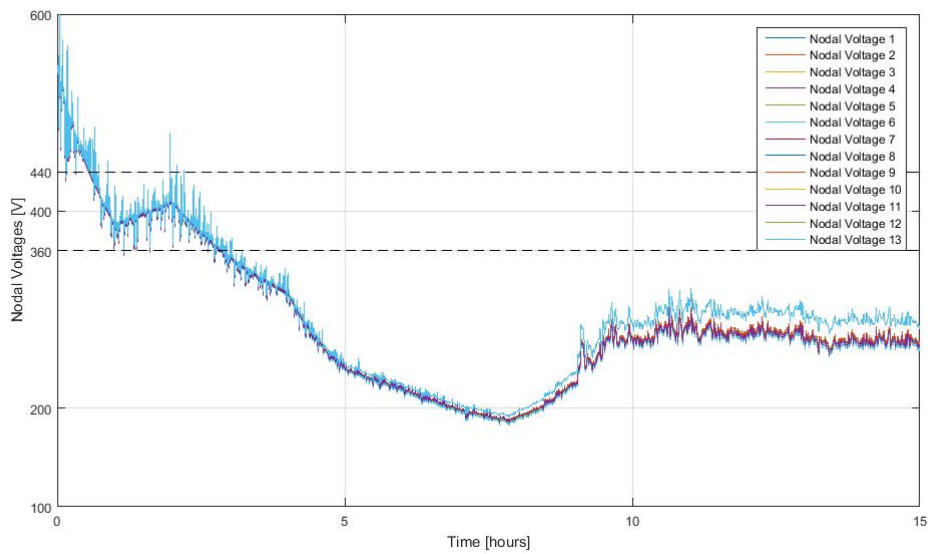
Figure 5.9: Open-Loop system: nodal voltages responses

As reported in the second chapter, the presented problem could be solved by designing a control system able to promptly vary the generated powers in case the network variables deviate from their nominal values.

69

This would considerable reduce the power unbalance, eventually leading the network variables to reach steady-state values not so far from their nominal values. However, another important requirement is that this control system performs a fast control action since we are dealing with a low-inertia system and therefore voltages and frequency may quickly reach steady-state values that are not allowed by the regulations. All these features can be achieved by implementing the primary control layer that has been described in the second chapter. In the following paragraph its actual implementation will be described, and also some simulations will be performed in order to test the relative performances.

5.3.3   Primary Control: Implementation and Tests

As discussed in previous chapters, the primary control consists in two sequential sublayers, i.e. the inverter output control and the droop control. The droop control can be considered the most significant layer since it is designed to vary the generated powers based on the deviation of the network variables from nominal values. For the purpose of this work, the inverse resistive droop control approach has been adopted. This links the variations of voltages to the variations of active power and the variations of frequency to the variations of reactive power through a proportional control action. Being defined as a decentralized structure, this system is located at each generation unit; its scheme is again represented in Figure 5.10.
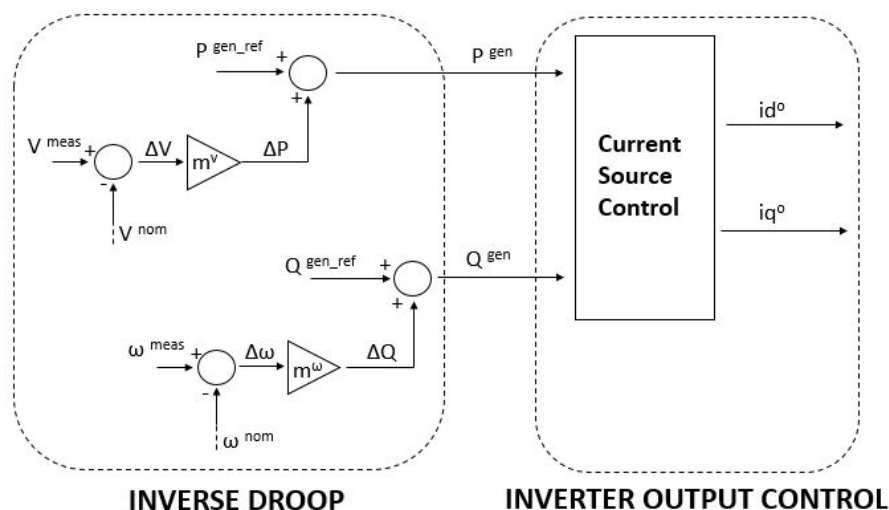
Figure 5.10: Inverse Resistive Droop

The resistive configuration implies that the proportional gains must be chosen such that $m_i^v < 0$ and $m_i^\omega > 0$, where $i \in (1, ..., ncg)$ corresponds to the i_{th} generator. This results from the considerations made in paragraph 2.4 about the relationships between powers and network variables in a resistive network with RLC loads; this actually corresponds to the analysed microgrid test case.

There is no a fixed rule to choose the exact values of m_i^v and m_i^ω, although their magnitudes have a significant impact on the network since they express how the requested power is distributed among the generators.

In this work the proportional gains have been defined as reported in equation 5.1, where V^{max}, V^{min}, ω^{max}, ω^{min} correspond to the bounds imposed by CEI norms [13].

$$
\begin{cases}
m_i^v & = -\left(P_i^{gen\_max} - P_i^{gen\_min}\right) / \left(V^{max} - V^{min}\right) \\
m_i^\omega & = \quad\left(Q_i^{gen\_max} - Q_i^{gen\_min}\right) / \left(\omega^{max} - \omega^{min}\right)
\end{cases}
\tag{5.1}
$$

By setting the droop parameters as above reported, the variations of generated powers will be not equally distributed but they will depend on the active and reactive power limits of each generation source. In this way, the bigger is the power variation range that a unit can afford, the bigger will be the relative droop proportional gain.

With regard to batteries and renewable sources, some small modifications to the droop scheme have been implemented. As far as the batteries are concerned, it should be noted that if the state of charge reaches its lower bound, the storage unit should no more generate active power but only absorb it. The same holds if the upper bound is reached, where the battery must no longer store charge but it could only generate power. To make the droop work according to these limitations, a simple algorithm has been designed as follows.

If the SOC reaches its lower bound, the droop functions will be modified setting the maximum output power to zero. In this way, since the maximum generating power is set to zero, only output negative powers are allowed and therefore it will be only possible to absorb energy. On the contrary, if the SOC upper bound is reached, the algorithm will prevent the battery to absorb additional power by setting the minimum output power to zero; in this way the battery can only generate power.

Concerning the renewable sources, it is quite obvious that the generated active power can not be increased with respect to the reference value since it is not a control variable, but it depends on the actual solar radiation or wind speed. Moreover, it should be noted that the active power generated by green energy sources does not cost anything and therefore it would be also a waste to decrease it only for small variables' deviations.

Hence, the implemented local droop controller has been designed such that the output active power is never increased; while it is decreased only in case of a serious voltage deviation from the nominal value. As for the reactive power droop control, it has been implemented in the same way of the other generation units, since the output reactive power does not depend on the weather conditions but only on how the inverter is controlled. The implemented droop characteristics for the renewable sources are depicted in Figure 5.11, where P^{gen_ref} corresponds to the power generated by the renewable source, while Q^{gen_max} and Q^{gen_min} take the values described in Table 5.4.
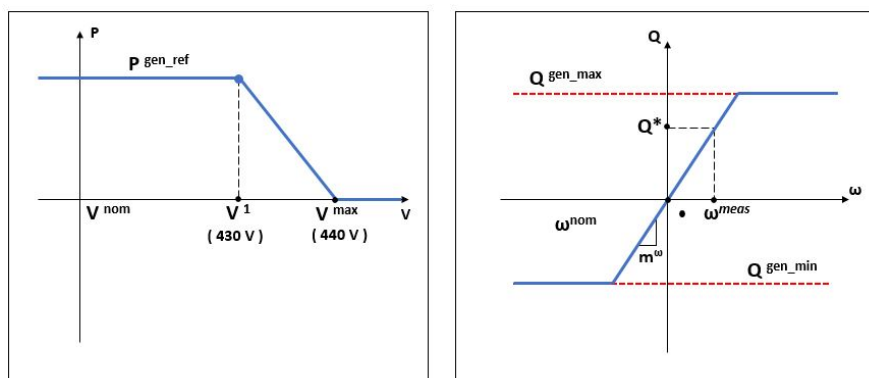
Figure 5.11: Renewable sources: implemented droop characteristics

Once the primary controllers for each generation unit having been defined, now the overall responses will be illustrated. These have been performed in the same set considered for the open-loop simulations, therefore by imposing the same power profiles to the uncontrollable units and the same initial conditions to the generation units. Given the primary control action, in this case the final effective generated powers will be not equal to the reference powers depicted in Table 5.4, but they will be varied according to the local network variable deviations from their nominal values. This can be easily seen from the Figure 5.12 and Figure 5.13, where the effective generated powers show a varying trend.
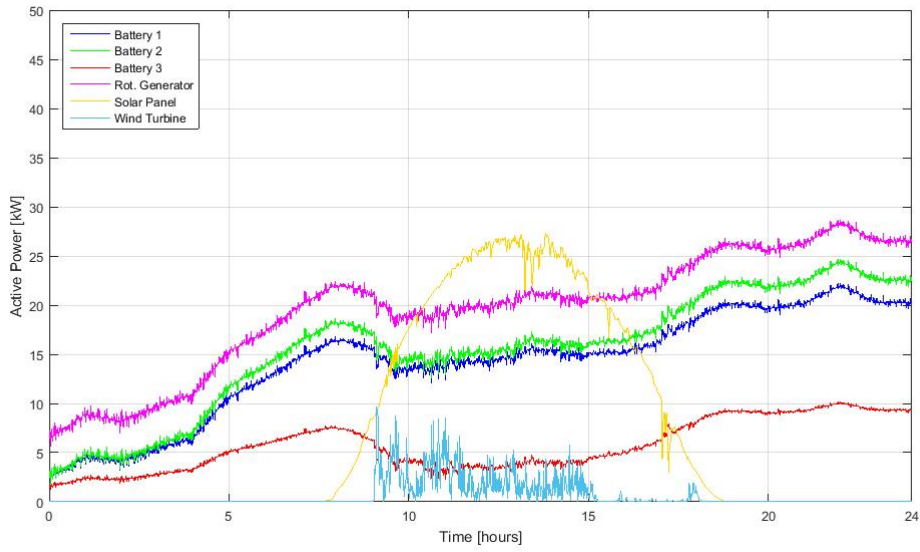
Figure 5.12: Primary control: generated active powers responses
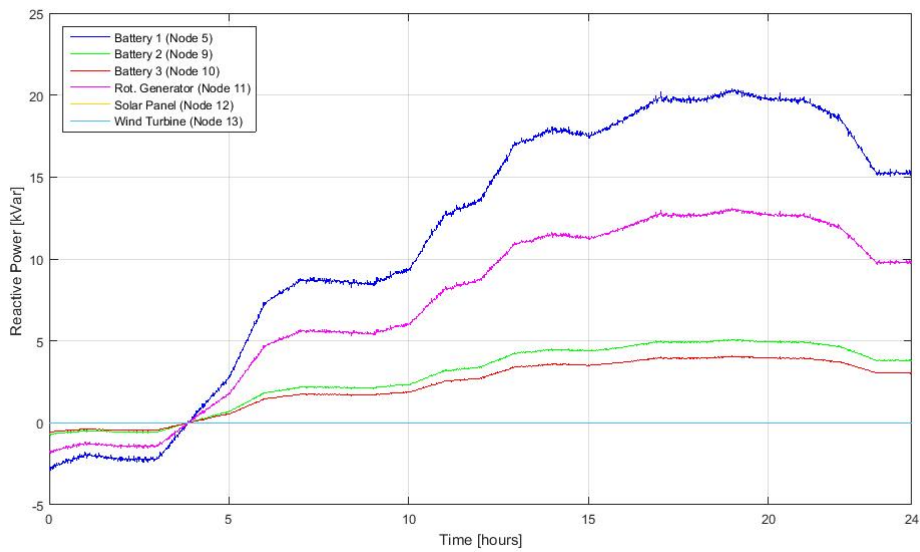
Figure 5.13: Primary control: generated reactive powers responses

Although the powers are varied by simple proportional gains, the requested load power has been efficiently distributed among the controllable generation sources. Regarding the dispatchable units (i.e. batteries and rotating generator), the power distribution is obviously not equal since it depends on the droop parameters. As above reported, the droop control has been designed such that the more power a unit can either generate or absorb, the larger will be the relative power variation.

With regard to the network variables, by looking at Figure 5.14 and Figure 5.15 it is possible to appreciate significant improvements with respect to the open loop case. Indeed, the droop scheme is able to keep the network variables around realistic values, respecting for most of the time the bounds imposed by the regulations.

However, it can be surely noted that neither the frequency nor the voltages keep their nominal values, which are 50 Hz and 400 V, respectively. This is more relevant feature for the frequency, since it is recalled that, in case of a possible reconnection with the main grid, it is strictly required that at the interconnection the two systems are synchronized at the same frequency. About nodal voltages, it is possible to notice that they show a decreasing behavior due since the load powers are continuously increasing over the whole day, as reported by Figure 5.6 and 5.7. It can be appreciated that the active power generated by renewable sources gives a great help since it prevents the nodal voltages to drastically exceed the lower bound. This is witnessed by an evident increase on the nodal voltages trend over the central hours of the day. However, once the active power from renewable sources come back to zero, the droop control is not able to keep the voltages above the lower bound.

Finally, in Figure 5.16 the states of charge are illustrated, showing obviously a decreasing trend; in fact the batteries have generated power for the whole simulation time. The amount of discharged energy is not equal among the different batteries both because they generated different values of active power and also because they are characterized by different capacities and charge/discharge coefficients, as previously shown in Table 5.1.

As the following figures show, although the primary controllers guarantee great improvements with respect to the open loop case, they are not the best solution to manage an islanded microgrid. Pure proportional actions are in fact extremely efficient in ensuring a fast and considerable reduction of network variable deviations, but they are not able to make the network variables evolve close to their nominal values. Moreover, through this simple control structure is not possible to implement any resource management logic, taking for example the remaining states of charge of the batteries or some economic factors.
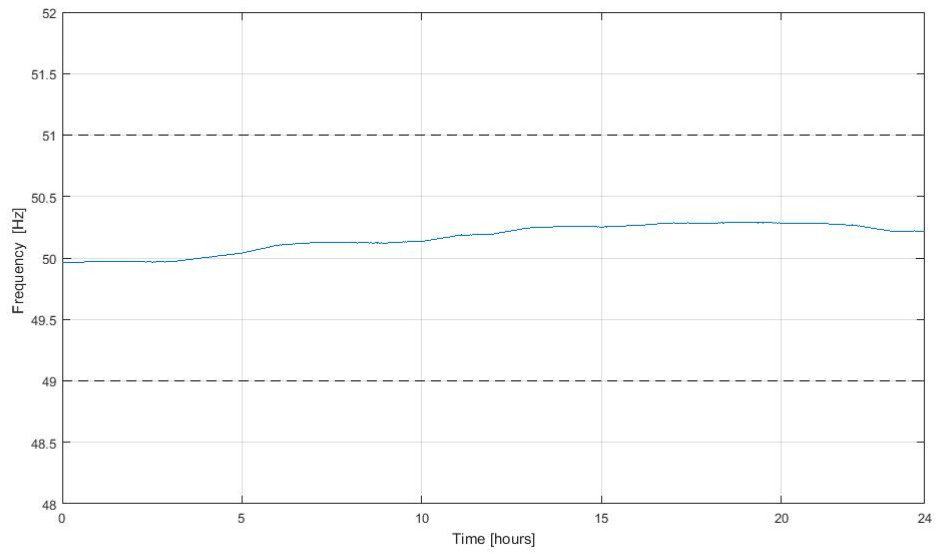
Figure 5.14: Primary Control: network frequency response
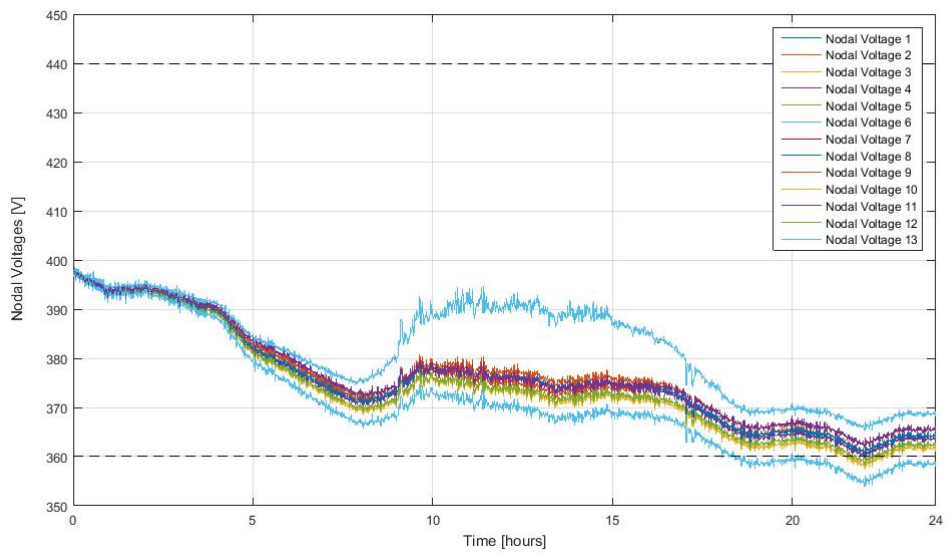
Figure 5.15: Primary Control: nodal voltages responses

75
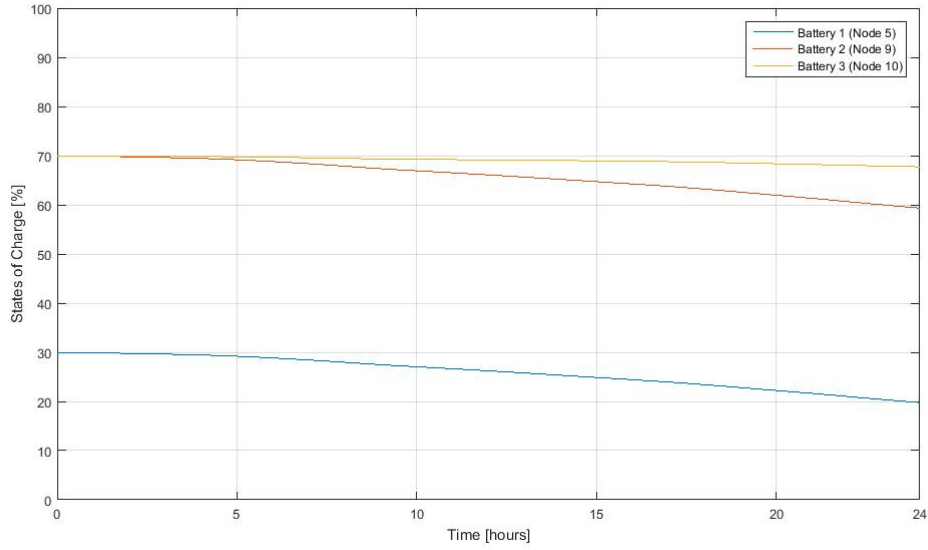
Figure 5.16: Primary Control: batteries' SOCs responses

There is an additional degree of freedom that this control structure is not exploiting, which corresponds to actually vary the reference active and reactive powers according to the network conditions. In this way in fact, the steady-state deviations can be furtherly decreased and an efficient resource power management can be implemented. These motivations lead to the design of a higher control layer, which actual implementation have been largely described in the fourth chapter. The numerical results of the complete hierarchical control structure will be shown in the next paragraph.

5.3.4 Hierarchical Control: Implementation and Tests

The use of a centralized secondary controller allows to ensure an efficient coordination of all the controllable units, achieving the defined control objectives. The secondary control layer is composed of two main elements: the frequency integrator and the Model Predictive Controller, which have been largely discussed in the previous chapters. Before showing the main results of the performed simulations, some considerations on the design specifications are worth to be described; these are reported in the next paragraph.

Secondary Control: Design Specifications

Time Frame: The secondary control acts at a lower rate with respect to the primary control layer so that it can be supposed that the network variables have already reached the steady-state condition. In the following simulations, the secondary control will be designed to run each minute. This leaves also enough time to the central controller to perform all the required computations. Actually, since the secondary controller relies on a centralized optimization algorithm that has both to measure all the nodal network variables and also to send inputs to the dispatchable generation units, it can not obviously be characterized by slow time constants.

Prediction Horizon: One of the main feature of the MPC algorithm is that the optimization is performed taking into account also future values of the system variables. For the purpose of this work, the number of the considered future time steps has been implemented to be the same for each control iteration, following the *Receding Horizon* approach. The extension of the prediction horizon has been designed to be 5 steps ahead, which actually correspond to a prediction of 5 minutes. A schematic representing the implemented Receding Horizon method is depicted Figure 5.17, where N_k indicates the prediction horizon that is taken into account at each iteration $t = k$.
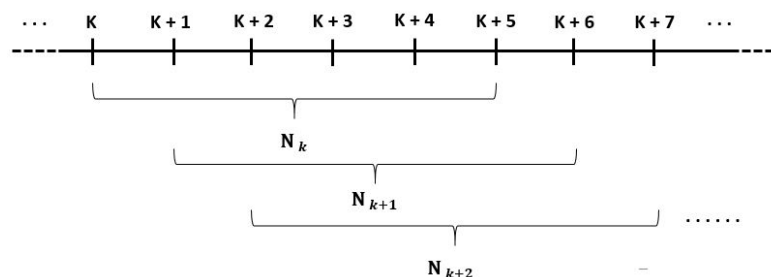
Figure 5.17: Receding Horizon Approach

It is recalled that that the prediction horizon should be of limited size for two main reasons. On the one hand, the longer is the prediction horizon, the more time will be required to perform the optimization algorithm. On the other hand, the predictive model relies on a linearization process that accurately describes the network dynamics only in the neighborhood of the considered equilibrium condition. This implies that the longer is the prediction horizon, the less accurate the future predictions will be.

Knowledge of the system: At this stage, it is supposed that the secondary controller has a complete knowledge of the network parameters, as well as of the units' characteristics. Moreover, also the predictions of the power trends of loads and renewable sources are supposed to be available. Since it is quite difficult to have such detailed information on the system, in the Section 5.4 a more realistic implementation will be taken into account.

Cost Function and Constraints: Looking at the actual optimization problem, the weights of the cost function have been set so that the network variables' deviations have more importance than the other system variables in the minimization process. At this stage, the optimization process does not take into account a possible resource management strategy and therefore all the generation sources are equally weighted in the cost function.

Concerning the variable constraints, their implementation have been already described in the fourth chapter, where most of them refer either to regulations' bounds or to physical limits. This does not hold for two precise constraints, whose the corresponding bounds are design parameters. The former defines the SOC maximum and minimum recommended bound, which have been set to be 20% and 80%. Moreover, since also the control inputs corresponding to the variations of reference powers are limited, and in the following simulations a maximum variation of ± 5 kW (kVar) will be allowed.

Moreover, an additional constraint needs to be defined since the rotating generator is not characterized by a pure squared capability curve but also a limitation on the minimum power factor exists (look at Figure 5.3). This means that a constraint taking into account the ratio between the actual generated active and reactive power has been also implemented.

Hierarchical control simulations

Once all the MPC parameters have been set, the actual simulations can be performed. As in the previous tests, the power trends illustrated in the Figures 5.5, 5.6 and 5.7 will be implemented, as well as the same initial conditions. However, it is recalled that now also the reference ones will be varied by the hierarchical control structure so that smaller voltages and frequency deviations are allowed. The final simulations' outcomes are illustrated in the following figures.
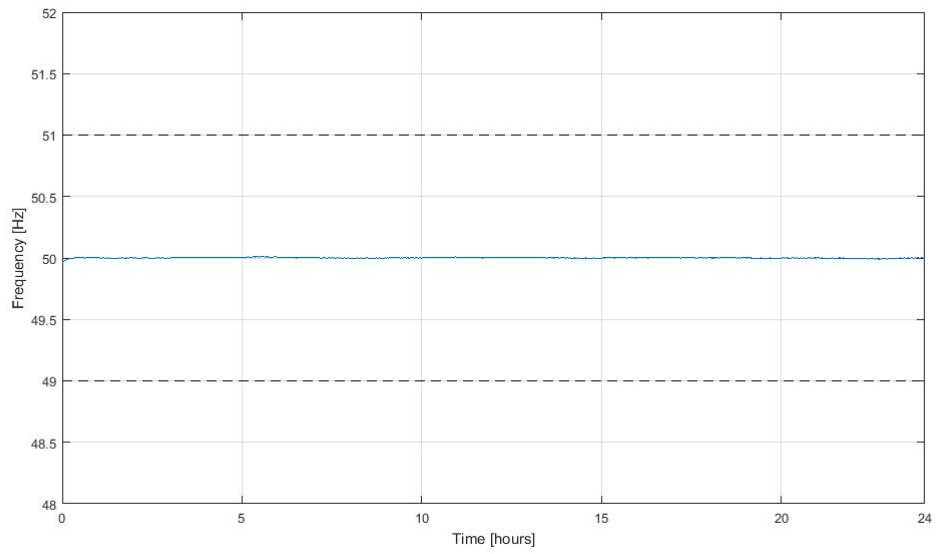
Figure 5.18: Hierarchical Control: network frequency response
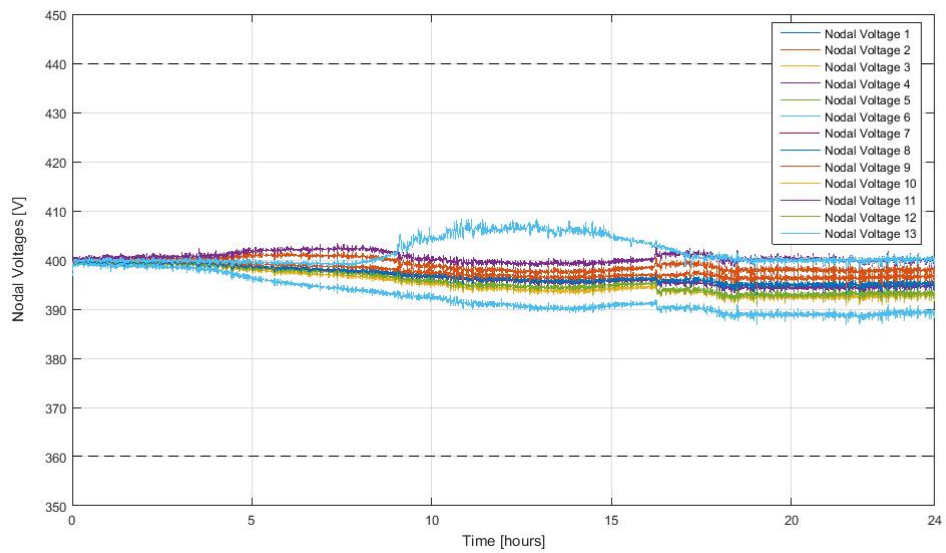
Figure 5.19: Hierarchical Control: nodal voltages responses

79
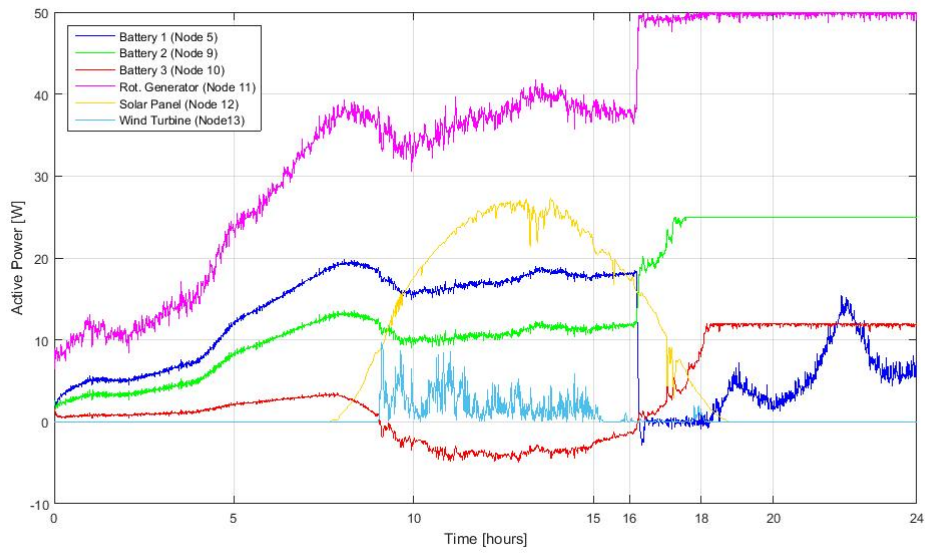
Figure 5.20: Hierarchical Control: generated active powers responses
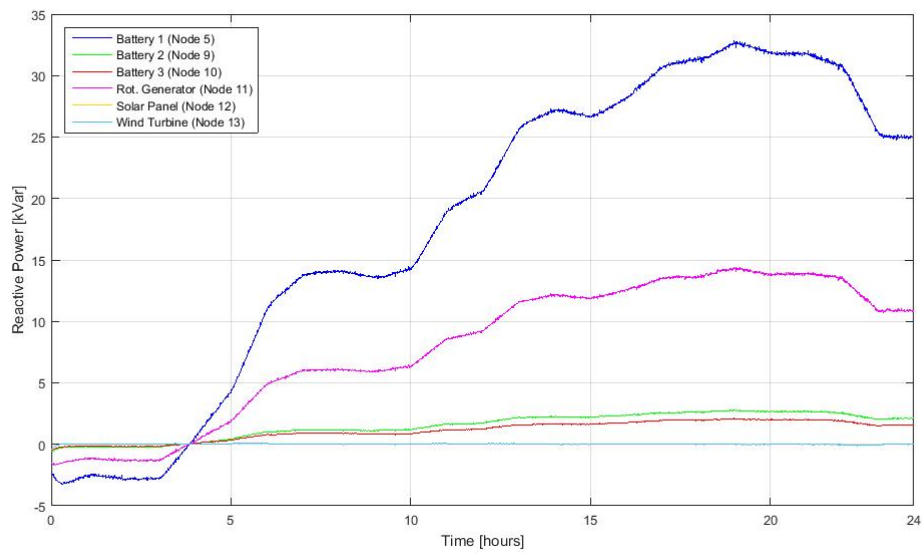
Figure 5.21: Hierarchical Control: generated reactive powers responses
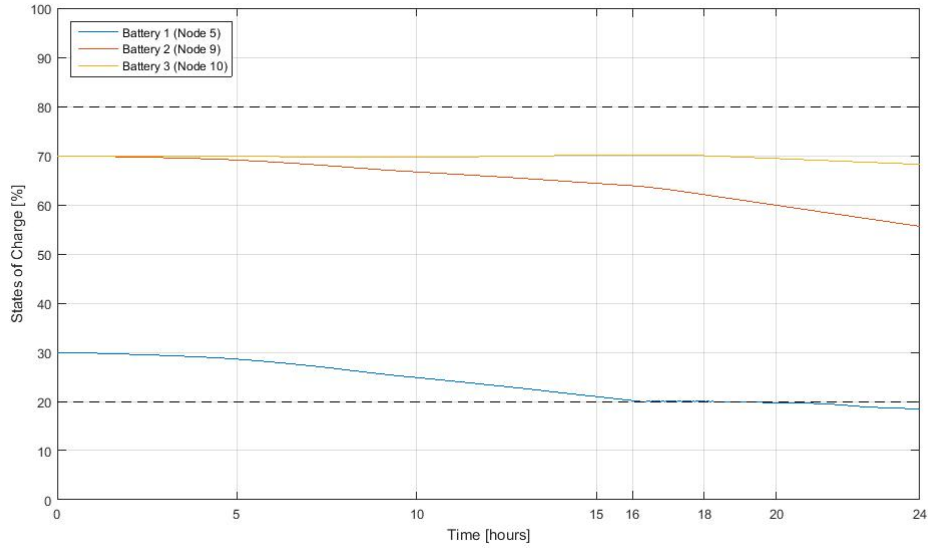
Figure 5.22: Hierarchical Control: batteries' SOCs responses

By looking at the first two graphs, the main achievements of the designed control structure can be appreciated. Actually, by performing the system simulations with exactly the same initial conditions, it can be noticed that now the network variables evolve really close to their nominal values for the whole simulation time. Moreover, the microgrid frequency shows an almost null static error due to the presence of the integrator, properly placed as described in the previous chapters. On the other hand, voltages are not exactly equal to their nominal value, but they are kept between 390 V and 410 V. This can be considered quite satisfactory since the network can afford small voltage deviations without any consequence. What is more, given the flexibility of the cost function, if a lower voltage offset was required it would be enough to increase the corresponding weight.

A more accurate look at the active and the reactive powers shows that a bigger amount of power is generated with respect to the previous cases. This is more evident for the active powers, since three out of four generation sources reach their maximum power limits in the final part of the day, according to their parameters previously defined. This is because the generation powers try to equal the actual power absorption in order to minimize the variable deviations, taking eventually greater values with respect to the previous simulations.

Remark: As far as the states of charge are concerned, it is worth noticing that they are kept inside the recommended bounds for most of the simulation time, apart from the battery placed at node 5, indicated as battery 1; this behavior is not surprising according to the implemented secondary control logic. Actually, the SOC of the battery 1 reaches the lower bound at about the 16th hour. Given the imposed constraint, the secondary control layer modifies the corresponding active power so that it is set to zero when the SOC reaches its lower bound, as it can be noticed from Figure 5.20 by looking at the blue trend. However, at about the 18th hour, all the remaining generators have reached their active power limits, although the active load power absorption continues to increase. Since the main control objective is to keep the network variables near to the nominal values, the MPC decides to allow the battery 1 to generate the remaining load power, furtherly discharging the battery SOC. It is in fact recalled that the operations bounds for the states of charge have been implemented as Soft Costraints, which in some cases can be violated.

To sum up, starting from the description of the considered test case, the hierarchical control structure shows great improvements with respect to the previous cases. Indeed, although the microgrid is subject to varying and noisy power trends, the network variables never exceed the bounds imposed by the regulations and, what is more, they maintain their nominal values for the whole simulation time. Nevertheless, to test the robustness of the designed control system, in the next sections additional simulations will be presented.

5.4 System Robustness Tests

In this section, the control framework will be tested in three different scenarios. Firstly, it will be supposed that the control system has a pretty limited knowledge of the system parameters, testing if the designed control structure shows robust characteristics with respect to model's uncertainties. Then, it will be shown how the flexibility of the MPC approach allows to implement different resource management logics by simply changing the cost function's weights. Finally, a more realistic context will be considered, testing the control structure with identified load models corresponding to real utilities.

5.4.1 Limited knowledge of the system

In this section, some features of the implemented MPC algorithm have been removed, although they could be considered feasible from a theoretical point of view.

In the previous chapters, it was supposed that the control system had a complete knowledge of the future power trends of the uncontrollable units, which have been modeled as known disturbances. Moreover, also the dependence of the load power with respect to the network variables was assumed to be available, being actually inserted in the network jacobian (see paragraph 3.3). This does not represent a realistic implementation since it is quite difficult to have such detailed data on the load characteristics. Therefore, taking into account a more realistic view, in the following simulations it will be supposed that all the information about the uncontrollable sources, both related to their internal parameters and future power trends, are not available to the central controller.

Moreover, it is unlikely the case that an exact knowledge of the line impedances is accessible. It should be also noted that, depending on the circulating currents, the line impedances' values can considerably grow with respect to the nominal values, as reported in [28]. Because of this, in the following simulations it will assumed that only the nominal values of line impedances are known to the controller, while the real implemented values have been increased by a 50% factor.

Obviously, introducing the above mentioned uncertainties of the real parameters implies that the hierarchical control structure will rely on a slightly wrong system model and consequently the computed control actions may be not the optimal ones to implement.

In the following simulations, the same initial conditions and power trends illustrated in paragraph 5.3.1 have been implemented. The figures show that, although the controller has not an exact knowledge of the system, the main control objectives have been achieved. It can be noticed that the voltages are slightly more noisy and slightly more distant from their nominal value with respect to the previous test. However, their trends are satisfactory since it is recalled that voltages are not required to evolve exactly at their nominal value, but it is more relevant that they never exceed the imposed bounds.

Finally, with regard to the generated active and reactive powers, respectively depicted in Figure 5.25 and Figure 5.26, it is possible to note that they do not show such a different behavior with respect to the base case. This is due to the fact that they do not significantly depend on the knowledge that the controller has about the system, but their trends are more related to the uncontrollable power profiles and to the implemented control strategy in the cost function.
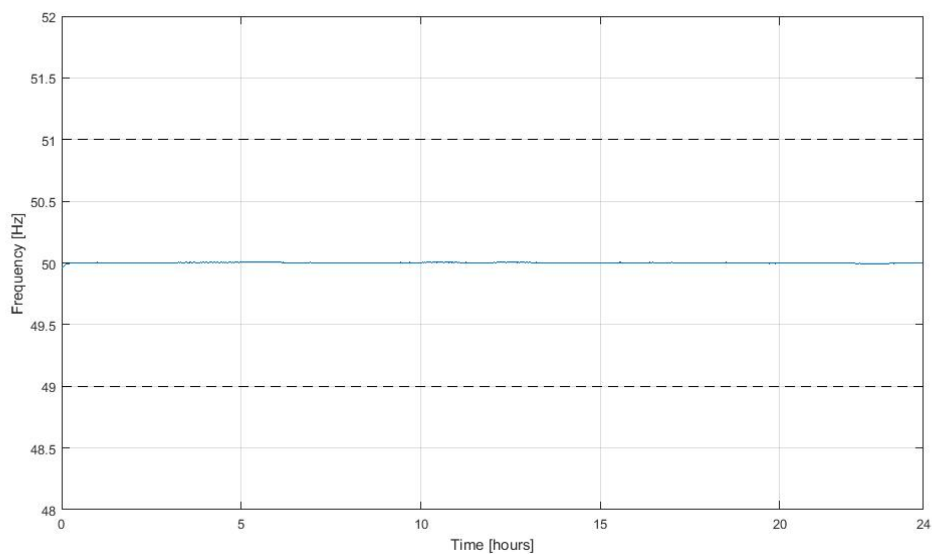
Figure 5.23: Limited System Knowledge: network frequency response
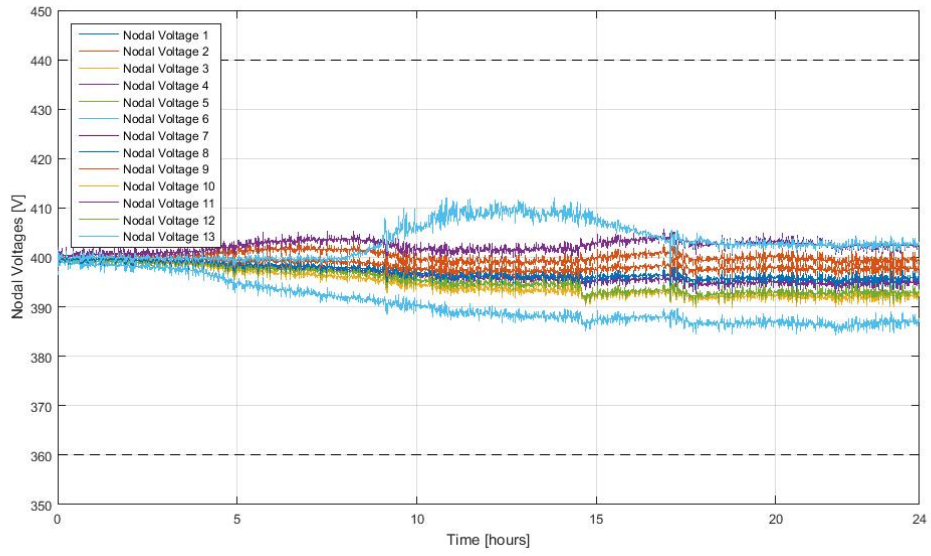
Figure 5.24: Limited System Knowledge: nodal voltages responses
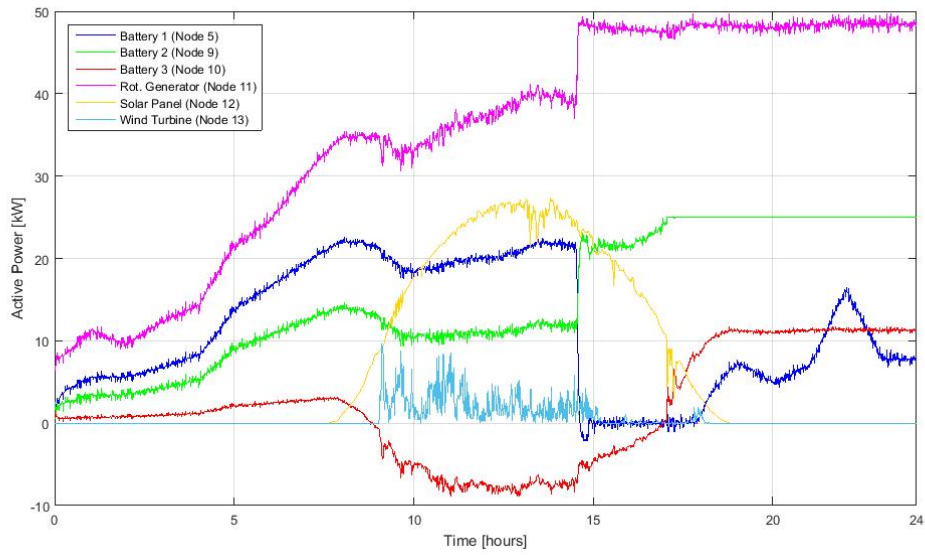
Figure 5.25: Limited System Knowledge: generated active power responses

85
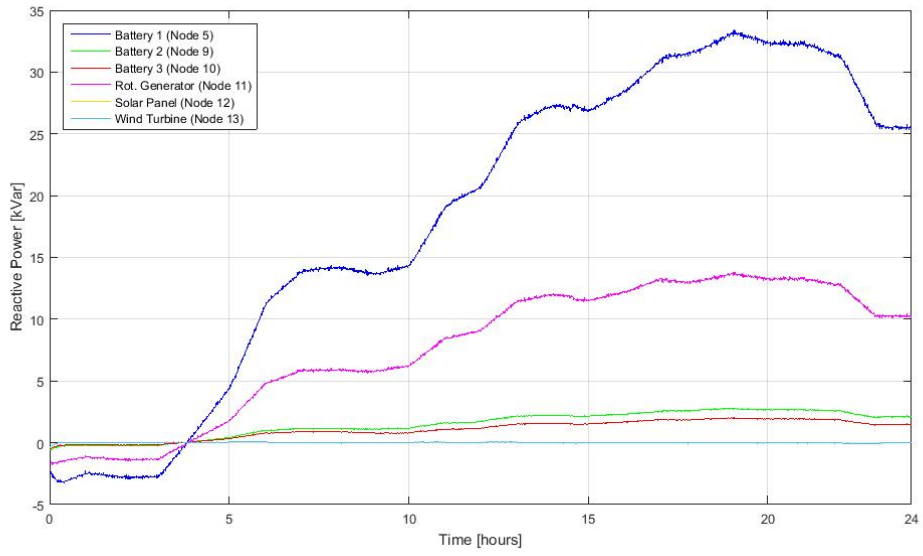
Figure 5.26: Limited System Knowledge: generated reactive power responses
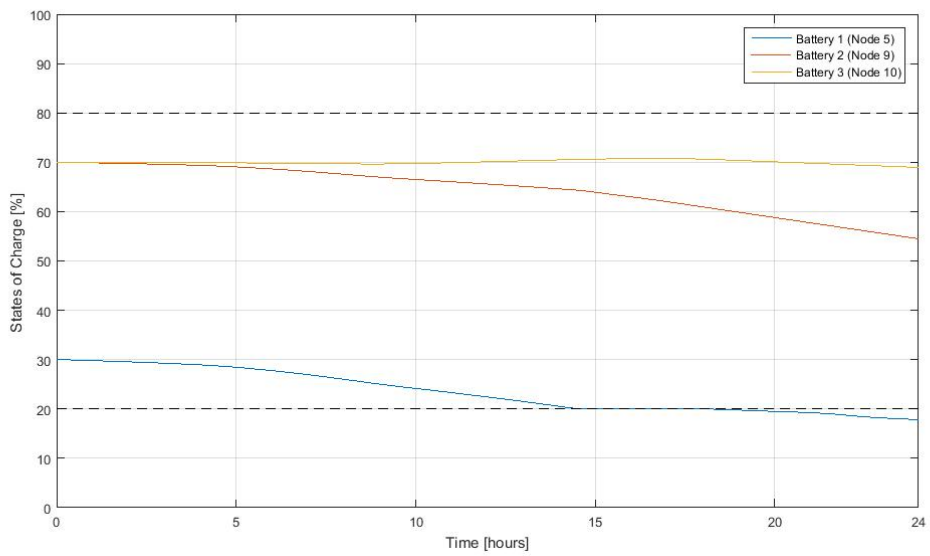
Figure 5.27: Limited System Knowledge: batteries' SOCs responses

86

The previous figures show that the developed control system is quite robust with respect to the introduced uncertainties. Actually, although a complete knowledge of the system parameters was not available, the combined action of the primary and secondary control layers was however able to manage the considered microgrid in the islanded operating mode accomplishing the defined control objectives.

5.4.2 Resource Management Control Logics

At this stage, a control logic that manages the different sources according to predefined targets has not still implemented. Depending on the considered scenario, there could be some circumstances where it is more convenient to exploit one kind of source rather than another. To implement simple resource management strategies, it is enough to change the values of some weights of the defined cost function. This will be shown taking into account two possible case examples, which be presented in the next paragraphs. In the following simulations, the uncontrollable power trends previously illustrated are implemented, while the initial conditions are set as reported in Table 5.6.

	P^{gen_ref}	Q^{gen_ref}	SOC
Battery 1	5 kW	0 kVar	50%
Battery 2	5 kW	0 kVar	50%
Battery 3	5 kW	0 kVar	50%
Rotating Generator	5 kW	0 kVar	——

Table 5.6: Resource Management Control Logics: Initial Conditions

Moreover, considering a more realistic implementation of the defined control structure, the model uncertainties introduced in the previous section will be kept for the following tests.

Economic Microgrid Management

There are some cases where it is better to minimize the energy provided by the rotating generator and to greatly exploit the storage units and the renewable sources. For instance, if it is expected that the microgrid will operate in islanded mode only for few hours, it is not fundamental to preserve the energy stored in the batteries for a future use, but it could more convenient to take into account some economic factors. Actually, differently from batteries, the energy provided by the rotating generator has a significant cost since it is based on a fuel combustion process.

A simply way to implement the corresponding control logic corresponds to modify cost functions parameters such that the active power provided by batteries is considerably less weighted with respect to the one generated by the rotating source. Implementing that case, the responses of the main variables are illustrated in the following figures.
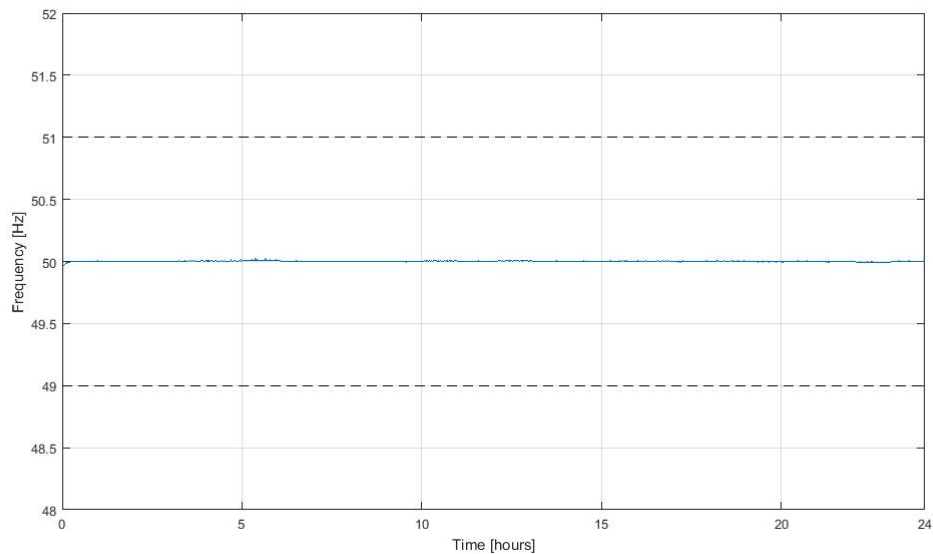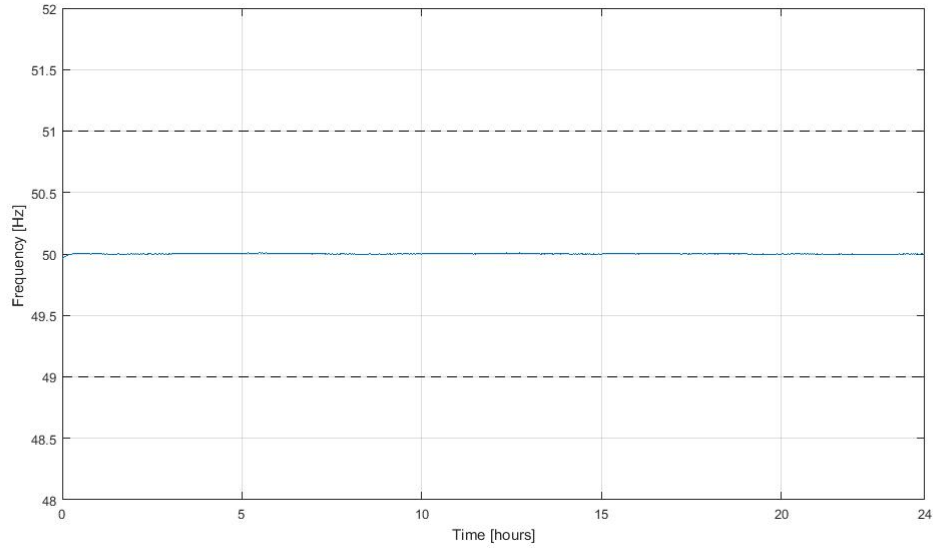

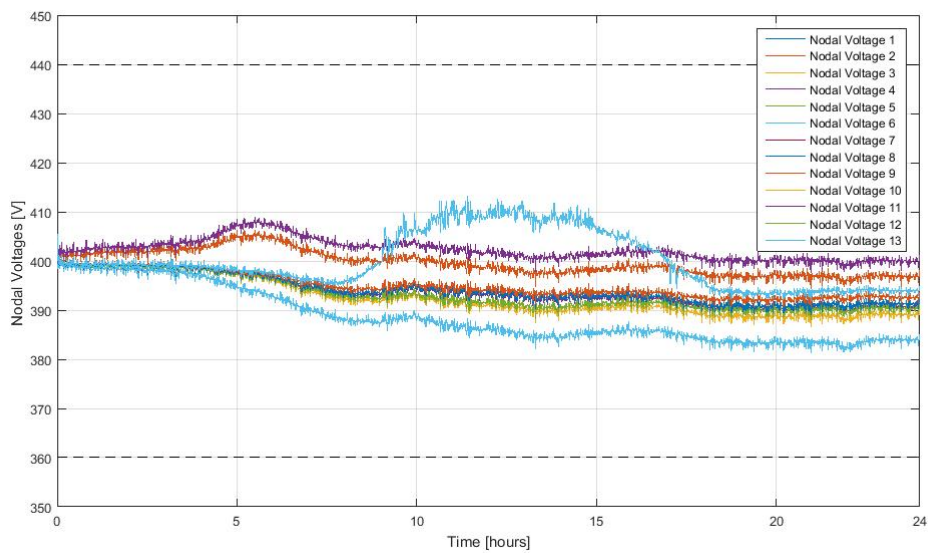Figure 5.28: Economic Microgrid Management: network frequency response
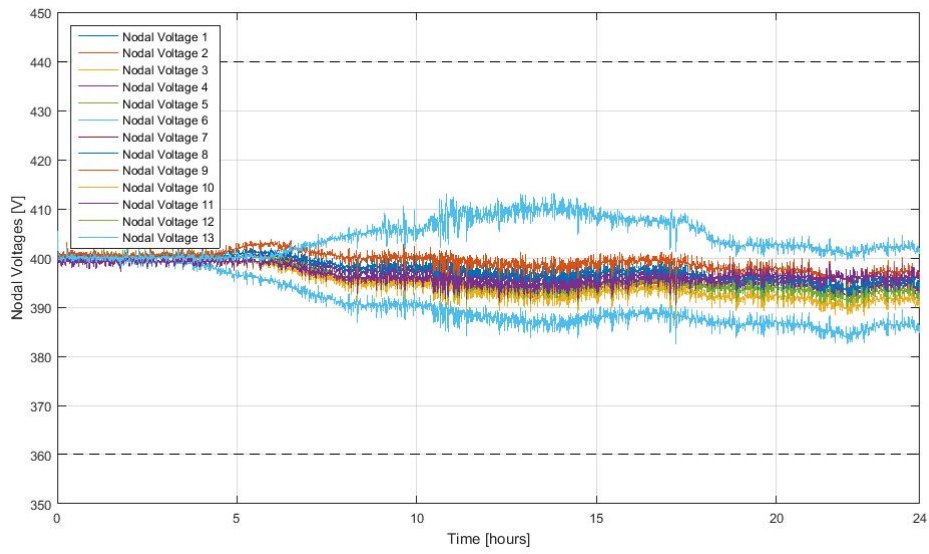
Figure 5.29: Economic Microgrid Management: nodal voltages responses
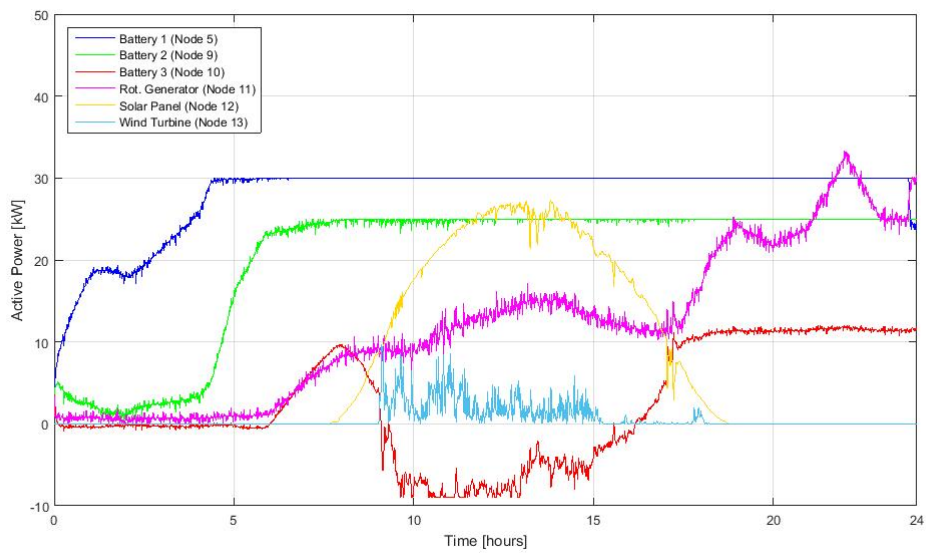
Figure 5.30: Economic Microgrid Management: generated active power responses
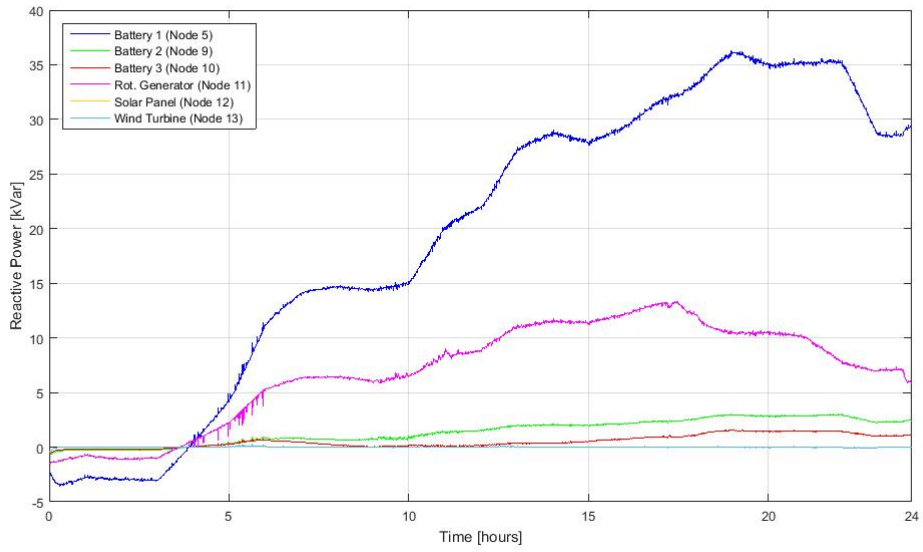
Figure 5.31: Economic Microgrid Management: generated reactive power responses
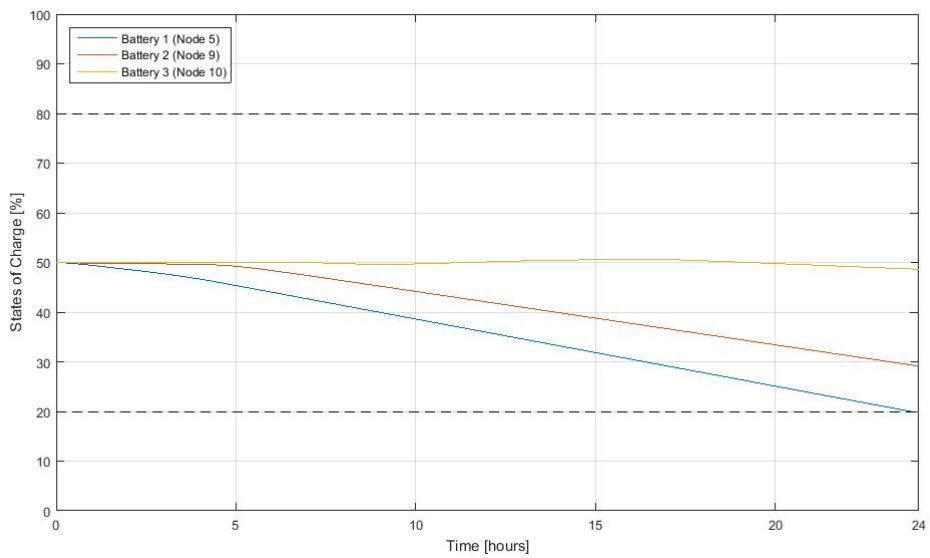
Figure 5.32: Economic Microgrid Management: batteries' SOCs responses

90

The figures show that it has been possible to implement a "cheaper" resource management strategy, without affecting the network system variables. Actually, the frequency is always kept at its nominal value while the voltages continue to evolve pretty far from the bounds imposed by the regulations. By comparing the Figure 5.30 and Figure 5.25, it is possible to notice that in this case the rotating generator delivers a considerably smaller amount of energy with respect to the previous cases. It in fact reaches a peak of 33 kW only in the final part of the day where it is recalled that the power absorption significantly increases.

Remark: Looking at Figure 5.30, it can be noticed that during the central part of the day the battery 3 absorbs energy, taking negative values of output power, while the rotating generator is generating an active power between 10 kW and 15 kW. This could seem a counter-intuitive behavior since it was reported that the implemented resource management strategy minimizes the energy delivered by the combustion-based generator and tries to make only the storage units generate the needed power. Looking at Figure 5.2, it can be also noted that the battery 3, which is located at node 10, is the closest storage unit to renewable sources, placed at node 12 and 13, respectively. Moreover, when the renewable sources start to generate, since their active powers are not regulated by primary controllers in normal conditions, the corresponding nodal voltages increase. Since the designed main control objective remains to keep the network variables near their nominal values, it happens that the MPC controller considerably decreases the reference power of the battery 3 such that it absorb as much energy as possible by the green energy sources. In this way, the battery compensates the power unbalances caused by renewable generators, and consequently the network variables do not considerably deviate from their nominal values. To sum up, although resource management strategies can be implemented, the control structure is designed such that the minimization of the network variables' deviations is always the first priority.

Robust Microgrid Management

There are others cases where it could be more relevant to preserve the batteries' charge and it is more reliable to make the rotating generator produces a considerably amount of active power. For instance, if the microgrid is supposed to operate in the islanded condition for a long time, which could be unknown a priori, it is not recommended to consume all the batteries' power, but it could be more safe to sustain the microgrid with fully dispatchable generators. This simply resource management strategy can be implemented by changing the cost functions parameters such that the active powers produced by batteries are more weighted with respect to the rotating generator one.

With same simulation specifications of the previous section, the main variable responses follow.

Figure 5.33: Robust Microgrid Management: network Frequency response

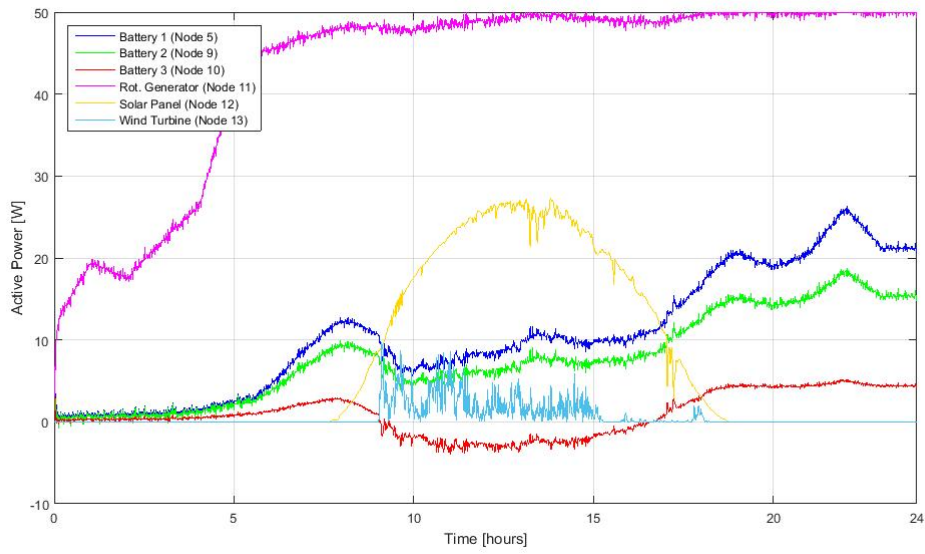Figure 5.34: Robust Microgrid Management: nodal voltages responses

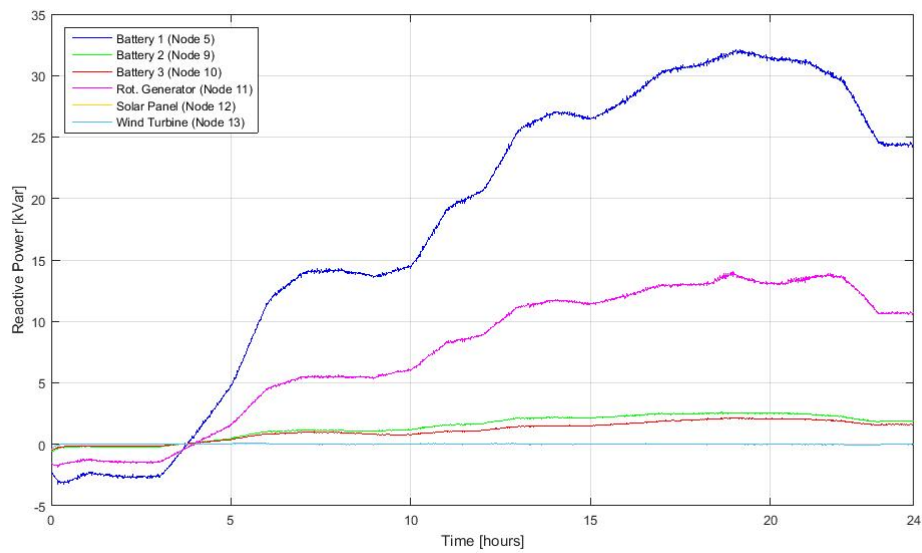Figure 5.35: Robust Microgrid Management: generated active power responses

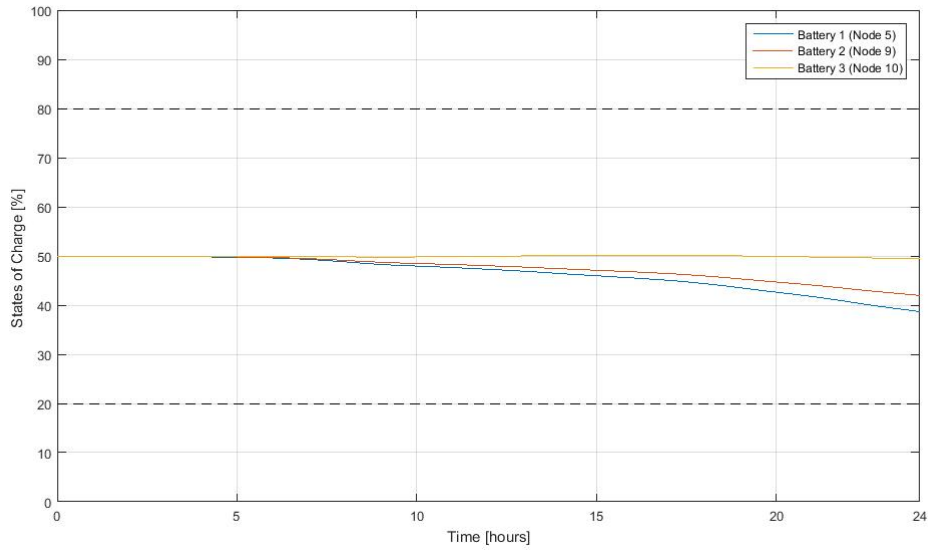Figure 5.36: Robust Microgrid Management: generated reactive power responses

Figure 5.37: Robust Microgrid Management: batteries' SOCs responses

Obviously, in this case the rotating generator produces a higher amount of energy with respect to the other sources, and this can be easily noted by looking at the Figure 5.35, where the active power trends are depicted. Moreover, by comparing the Figure 5.32 and Figure 5.37, it is possible to notice that the batteries have been considerably less discharged. Finally, also in this case the implementation of a resource management logic does not affect the main control objectives in the illustrated simulations, since the frequency remains at 50 Hz and the voltages evolve far enough from the imposed limits for the whole simulation time.

To conclude, it has been shown how flexible the designed control structure is, accomplishing different objectives with only small changes in the cost function parameters. Nevertheless, many other and more sofisticated resource management strategies could be implemented, taking into account for example the available states of charge or an equal distribution of generated powers among the sources. Actually, as described in the fourth chapter, the cost function must not take a fixed form but different objectives can be implemented.

5.4.3   Realistic loads

It is worth underlining that so far the designed control structure has been tested considering two parallel RLC loads. As reported in paragraph 2.4, they are defined by a pure resistive dependence between the network variables and the absorbed powers, for instance implying that the active power and the network frequency are completely decoupled. This does not represent real utilities characteristics, where all the variables are usually coupled. Moreover, since the primary controllers have been implemented through droop resistive relationships, it is not so surprising that they are able to prevent the network variables to largely deviate in case only RLC loads are present.

Taking into account a more realistic microgrid context, in this section the designed control structure will be tested considering two different loads, which are not characterized by an ideal resistive behavior. As reported in paragraph 3.4.4, the load static models can be obtained through identification procedures, that eventually define some nonlinear functions expressing the dependence between powers and network variables. Going into the details, it has been chosen to substitute the RLC loads with two real loads: the first corresponds to a 10 kW water pump, while the second represents an aggregate of many loads corresponding to a whole residence. Moreover, their models come from identification experiments, which have been performed in [29] and in [30]. The identified models are based on slightly different nonlinear functions, which are depicted in (5.2) and (5.3). In Table 5.7 and Table 5.8 the corresponding model parameters are reported.

$$
\begin{cases}
P &= P^{nom} \left(\frac{V}{V^{nom}}\right)^{k_{pv}} \left(\frac{\omega}{\omega^{nom}}\right)^{k_{p\omega}} \\
\\
Q &= Q^{nom} \left(\frac{V}{V^{nom}}\right)^{k_{qv}} \left(\frac{\omega}{\omega^{nom}}\right)^{k_{q\omega}}
\end{cases}
\tag{5.2}
$$

<div align="center">Water Pump Model</div>

	k_{pv}	$k_{p\omega}$	k_{qv}	$k_{q\omega}$
Water Pump	1.4	5.3	1.4	4.1

<div align="center">Table 5.7: Water Pump Model Parameters</div>

$$\begin{cases} P = P^{nom} \left(\frac{V}{V^{nom}}\right)^{k_{pv}} \left(1 + k_{p\omega}(\omega - \omega^{nom})\right) \\[4mm] Q = Q^{nom} \left(\frac{V}{V^{nom}}\right)^{k_{qv}} \left(1 + k_{q\omega}(\omega - \omega^{nom})\right) \end{cases} \tag{5.3}$$

Residential Model

	k_{pv}	$k_{p\omega}$	k_{qv}	$k_{q\omega}$
Residential Load	1.2	0.7	2.7	-2.3

Table 5.8: Residential Model Parameters

Looking at these loads, it can be noted that they are not characterized by pure resistive relationships but all variables are correlated. It is in fact recalled that the parameters shown in the tables express how one variable is correlated to the other. This is more relevant for the water pump, where a significant dependence between the active power and the network frequency is present (the parameter $k_{p\omega}$ has in fact a bigger value with respect to the others). This is due to the fact that the water pump is a rotating load, which is usually characterized by an inductive relationship.

Having defined the load characteristics, their nominal power trends are now illustrated. At this stage, two different profiles are defined for each load: one profile will represent the active power trend, while the other shows how the power factor evolves during the whole simulation time. Actually, real loads are never characterized by two independent active and a reactive power profiles, as performed in the previous simulations, but their power factor is usually varied. However, it is recalled that given the active power and the power factor, the resulting reactive power can be easily computed by performing the following computation.

$$Q = P \, tan \, (\, acos(\, cos(\phi) \,) \,)$$

The implemented load profiles are illustrated in Figures 5.33 and 5.34.
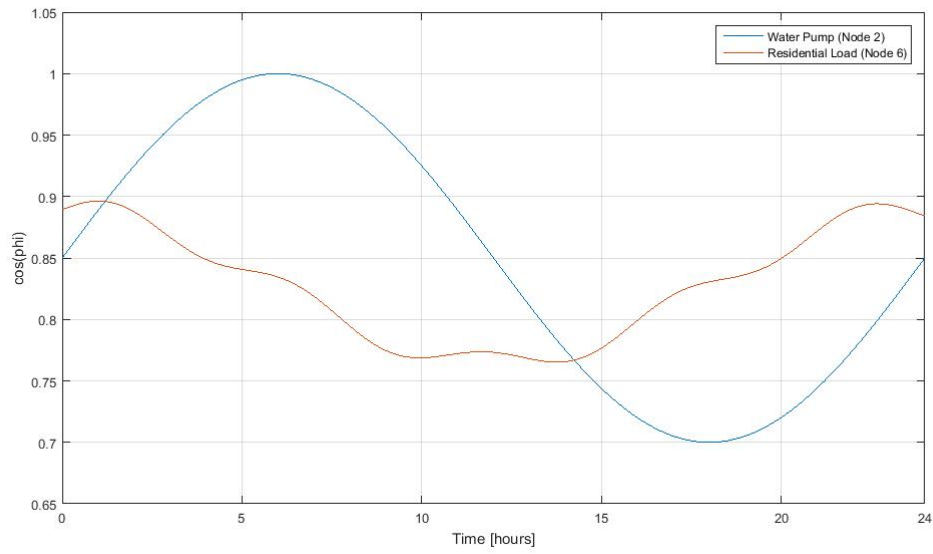
Figure 5.38: Realistic Loads: Power Factor Profile
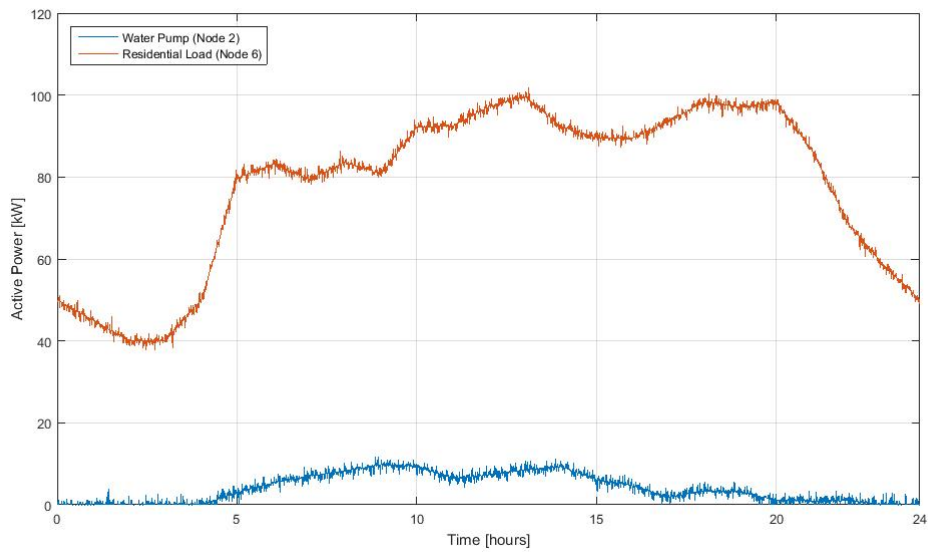
Figure 5.39: Realistic Loads: Active Power Profile

With regard to initial conditions of the generation sources, the data depicted in Table 5.6 have been implemented, while the renewable sources follow the same

97

power trends of the previous simulations. Moreover, also in this case the same scenario considered in paragraph 5.4.1 has been assumed, taking into account a more realistic test. The main results of the implemented simulation are depicted in the following figures.
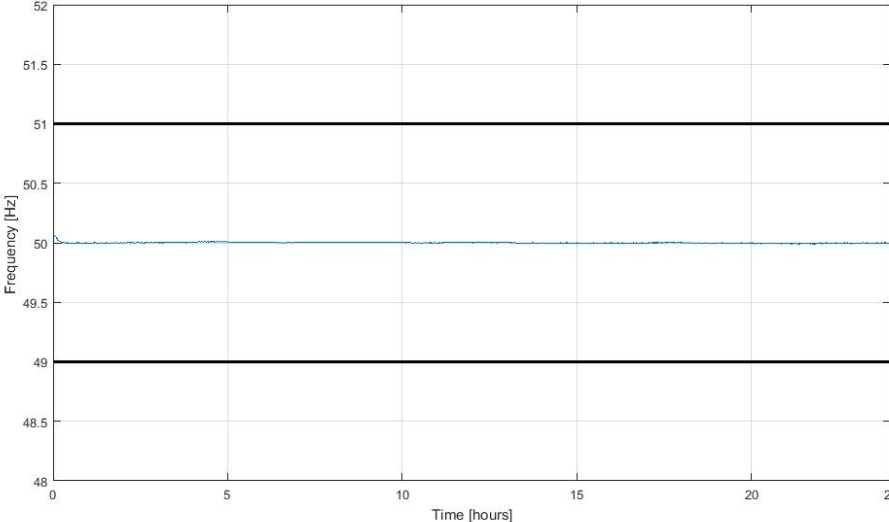
Figure 5.40: Robust Microgrid Management: network frequency response
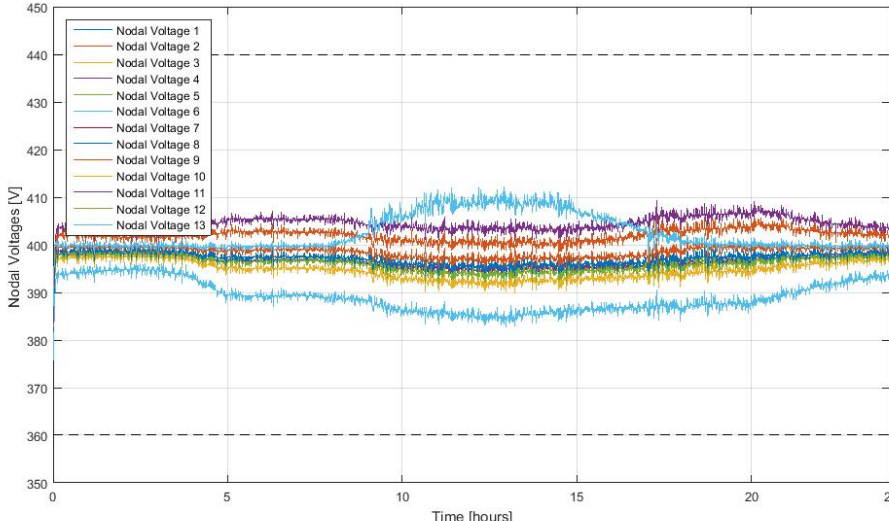
Figure 5.41: Realistic Loads: nodal voltages responses

98
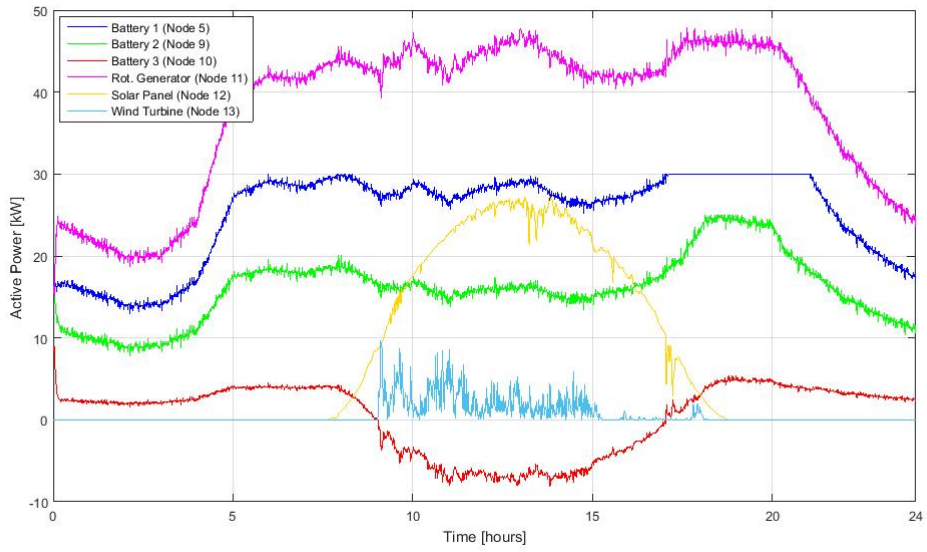
Figure 5.42: Realistic Loads: generated active power responses
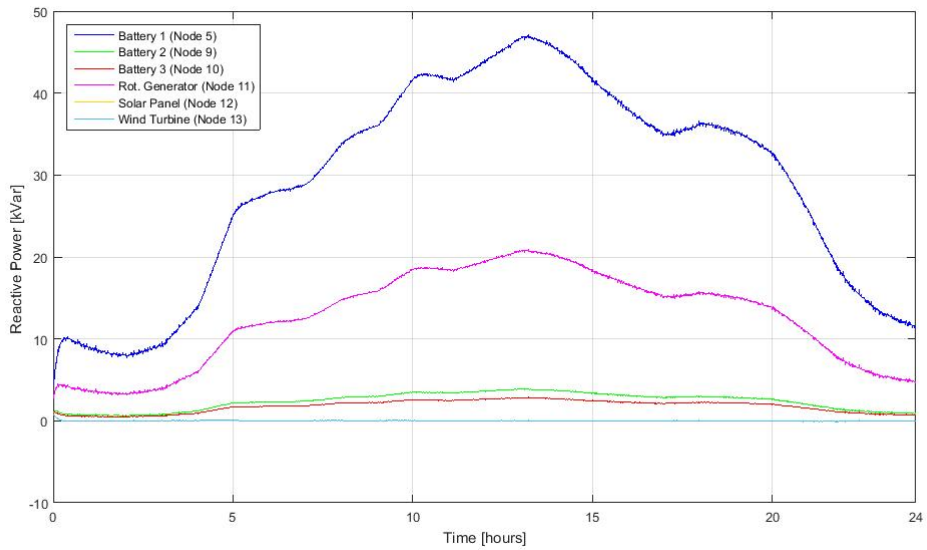
Figure 5.43: Realistic Loads: generated reactive power responses
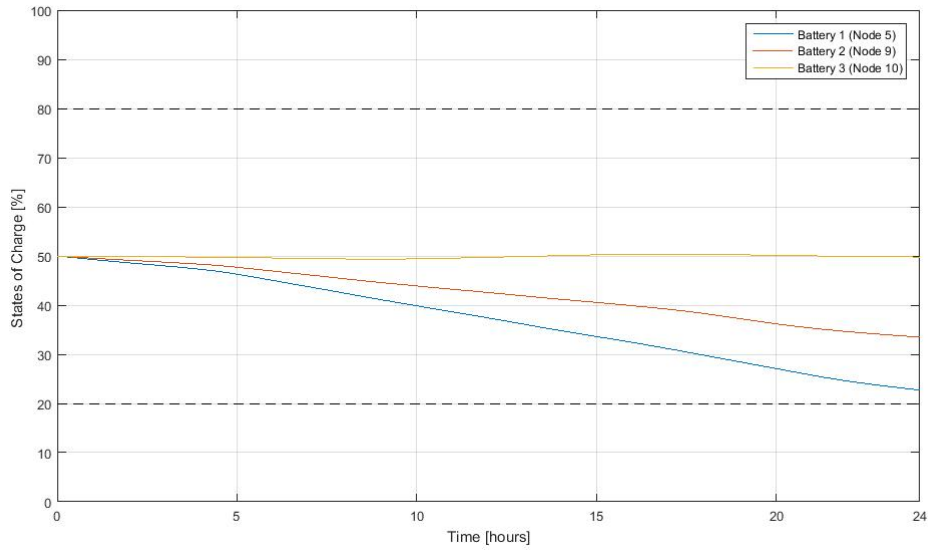
Figure 5.44: Realistic Loads: batteries' SOCs responses

The figures show that also in this case the control objectives are achieved. To sum up, in this simulation the control system does not have information about load power forecasts and on the load characteristics. Moreover, the implemented loads are not described by pure resistive relationships.

It has to be noted that from the simulated case it is not possible to conclude the designed hierarchical control structure perfectly works in any microgrid context. Actually, as discussed in the second chapter, to design the primary control layer it is really important to understand which is the prevailing impedance of the microgrid. Obviously, if the microgrid was characterized by inductive lines and only rotating loads were implemented, the designed control structure would be not able to keep the network variables at their nominal values. However, two facts are worth to be underlined.

Firstly, in the future most microgrids will be characterized by a resistive prevailing impedance. Indeed they are characterized by short resistive lines and it will be really unusual to find rotating loads directly connected to lines. Given the recent developments in power electronics converters, it will be more and more common that all microgrid elements are interfaced with electronically-controlled inverters instead of being directly plugged into the network.

On the other hand, it can be also noted that the defined control structure is not dependent on the implemented droop relationship. Actually, the inductive inverse droop control can be easily adopted without changing the secondary controller, but only by updating the system model used to perform the optimization algorithm. Therefore, in case we are dealing with a microgrid that shows a prevailing inductive relationship, the hierarchical control approach can be all the same implemented, achieving the defined control objectives.

5.5 Conclusions

In this chapter the microgrid test case has been presented and the performances of the designed control structure have been discussed. Summarizing, it has been proved that the implementation of a predictive secondary control layer gives considerable improvements since the network variables do not significantly deviate from their nominal values. Moreover, it allows to implement different policies for the resource management according to predefined objectives. It has been also shown that the hierarchical control structure is not strictly dependent on the exact knowledge of the system.

Chapter 6

Conclusions and Future Developments

In the first chapter, a complete overview of the future microgrid context has been presented, describing the main issues involving this new electrical paradigm. These are more relevant in the so called islanded operating mode, where frequent unbalances between the total generated and requested power occur. Actually, as shown in the second chapter, these unbalances significantly affect the network voltages and frequency, making them deviate from their nominal values. To solve this problem, in the same chapter a primary decentralized control layer has been described, analyzing both its theoretical definition and the adopted configuration. However, in the final part of the second chapter it is reported that this control layer is not enough to ensure that the network variables evolve around their nominal values.

Therefore, the implementation of a higher control layer has been considered, which actually corresponds to the main innovation introduced by this work. This secondary control layer has been chosen to be based on an advanced control strategy, i.e. the Model Predictive Control. Actually, the corresponding flexibility and potentialities make this control approach an efficient solution to the mentioned problems, allowing also the implementation of different resource management strategies during the islanded operating mode. However, since this control approach relies on a mathematical model of the system, the third chapter focused on the analysis of the main system dynamics. Once the final state-space equation describing the behavior of the main variables of the microgrid has been defined, in the final part of the chapter a description of the network simulator has been given, which has been developed by RSE SpA.

The fourth chapter covered the designing of the secondary control layer, analyzing its main elements. It is recalled that Model Predictive Control is based on an online optimization algorithm which relies on three principal elements: the system model, the variables' constraints and the cost function. While the first has been largely described in the third chapter, the implemented constraints and cost function have been presented in this chapter. However, given the flexibility of this advanced control technique, it is recalled that the designed control objectives can been easily extended or modified.

Finally, in the fifth chapter the designed hierarchical control structure has been tested. In the first part, the considered microgrid test case and its main elements have been described, which actually correspond to a real small-scale network that RSE owns at their main headquarters. Then, a series of simulations have been reported and it has been shown how the designed control structure is able to efficiently manage the considered microgrid in the islanded mode.

At the end of the chapter, additional tests have been presented where a more realistic implementation has been taken into account, for instance limiting the knowledge that the controller has on the system parameters or by testing the designed control structure with real utilities instead of simple RLC loads. Furthermore, it has been also proved that the flexibility of designed control structure allows to implement different resource management strategies without affecting the network variables' stabilization.

Considering the proposed solution, the main advantages of implementing the secondary control layer with a predictive control approach can be underlined:

- Coordinating all the primary controllers of the microgrid sources, this allows to keep the network variables at their nominal values in each power condition.

- Its flexibility allows to easily implement different resource management strategies without varying the designed control structure, but only by changing some parameters.

- It can perform an efficient microgrid management by taking into account some forecasts about the renewable sources production and load power future trends, if available.

Although the results of the designed control structure are satisfying, there are many other aspects that would be worth investigating through additional research activities; some of them are now presented.

- The implemented optimization algorithm takes into account only the minimization of the generated output powers for the resource management. However, more complex control strategies could be implemented. For instance, it could be interesting to control the generator reference powers based on their distance from the power limits, rewarding the units that allow bigger regulation margins. Another relevant resource management strategy could take into account the units' efficiency, trying to minimize the resource consumption in terms of batteries' states of charge or consumed fuel of the combustion-based generators.

- Analyzing the implemented primary layer, it can be noted that there is an additional degree of freedom that has been not exploited. Actually, the droop functions are characterized by fixed slopes and only their reference powers are varied. A more complex hierarchical control structure could be implemented, which can consist in more than two layers, and that is able to vary both the reference powers and the droop proportional gains according to some predefined objectives.

- The actual control structure is characterized by a centralized secondary controller that coordinates all the generation sources. However, this approach implies that a high computational power is required. Moreover, if a new microgrid element is plugged into the network or a unit is disconnected, this centralized control structure needs to be reformulated with a new system model. To overcome this issue, it would be interesting to investigate the possibility of implementing a decentralized secondary control layer that it is however based on an optimization based control algorithm, such as a distributed Model Predictive Control. This would allow in fact a flexible control framework, which all the same ensures an efficient management of the microgrid elements.

- Finally, the proposed control system has been designed to manage the microgrid only in islanded condition, and it does not consider neither the islanding nor the reconnecting event. The hierachical control structure could be actually improved so that it is performed both in islanded and in grid-connected mode, ensuring an efficient energy management in both conditions. Moreover, it has to be noted that an accurate analysis of the network variables transients should be performed during both the islanding and the recconnecting event; they may in fact experience unstable behaviors if the generation sources are not properly controlled.

List of Figures

List of Tables

Bibliography

[1] K. De Brabandere, B. Bolsens, J. Van den Keybus, A. Woyte, J. Driesen, R. Belmans. *"A Voltage and Frequency Droop Control Method for Parallel Imverters"*. IEEE Transaction on Power Electronics, 22(4): 1107-1115, 2007.

[2] Y. Wei Li, Ching-Nan Kao. *"An Accurate Power Control Strategy for Power-Electronics-Interfaced Distributed Generations Univs Operating in a Low-Voltage Multibus Microgrid"*. IEEE Transaction on Power Electronics, 24(12): 2977-2988, 2009.

[3] D. Wu, J. M. Guerrero, J. C. Vasquez, T. Dragicevic, F. Tang. *"Coordinated Power Control Strategy based on Primary-Frequency-Signaling for Islanded Microgrids"*. Industrial Electronics Society, IECON 2013 - 39th Annual Conference of the IEEE

[4] T.L. Vandoorn, J.D.M. De Kooning, B. Meersman, L. Vandevelde. *"Review of primary control strategies for islanded microgrids with power-electronic interfaces"*. Renewable and Sustainable Energy Reviews 19: 613–628, 2013.

[5] J. W. Simpson-Porco, F. Dörfler, Francesco Bullo. *"Synchronous and Power Sharing for Droop-Controlled Inverters in Islanded Microgrids"*. Automatica, 49(9): 2603-2611, 2013.

[6] H. Bouattour, J. W. Simpson-Porco, F. Dörfler, Francesco Bullo. *"Further Results on Distributed Secondary Control in Microgrids"*. 52nd IEEE Conference on Decision and Control. December 10-13, 2013. Florence, Italy.

[7] A. Bidram, F. L. Lewis, A. Davoudi. *"Distributed Control in Systems for Small-Scale Power Networks: Using Multiagent Cooperative Control Theory"*. IEEE Transaction on Control Systems, 34(6): 56-77, 2014.

[8] D. Wu, T. Dragicevic, J. C. Vasquez, J. M. Guerrero, Y. Guan. *"Secondary Coordinated Control of Islanded Microgrids Based on Consensus Algorithms"*. IEEE Energy Conversion Congress and Exposition (ECCE). September 14-18, 2014. Pittsburgh, PA.

[9] J. A. Peças Lopes, C. L. Moreira, A.G. Madureira. *"Defining Control Strategies for MicroGrids Islanded Operation"*. IEEE Transaction on Power Electronics, 21(2): 916-924, 2006.

[10] J. M. Guerrero, J. C. Vasquez, J. Matas, L. García de Vicuña, M. Castilla. *"Hierarchical Control of Droop-Controlled AC and DC Microgrids - A General Approach Toward Standardization"*. IEEE Transaction on Industrial Electronics, 58(1): 158-172, 2011.

[11] P. Bolzern, R. Scattolini, N. Schiavoni. *"Fondamenti di Controlli Automatici"*. McGraw-Hill Press, 2008.

[12] CEI. Norm CEI 021, *"Regola tecnica di riferimento per la connessione di Utenti attivi e passivi alle reti BT delle imprese distributrici di energia elettrica"*.

[13] CEI. Norm EN 50160, *"Caratteristiche della tensione fornita dalle reti pubbliche di distribuzione dell'energia elettrica"*.

[14] N. Mohan, T. M. Undeland, W. P. Robbins. *"Power Electronics, Third Edition"*. John Wiley Press, 2003.

[15] J. Rocabert, A. Luna, F. Bllbjerg, P. Rodriguez. *"Control Power Converters in AC Microgrids"*. IEEE Transaction of Power Electronics, 27(11): 4734-4749, 2012.

[16] C. A. Gross, T. A. Roppel. *"Fundamental of Electrical Engineering"*. CRC Press, 2012.

[17] A. Timbus, M. Liserre, R. Teodorescu, P. Rodrigues, F. Bllabjerg. *"Evaluation of current controllers for distributed power generation systems"*. IEEE Transaction of Power Electronics, 24(3): 654-664, 2009.

[18] K. D. Brabandere. *"Voltage and Frequency Droop control in low voltage grids by distributed generators with inverter front-end"*. PhD Final Thesis, Katholieke Universiteit Leuven. October 2006.

[19] R. E. Thomas, A. J. Rosa, G. J. Toussaint. *The Analysis and Design of Linear Circuits, 7th Edition"*. Wiley Press, 2012.

[20] A. Villa, F. Belloni, C. Gandolfi. *"Caratterizzazione sperimentale del comportamento di una porzione della Test Facility durante il funzionamento in isola elettrica e studio delle interazioni tra generatori statici con controllo droop in isola"*. RSE Report, February 2014.

[21] D. P. Kothari, I. J. Nagrath. *"Modern Power System Analysis, 3rd Edition"*. McGraw-Hill Press, 2003.

[22] S. Raimondi Cominesi, M. Farina, L. Giulioni, B. Picasso, R. Scattolini. *"Two-layer predictive control of a micro-grid including stochastic energy sources"*. American Control Conference (ACC), Chicago 2015.

[23] C. Carlini, C. Michelangeli, M. Rossi, D. Moneta, P. Mora. *"Evoluzione delle reti MT attive: algoritmi di controllo centralizzato e test in campo reale"*. RSE Report, January 2013.

[24] D. V. Griffiths, I. M. Smith. *"Numerical Methods for Engineers, 2nd Edition"*. Chapman & Hall Press, 2006.

[25] L. Magni, R. Scattolini. *"Advanced and Multivariable Control"*. Pitagora Editrice Bologna, 2014.

[26] J.M. Maciejowski. *"Predictive Control with Constraints, 1st Edition"*. Prentice Hall Press, 2000.

[27] E. F. Camacho, C. B. Alba. *"Model Predictive Control, 2nd Edition"*. Springer Press, 2007.

[28] M. Bockarjova, G. Andersson. *"Transmission Line Conductor Temperature Impact on State Estimation Accuracy"*. Power Tech Conference, 2007 IEEE Lausanne.

[29] R. Marconato *"Electrical Power Systems, Volume 1 - Second Edition"*. CEI-Italian Electrotechnical Committee, 2002.

[30] *"Load representation for dynamic performance analysis of power systems"*. IEEE Transactions on Power Systems, 8(2): 472 - 482, 1993.

Ringraziamenti

Non è facile concentrare in una sola pagina a chi devo il conseguimento di questo traguardo. Esso è stato infatti frutto di impegno e sacrifici, ma sicuramente il grazie principale va alle persone che mi hanno accompagnato durante questo percorso.

Ringrazio innanzitutto il Professor Scattolini, il quale con grande dedizione e impegno mi ha seguito in questo lavoro di tesi; la sua professionalità e sicurezza rimarranno sempre fonte di ammirazione. Lo ringrazio inoltre per il sostegno e la fiducia mostrata non solo per questo lavoro, ma anche per le esperienze future che mi aspetteranno.

Un particolare grazie va al Dr. Stefano Raimondi Cominesi, il quale è stato fonte di continuo sostegno e aiuto per il completamento di questo lavoro. Egli si è rivelato inoltre una preziosa fonte di consiglio, indispensabile nei momenti più difficili di questo percorso.

Un doveroso grazie va RSE S.p.A., e in particolare all' Ing. Carlo Sandroni, per l'attenzione e gli importanti consigli che hanno permesso il compimento di questo lavoro. Ringrazio anche il Prof. Carlo Novara, che con grande disponibilità mi ha seguito dal Politecnico di Torino durante questi mesi di lavoro.

Un immenso grazie va sicuramente alla mia famiglia, alla quale questo lavoro è dedicato. Ringrazio soprattutto i miei genitori per il sostegno e fiducia che hanno sempre mostrato verso me e mia sorella per ogni nostra scelta; credo che a loro dobbiamo ogni nostro traguardo.

Ringrazio inoltre Nina, che ormai da più di sei anni riempe la mia vita. Il suo continuo incoraggiamento e amore sono stati fondamentali in questi ultimi 5 anni, permettendomi di affrontare qualunque difficoltà e di perseguire i miei più innati sogni.

Ringrazio infinitamente i miei più grandi amici, in particolare Anastasia, Alessandra, Marco, Vincenzo, Eugenio, Guido, Peppe e Salvo, con i quali ho condiviso momenti di grande gioia e spensieratezza. Sono convinto che uno dei più grandi successi sia avere persone come loro al mio fianco.

Infine, ma non per importanza, ringrazio Enrico, Fabio, Caterina, Marcella, Mattia e Luca, con i quali abbiamo condiviso ogni difficoltà e vittoria, e che hanno reso questi 5 anni di università molto più belli di quanto si possa immaginare.